UNIVERSITY OF NAPOLI FEDERICO II

Doctorate School in Molecular Medicine

Doctorate Program in

Genetics and Molecular Medicine

Coordinator: Prof. Lucio Nitsch

XXV Cycle

"MOLECULAR ALTERATIONS LEADING TO MITOCHONDRIAL DYSFUNCTION IN DOWN SYNDROME"

ROSANNA MANCO

Napoli 2013

TABLE OF CONTENTS

LIST OF PUBLICATIONS **3**

ABSTRACT **4**

INTRODUCTION **5**

DOWN SYNDROME 5

GENE EXPRESSION IN DS 5

MITOCHONDRIAL DYSFUNCTION IN DS 8

TRANSCRIPTIONAL REGULATION OF MITHOCONDRIAL BIOGENESIS, FUNCTION AND MORPHOLOGY 9

HSA21 GENES: MOLECULAR BASIS OF MITOCHONDRIAL DYSFUNCTION IN DS 13

ANT1/SLC25A4 REGULATES THE ADP/ATP EXCHANGE WITHIN MITOCHONDRIA 17

AIMS OF THE STUDY **20**

MATERIALS AND METHODS **21**

RESULTS **30**

HSA21 GENES AND NEMG ARE DYSREGULATED IN DS-HFF 30

THE MITOCHONDRIAL FUNCTION IS ALTERED IN DS-HFF 32

WHICH HSA21 GENE OR TRANSCRIPT MIGHT BE RESPONSIBLE FOR MITOCHONDRIAL DYSFUNCTION IN DS? 41

META-ANALYSIS OF PUBLIC EXPRESSION DATA STRONGLY SUGGESTS THAT RIP140 AFFECTS MITOCHONDRIAL FUNCTION 41

THE HSA21 GENE RIP140 IS A MAJOR REGULATOR OF PGC-1A 42

RIP140 SILENCING AFFECTS MITOCHONDRIAL FUNCTION IN DS-HFF 44

HSA21 MIRNA LET-7C MAY NEGATIVELY REGULATE MITOCHONDRIAL ENERGY MOBILIZATION THOROUGH THE DOWNREGULATION OF ANT1 46

DISCUSSION **50**

ACKNOWLEDGEMENTS **57**

REFERENCES **58**

LIST OF PUBLICATIONS

1) Piccoli C, Izzo A, Scrima R, Bonfiglio F, **Manco R**, Negri R, Quarato G, Cela O, Ripoli M, Prisco M, Gentile F, Calì G, Pinton P, Conti A, Nitsch L, Capitanio N. *Chronic pro-oxidative state and mitochondrial dysfunctions are more pronounced in fibroblasts from Down syndrome foeti with congenital heart defects.* Human Molecular Genetics, 2013, Vol. 22, No. 6 1218–1232

ABSTRACT

Down Syndrome (DS) is the most frequent autosomal aneuploidy compatible with post-natal life. It has been attributed to the overexpression of chromosome 21 (Hsa21) genes. At least 80 phenotypic signs such as mental retardation, cardiac defects, muscle hypotonia, immunological disorders have been described in DS, however, it is unknown which, and how many, Hsa21 genes are responsible for each sign.

Hsa21 trisomy has been associated to mitochondrial dysfunction in different tissues and a global downregulation of nuclear genes encoding mitochondrial enzymes (NEMG) has been demonstrated in heart tissues from DS suggesting that the dysfunction may contribute to the DS phenotype.

To establish which correlation there might be between NEMG regulation and mitochondrial function in DS, we undertook molecular, functional and morphological studies on mitochondria in primary lines of fetal fibroblasts (DS-HFF). Hsa21 genes were globally upregulated and NEMGs were downregulated in DS-HFF, like in fetal hearts, and a mitochondrial dysfunction was observed.

The aim of this work is to understand how alterations in the expression of specific Hsa21 genes might cause mitochondrial dysfunction.

Based on literature and prediction databases, the nuclear receptor interacting protein RIP140 and the miRNA let-7c both mapping to Hsa21 were hypothesized to affect oxidative metabolism and mitochondria biogenesis in DS. RIP140 negatively controls the expression of the transcriptional coactivator PGC-1α, a key gene for mitochondrial biogenesis and NEMG expression, which was found downregulated in DS-HFF. To verify the hypothesis that RIP140 overexpression might cause PGC-1α downregulation, RIP140 silencing experiments were performed in DS-HFF demonstrating an inverse correlation between RIP140 and PGC-1α expression and a partial recovery of mitochondrial activity upon downregulation of RIP140 expression.

The role of miRNA let-7c in mitochondrial dysfunction was also investigated. Let-7c is upregulated in DS fetal tissues and among its predicted it is included the adenine nucleotide translocator-1 (ANT1), a gene responsible for the ATP/ADP exchange through the mitochondrial inner membrane. We found that in vitro let-7c upregulation caused ANT1 downregulation, suggesting that the upregulation of let-7c, due to primary gene dosage effect, might contribute to the energy deprivation in mitochondrial dysfunction.

These findings have potential therapeutic implications based either on in vivo inhibition of RIP140 gene or on the activation of key genes repressed by the overexpression of Hsa21 regulators.

INTRODUCTION

Down Syndrome

Down Syndrome (DS), caused by a complete or partial trisomy of chromosome 21 (Hsa21), occurs with a frequency of 1/700 births. Its complex phenotype is characterized by about 80 features with various degrees of expression and frequency (Epstein et al. 1991). Constant features are mental retardation, hypotonia, developmental delay, a partial immune deficiency, and an increased risk of leukemia. DS is a major cause of congenital heart defects (CHD) associated mostly to endocardial cushion defects (Ferencz et al. 1989, Park et al. 1977), mainly atrioventricular canal defects (AVCD) followed by ventricular septal defects (VSD) and complex malformations such as tetralogy of Fallot (TOF) (Park et al. 1977).
The life expectancy of DS subjects is 45-50 years. Starting from the age of 40 years old, DS subjects very commonly suffer from Alzheimer's disease (Cork 1990), autoimmune diseases and thyroid dysfunction typical of older population.

Gene expression in DS

It has been widely demonstrated that three copies of Hsa21 cause the overexpression of Hsa21 genes as a primary dosage effect. This produces, as secondary effect, the dysregulation of genes mapping to different chromosomes and as final effect the DS phenotype (**Figure 1**).

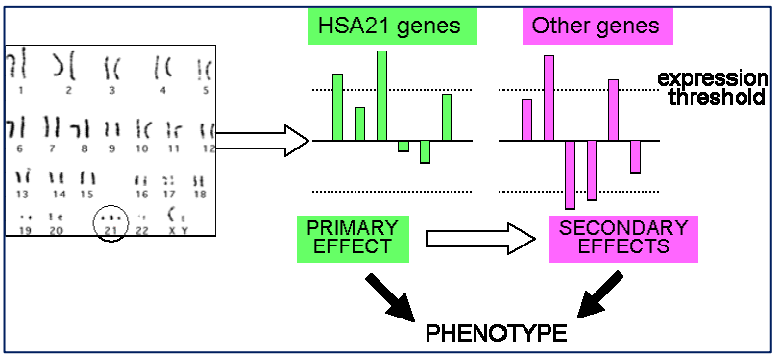

Figure 1. Primary and secondary effects of trisomy 21. Three copies of Hsa21 may cause a 50% increase in the expression of trisomic genes as primary dosage effect. The dysregulation of Hsa21 genes may cause alteration of disomic gene expression as secondary effects. Both primary and secondary effects will finally result in developmental defects and phenotypic alterations.

Several studies reported a global 1,5 fold overexpression of triplicated genes in mouse models of DS and in DS subjects (Kahlem et al. 2004; Lyle et al. 2004; Dauphinot et al. 2005). Interestingly, only a subset of chromosome 21 (Hsa21) genes is overexpressed in trisomic samples (FitzPatrick et al. 2002; Mao et al. 2005, Conti et al. 2007). The increase in expression may slightly differ from the expected ~1.5-fold and the set of over-expressed Hsa21 genes differs across the trisomic cell types (Amano et al. 2004; Li et al. 2006) and developmental stages indicating that other factors might also affect gene expression (Sommer and Henrique-Silva 2008).

In order to evaluate primary and secondary dosages gene effects in DS fetuses a gene expression profiling of fetal heart tissue by microarray technology has been performed (Conti et al. 2007). This study analyzed 15 fetal hearts at 18-22 weeks of gestation divided into 3 groups: 5 DS with CHD, 5 without CHD and 5 euploid fetuses. This analysis concerned 15.000 genes, including 168 Hsa21 genes. Microarray data demonstrated that Hsa21 genes were globally upregulated and that 441 genes, located on other chromosomes, were significantly dysregulated in trisomic heart samples. Downregulation of genes encoding mitochondrial enzymes (NEMG) and upregulation of genes encoding extracellular matrix (ECM) proteins appeared to be a hallmark of trisomy 21 in fetal heart samples: 65 out of 600 NEMG were downregulated and 40 out of 700 ECM genes were upregulated (**Table 1**). Downregulated NEMG were involved in all the respiratory complexes.

Table 1. List of genes encoding mitochondrial proteins downregulated in DS fetal hearts.

Probe ID	Fold Change (DS/euploid ratio)	Gene Name	Genbank ID
214274_s_at	0.647	ACAA1	AI860341
215210_s_at	0.548	ACADM	S72422
205412_at	0.756	ACAT1	NM_000019
208967_s_at	0.757	AK2	U39945
201322_at	0.739	ATP5B	NM_001686
208972_s_at	0.739	ATP5G1	AL080089
211715_s_at	0.554	BDH1	BC005844
205295_at	0.699	CKMT2	NM_001825
209746_s_at	0.721	COQ7	AF032900
203858_s_at	0.74	COX10	NM_001303
218057_x_at	0.738	COX4NB	BC001472
201597_at	0.764	COX7A2	NM_001865
201633_s_at	0.727	CYB5B	AW235051
208905_at	0.702	CYCS	BC005299

209759_s_at	0.729	DCI	BC002746
211150_s_at	0.568	DLAT	J03866
204824_at	0.638	ENDOG	NM_004435
201931_at	0.698	ETFA	NM_000126
202942_at	0.692	ETFB	NM_001985
213133_s_at	0.713	GCSH	AW237404
221415_s_at	0.545	GJA10	NM_030772
200947_s_at	0.758	GLUD1	NM_005271
208813_at	0.671	GOT1	BC000498
203745_at	0.678	HCCS	AI801013
200691_s_at	0.645	HSPA9B	NM_004134
210046_s_at	0.743	IDH2	U52144
202070_s_at	0.709	IDH3A	NM_005530
210418_s_at	0.751	IDH3B	AF023265
200955_at	0.704	IMMT	NM_006839
36830_at	0.711	MIPEP	U80034
219527_at	0.701	MOSC2	NM_017898
218027_at	0.716	MRPL15	NM_014175
203781_at	0.741	MRPL33	NM_004891
218890_x_at	0.745	MRPL35	NM_016622
204331_s_at	0.735	MRPS12	AA587905
220864_s_at	0.638	NDUFA13	NM_015965
202077_at	0.748	NDUFAB1	NM_005003
218201_at	0.669	NDUFB2	NM_004546
201226_at	0.663	NDUFB8	NM_005004
201966_at	0.62	NDUFS2	NM_004550
201740_at	0.72	NDUFS3	NM_004551
201757_at	0.763	NDUFS5	NM_004552
202941_at	0.76	NDUFV2	NM_021074
218455_at	0.712	NFS1	NM_021100
202780_at	0.705	OXCT1	NM_000436
200980_s_at	0.598	PDHA1	BF739979
214225_at	0.677	PIN4	BE674061
203649_s_at	0.657	PLA2G2A	NM_000300
205241_at	0.724	SCO2	NM_005138
201093_x_at	0.591	SDHA	NM_004168
202675_at	0.744	SDHB	NM_003000

202004_x_at	0.722	SDHC	NM_003001
203340_s_at	0.688	SLC25A12	AI887457
217961_at	0.705	SLC25A38	NM_017875
202825_at	0.607	SLC25A4	NM_001151
216841_s_at	0.734	SOD2	X15132
218119_at	0.634	TIMM23	NM_006327
203092_at	0.612	TIMM44	AF026030
220415_at	0.635	TNNI3K	NM_015978
209077_at	0.74	TXN2	AL022313
201903_at	0.75	UQCRC1	NM_003365
200883_at	0.716	UQCRC2	NM_003366
208909_at	0.744	UQCRFS1	BC000649
217140_s_at	0.637	VDAC1	AJ002428
217249_x_at	0.68	WUGSC:H_RG162B04.1	AC004544

Mitochondrial dysfunction in DS

Trisomy of chromosome 21 (TS21) has been associated to mitochondrial dysfunction, in several DS cells (Busciglio et al. 1995; Roat et al. 2007) and in mouse models (Shuchman et al. 2000; Shukkur et al. 2006), suggesting that a mitochondrial dysfunction might contribute to the DS phenotype. Data from functional studies suggest that Hsa21 trisomy affects mitochondrial function and reactive oxygen species production (Gardiner 2003). DS has been associated to oxidative stress, increase of reactive oxygen species (ROS) formation, altered intracellular calcium homeostasis, increase of apoptosis, decrease of protein level of complexes I, III and V in cerebellar and brain regions (Bambrick et al. 2008). Complex I was also deficient in mouse models of trisomy of chromosome 16. Impaired mitochondrial function, indicated by reduced mitochondrial redox activity and membrane potential, has been observed in DS astrocytes and in primary cultures of DS fibroblasts (Arbuzova et al. 2002, Busciglio et al. 2002). Deregulation of Ca^{2+} homeostasis and Ca^{2+}-mediated signaling has been described in cells derived from trisomic patients and in mouse models of DS (Caviedes et al. 2006; Yamato et al. 2009) since mitochondria function as a Ca^{2+} buffer. It has also been reported that the brain of the DS mouse model Ts1Cje has decreased mitochondrial membrane potential and ATP production (Shukkur et al. 2006). Recently it has been also reported that fetal DS fibroblasts show a decreased efficiency of the mitochondrial energy production apparatus, selectively involving ANT (adenine nucleotide translocator), ATP synthase and AK (adenylate kinase) and a selective deficit of complex I, which contributes to ROS overproduction by

DS mitochondria possibly related to changes in the cAMP/PKA signaling pathway (Valenti et al. 2010; Valenti et al. 2011).
Even though these results are indicative of widespread mitochondrial dysfunction in DS, molecular studies have not yet been performed to investigate the basis of mitochondrial dysfunction at the transcriptional level. Furthermore, no hypotheses have been formulated about the mechanisms by which trisomy of Hsa21 genes might induce such a dysfunction.
DS mitochondrial dysfunction is similar to the dysfunction associated to models of Parkinson's disease. This evidence suggests that different neurodegenerative diseases may be associated with the same mitochondrial dysfunction (Bambrick et al. 2008).

Transcriptional regulation of mithocondrial biogenesis, function and morphology

Mitochondria are cytoplasmatic organelles elongated in shape. They are present in all eukaryotic cells and can vary in size, indeed their average diameter is approximately 1μm. The overall volume of mitochondria is high (from hundreds to thousands per cell) in tissues and organs with high metabolic activity such as brain, retina, skeletal muscle, heart, kidney, and endocrine glands. The shape and number of these organelles are regulated by fission and fusion processes which vary depending on the function of the cell and tissue. Mitochondria are surrounded by outer and inner membranes that are consistent with their symbiontic origin. The outer membrane is smooth and permeable, whereas the inner envelope is highly folded and structured in cristae and offers the major permeability barrier to ions and molecules that traverse to the inner mitochondrial compartment by active transport.
The two envelopes enclose an intermembrane space and matrix, where the basic mitochondrial macromolecular syntheses (DNA replication, transcription, and translation) take place.
The main function of the mitochondrion is the production of energy, in the form of adenosine triphosphate (ATP), by the oxidative phophorylation (OXPHOS) process (**Figure 2**).

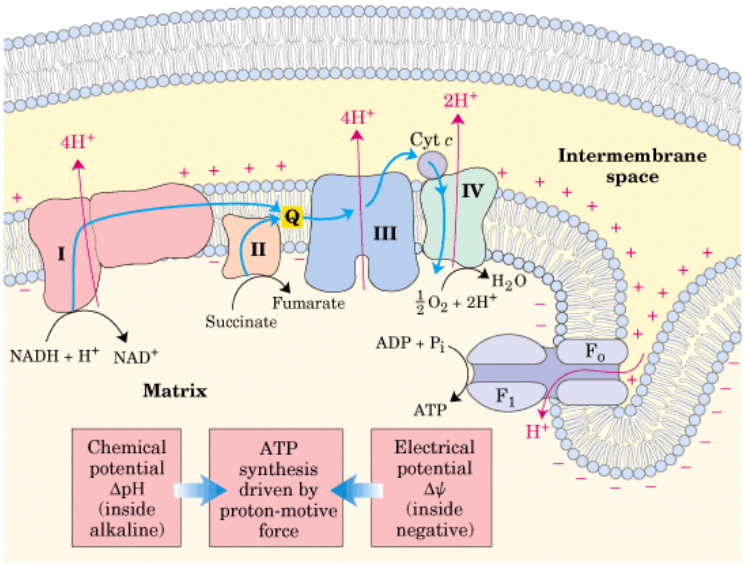

Figure 2. The OXPHOS process. Schematic representation of the complexes activity during the OXPHOS. The transition of the electrons is accompanied by a translocation of protons across the mitochondrial membrane. This phenomenon produces a chemical gradient (Phi) and an electrical gradient (Δψ).

The OXPHOS system is embedded in the lipid bilayer of the mitochondrial inner membrane and is composed by five multiprotein enzyme complexes (I–V) and two electron carriers – coenzyme Q and cytochrome c. During OXPHOS the charged molecules are processed within the five electron transport chain complexes to finally combine with oxygen to release the energy needed to make ATP. Complex I is called NADH ubiquinone oxidoreductase and it can be inhibited by rotenone; complex II is called succinate ubiquinone reductase and it can be inhibited by malate which competes with the substrate; complex II is called cytocrome bc_1 or ubiquinone cytocrome c oxidoreductase and it can be inhibited by antimycin and/or myxothiazol; complex IV is called cytocrome oxidase and it can be inhibited by potassium cyanide (KCN); finally, there is the ATP synthase enzyme. Mitochondrial OXPHOS constitutes the major cellular ATP-producing mechanism under aerobic conditions. A consequence of mitochondrial activity is the production of ROS that refers to a group of oxygen containing compounds with the ability to react with reduced compounds. They comprise superoxide (O^{2-}•), hydrogen peroxide (H_2O_2), and the highly reactive hydroxyl radical (•OH), although minor amounts of singlet oxygen can also be formed by cells. The initial product of the electron transport chain is O^{2-}•, which is quickly transformed into H_2O_2 by the enzyme superoxide dismutase (SOD). H_2O_2 can be reduced to water by catalase or glutathione peroxidase or can be converted into •OH in presence of reduced transition metals (reduced copper or iron).
The main source of O^{2-}• are respiratory complexes I and III located at the inner mitochondrial membrane (Chen et al. 2003; Camello-Almaraz et al. 2006).

With only 13 OXPHOS polypeptides encoded by mitochondrial DNA (mtDNA) (**Figure 3**), most of the OXPHOS subunits (at least 70) are encoded by the nuclear genome.

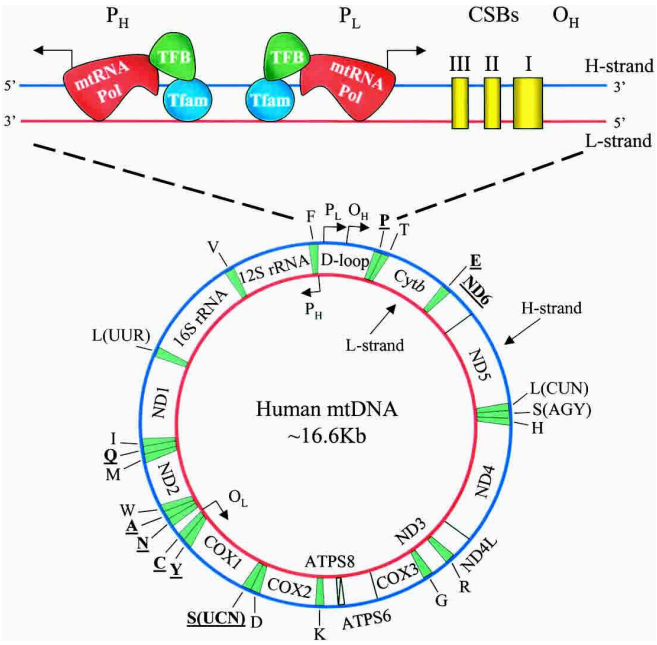

Figure 3. Human mitochondrial DNA (mtDNA). The genomic organization and structural features of human mtDNA in a circular double strand.

The transcriptional regulatory network controlling the expression of nuclear and mitochondrial genes includes nuclear respiratory factors NRF-1 and NRF-2 and mitochondrial transcription factor A (Tfam or mtTFA). NRF-1 transcriptionally controls many genes involved in mitochondrial function and biogenesis, genes involved in assembly of the respiratory apparatus, constituents of the mtDNA transcription and replication machinery, mitochondrial and cytosolic enzymes of the heme biosynthetic pathway (Huo and Scarpulla 2001). It is interesting to note that NRF-1 was found downregulated in TS21 fetal hearts and 34 of the NEMG downregulated in the same hearts showed an NRF-1-binding site within their promoters (**Table 2**).

Table 2. Mitochondrial genes downregulated in DS heart tissues with an NRF1 binding site in their promoter regions.

Gene name	Score	Promoter region position	Binding site Sequence
ECGF1	1	-13	CGCATGCGCA
SCO2	1	-14	CGCATGCGCA
PIN4	0,98	-282	CGCGTGCGCA

IDH3A	0,97	-24	CGCTTGCGCA
UQCRC1	0,96	7	CGCTTGCGCG
NDUFB8	0,96	-9	CACATGCGCA
RPL10	0,96	-12	CACATGCGCA
ENDOG	0,91	-161	CGCCTGCGCA
FPGT-TNNI3K	0,91	23	CGCATGCGCC
SDHA	0,91	-88	CGCCTGCGCA
UQCRC2	0,91	-264	CGCATGCGCC
ETFB	0,9	-9	CGCCTGCGCG
GLUD1	0,9	-31	CGCCTGCGCG
NDUFAB1	0,9	-43	CGCCTGCGCG
CYCS	0,9	-208	CGCAAGCGCA
SDHB	0,9	-65	CGCATGCCCA
HSPA9	0,89	-171	CGCATGTGCG
MRPL15	0,88	-52	CGCGCGCGCA
SLC25A12	0,88	-63	CGCGTGCGGA
VDAC1	0,88	-59	TGCGTGCGCA
HCCS	0,88	-25	CGCGTGCCCG
IDH3B	0,87	-166	TGCTTGCGCA
IDH2	0,86	-262	CGCTTGCGAG
COX4NB	0,84	-292	CACGTCCGCA
COQ7	0,81	-363	CGCCCGCGCA
ETFA	0,81	-71	CGCCTGCCCA
GOT1	0,81	-395	CGCCCGCGCA
NDUFA13	0,81	-265	GGCCTGCGCA
NDUFS2	0,81	-78	CGCCTGCGTA
PDHA1	0,81	-165	CGCAGGCGCT
DLAT	0,8	33	AGCCTGCGCG
GCSH	0,8	-18	CGCCTCCGCG
MOSC2	0,8	-6	AGCCTGCGCG
AK2	0,8	-303	CCCACGCGCA

NRF1 target genes are sorted with a cut-off affinity score = 0.80.

A second regulatory factor of mitochondrial biogenesis and function is NRF-2 which is the human homolog of mouse Gabp gene (Scarpulla 1997; Scarpulla 1999).

NRF-1 and NRF-2 are binding partners for the transcriptional coactivator PGC1α (peroxisome proliferator-activated receptor coactivator 1α) which

coactivates numerous transcription factors, including nuclear receptors such as PPARγ and PPARα, and estrogen receptor α, exerting the final effect to promote mitochondrial biogenesis and to regulate mitochondrial respiratory capacity (Leone et al. 2005; Scarpulla 2011; Scarpulla 2012). PGC-1α knock-out mice manifest a reduction of mitochondrial number and of respiratory capacity in skeletal muscle (Leone et al. 2005). PGC-1α transcription and activity are positively regulated by Ca^{2+} signaling and negatively regulated by the corepressor RIP140/NRIP1 (Receptor interacting protein 1/Nuclear receptor interacting protein 1) (Scarpulla 2011).
The functional versatility of mitochondria is paralleled by their morphological complexity. In certain cell types mitochondria are organized in networks of interconnected organelles. The ultrastructural changes in the architecture of mitochondria are due to differences that are established in the amount and form of the cristae, which result from folding of the inner membrane and can be either laminated or tubular, depending on the metabolic states of the organelle. This interconnected networks represent an efficient system to deliver energy or a calcium channel between different areas of the cell (De Giorgi et al. 2000; Skulachev et al. 2001).
The ultrastructure and the reticular organization of the organelle are determined by mitochondria-shaping proteins that affect the equilibrium between fusion and fission processes. The mitofilin, encoded by the gene IMMT, is a transmembrane protein localized at the base of the cristae. IMMT down-regulation results in a drastic change in the organization of the inner membrane that appears as densely packaged concentric layers and free of tubular connections (John et al. 2005). IMMT is downregulated in DS fetal hearts (Conti et al. 2007).

Hsa21 genes: molecular basis of mitochondrial dysfunction in DS

Some Hsa21 genes that regulate mitochondrial biogenesis and function have been identified. The kinase DYRK1A and DSCR1/RCAN1 (Bushdid et al. 2003) were considered to be involved in mitochondrial dysfunction in DS. RCAN1 and DYRK1A genes are localized on Hsa21 and their overexpression, through the downregulation of NFATc genes (**Figure 4**), might result in the depression of PGC-1α expression.

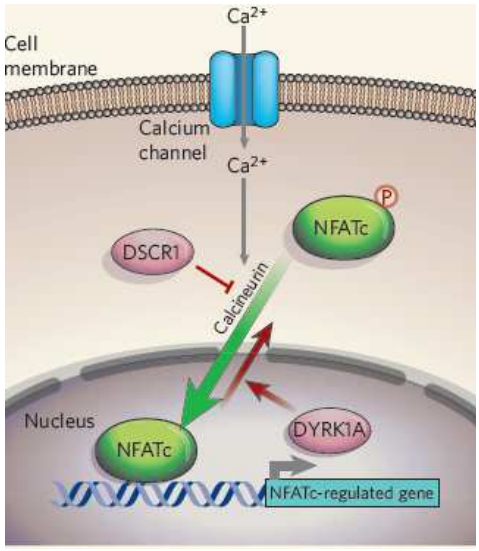

Figure 4. Calcineurin/NFAT signaling. The entry of calcium ions into the cell activates the enzyme calcineurin to remove phosphate groups (P) from NFATc factors in the cytoplasm, allowing NFATc to enter the nucleus and to activate its target genes. However, once in the nucleus, NFATc can be phosphorylated, and so returns to the cytoplasm. Arron et al. and Gwack et al. (2006) implicated the DSCR1 and DYRK1A proteins in regulating the levels of NFATc phosphorylation.

Another Hasa21 gene involved in mitochondrial function is RIP140, that has been already introduced above.

Literature on RIP140 function and modulation in mouse models strongly supports the hypothesis that this gene is involved in mitochondrial dysfunction (Powelka et al. 2006; Seth et al. 2007; Fritah et al. 2010; Chen et al. 2012). RIP140 is a corepressor that interacts with nuclear receptors and regulates the expression of genes that control metabolic processes such as energy homeostasis (Mangelsdorf et al. 1995; Robinson-Rechavi et al. 2003; Lin et al. 2005; Lelliot et al. 2006). It links nuclear receptors to chromatin remodeling enzymes, including the HDAC enzymes, involved in chromatin condensation and transcriptional repression, and this function is modulated by post-translational modifications which include phosphorylation and methylation (White et al. 2008). RIP140 is also target of acetylation, that inhibits the recruitment the C-terminal binding protein (CtBP) (Vo et al. 2001).

RIP140 interacts with 4 different repressive enzymatic complexes trough 4 distinct repression domains (**Figure 5**).

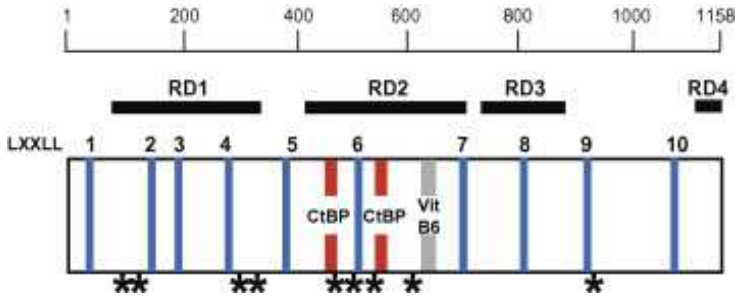

Figure 5. Functional domains and sites of post translational modifications of RIP140. LXXLL motifs and the LXXML motif are shown in blue (from 1 to 10). Positions of the 4 repression domains RD1–RD4 are in black. Stars indicate positions of potential sites of lysine acetylation and the vertical bars show positions of the interaction sites for CtBP and Vitamin B6. The protein contains approximately 15% serine/threonine residues and sites identified as phosphorylation targets (White et al. 2008)

This highly conserved gene shows a 1.5- to 4-fold upregulation both in the heart and fibroblasts from DS subjects (Conti et al. 2007; Piccoli et al. 2013). The upregulation of RIP140 protein was also demonstrated in the DS hippocampus (Gardiner 2006) together with the upregulation of SUMO3, another gene mapping to Hsa21, which might modulate RIP140 repressive activity. Indeed, the lysines located in RIP140 repression domain 3 and 4 represent the SUMO3 attachment consensus region and they are evolutionary conserved across vertebrate (Rytinki and Palvimo 2009). The simultaneous upregulation of both Hsa21 genes, might exert a synergistic effect.
Powelka et al. (2007) demonstrated that RIP140 significantly affects oxidative metabolism and mitochondrial biogenesis. On the contrary Seth et al. (2007) demonstrated that RIP140 overexpression represses nuclear mitochondrial genes involved in all respiratory chain complexes (**Figure 6A and 6B**).

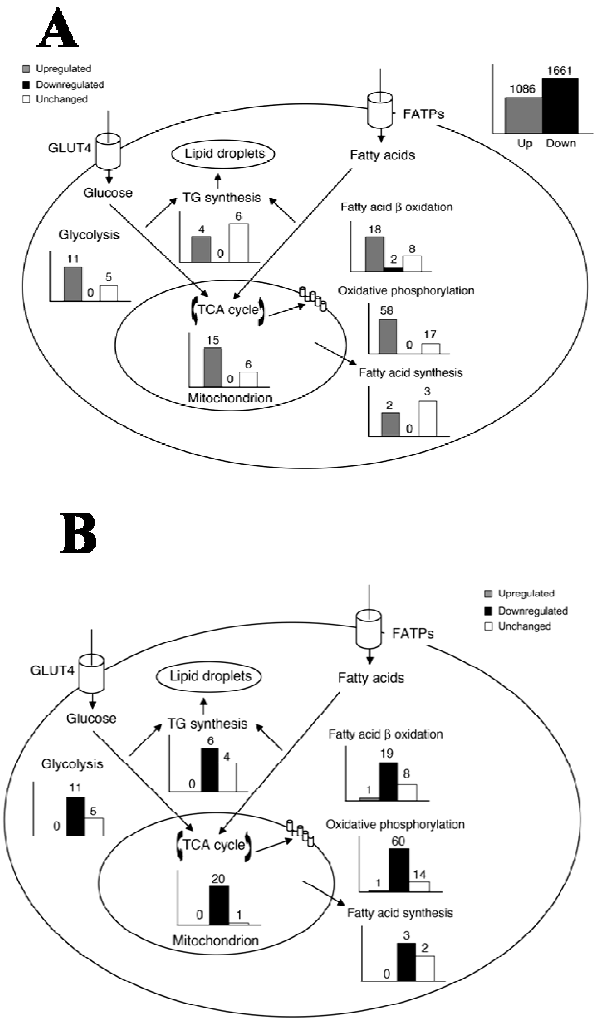

Figure 6. Representation of metabolic pathways influenced by RIP140 modification. (A) Metabolic pathways, in gray, upregulated after RIP140 silencing in adipocytes. (B) Metabolic pathways downregulated, in black, after RIP140 overexpression in mouse adipocytes (Seth et al. 2007).

The transcription factors NRF1 and ERRα and their targets are repressed by RIP140 and induced by PGC-1α in a dose dependent manner in neonatal rat cardiomyocytes (Chen et al. 2012). The PGC-1α protein, that plays a central role in regulating mitochondrial biogenesis and respiratory functions through the interaction with transcriptional partners, like NRF1, ERRα and PPARγ, is repressed by RIP140 (Scarpulla 2011) (**Figure 7**).

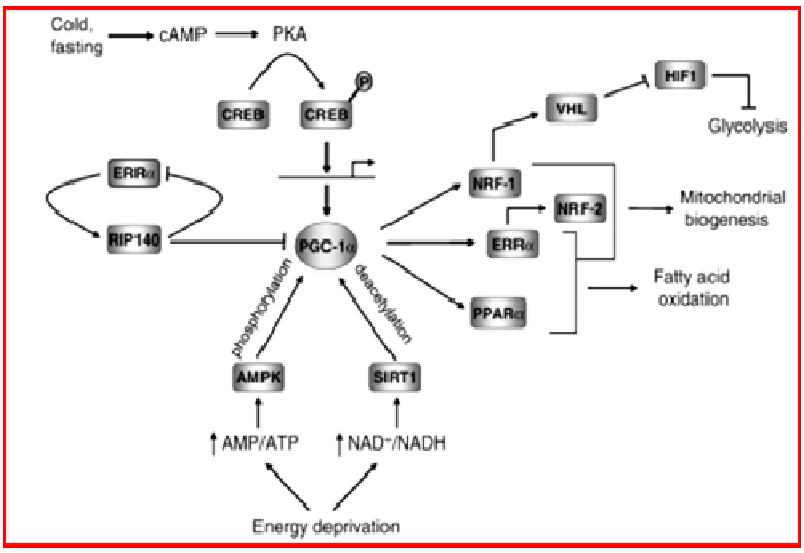

Figure 7. Representation of PGC-1α regulation by RIP140 and Ca^{2+} signaling (Scarpulla 2011).

Conti et al. (2007) and Piccoli et al. (2013) demonstrated that PGC-1α mRNA is significantly downregulated in DS fetal hearts and fibroblasts, respectively, while RIP140 is upregulated.
It can be hypothesized that the concurrent over expression of the Hsa21 genes RIP140, SUMO3, RCAN1 and DYRK1A and the downregulation of NFATc genes, observed in DS samples, result in the depression of PGC-1α expression.

ANT1/SLC25A4 regulates the ADP/ATP exchange within mitochondria

Genes mapping on other chromosomes are involved in a number of mitochondria functional alterations. Among those some authors have considered the role of ANT1 in the alteration of ADP/ATP exchange in mitochondria (Graham et al. 1997; Palmieri et al. 2005). ANT1/SLC25A4 (Adenine Nucleotide Translocator 1/Solute carrier family 25 member 4) is a dimeric protein complex of two identical 32kDa subunits embedded in the inner mitochondrial membrane that facilitates the transport of ADP and ATP (Klingenberg 1989; Fiore et al. 1998) (**Figure 8**). It has been demonstrated that ANT1 is downregulated in DS fetal hearts (Conti el al. 2007) possibly because it is a target of the Hsa21 miRNA let-7c.

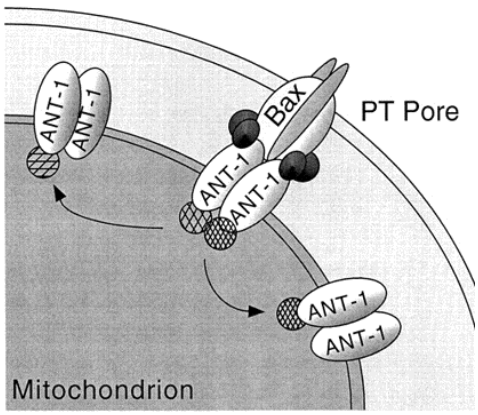

Figure 8. Position of ANT1 in the inner mitochondrial membrane. ANT1 interacts with PTP proteins and is embedded in the inner mitochondrial membrane. It has a central role in the ADP/ATP exchange and regulation of apoptosis. (Bauer et al. 1999)

ANT1 has a central role in OXPHOS: it acts as a solute carrier and exchanges matrix ATP for cytosolic ADP providing mitochondrial energy to the cytosol. ANT1 functions in mitochondria, which are structures within cells that convert the energy from food into a form that cells can use. ANT1 has also been proposed to participate in the formation of the mitochondrial permeability transition pore (PTP), a high-conductance channel of low selectivity that occurs on mitochondrial membranes (Zoratti and Szabò 1995; Haworth et al. 2000). The opening of PTP allows the free passage of solutes with a molecular mass below 1.5 kDa, thereby leading to membrane depolarization, substrate depletion, equilibration of solutes across the inner membrane, swelling of mitochondrial matrix and rupture of the outer membrane.
PTP is involved in programmed cell death through its action in permeabilizing the mitochondrial membranes. It has been demonstrated that PTP is regulated by ANT1 inhibitors, this suggests that ANT1 is the core pore-forming element of PTP. This proposal was supported by the observation that, in reconstituted lipid bilayers, purified ANT1 forms a large Ca^{2+}-dependent channel resembling PTP. However, the contribution of ANT1 to PTP remained a matter of active debate due to the lack of direct in vivo evidence to support ANT1 pore formation ability. Also, the complexity of PTP modulation in isolated mitochondria does not tend to support the ANT1-based single channel model (Chen 2002). It has been demonstrated that an ANT1 isoform is involved in some mitochondrial alterations. Indeed, the complete loss of function of ANT1 is associated to mitochondrial myopathy and cardiomyopathy. ANT1 knock out mouse model is characterized by a decrease of respiratory activity, increased redox stress and ROS production, proliferation of mitochondria and ragged-red fibers, heart progressive hypertrophy, metabolic abnormalities with increase of serum lactate level and severe exercise intolerance (Graham et al. 1997; Palmieri et al. 2005). Moreover, genetic inactivation of the ANT1 heart isoform results either in mtDNA damage and increased reactive oxygen species

either in dysregulation of many genes coding for mtDNA OXPHOS subunits, nuclear OXPHOS subunits and mitochondrial components (Subramanian et al. 2008). Palmieri et al. (2005) demonstrated that the accumulation of mtDNA deletion causes, in post-mitotic tissues, some mendelian disorders such as adult-onset progressive external ophthalmoplegia (PEO) due to weakness of the external eye muscles. Most of the ad-PEO families carry heterozygous mutations in ANT1.

In conclusion, it might be hypothesized that the concurrent over expression of the Hsa21 genes RIP140, SUMO3, RCAN1 and DYRK1A, and the downregulation of NFATc genes, observed in DS samples, result in the depression of PGC-1α expression (**Figure 9**).

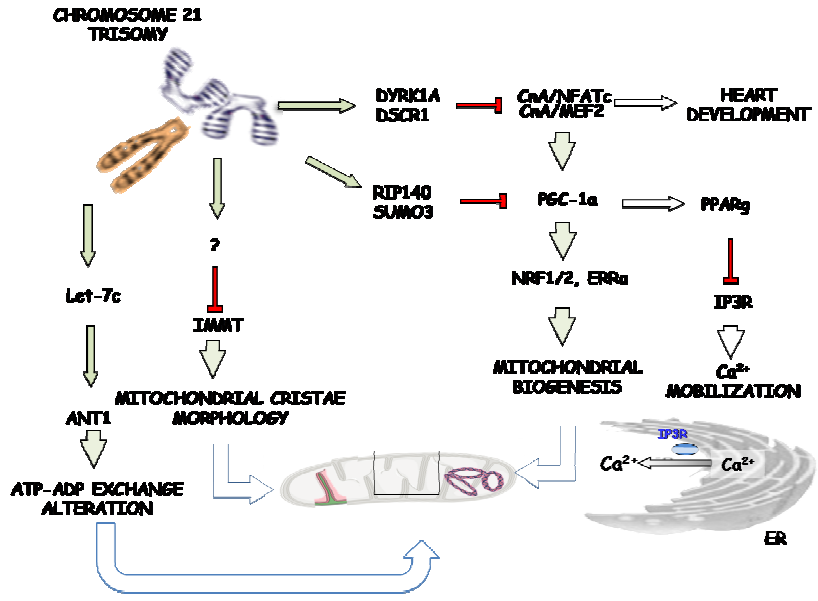

Figure 9. Hsa21 genes and transcript involved in mitochondrial pathways. Working hypothesis. TS21 leads to the upregulation of DYRK1A, DSCR, RIP140 and miRNA let-7c. DYRK1A and DSCR inhibit Calcineurin/NFAT axis in its control of PGC-1α expression and, as a consequence, the activity of PPARγ that controls Ca^{2+} homeostasis. By this pathway, the inhibition of PGC-1α may indirectly increase Ca^{2+} level. Also RIP140 may interfere with mitochondrial function as a consequence of the PGC-1α downregulation. The microRNA let-7c is involved in mitochondrial function possibly through the downregulation of ANT1 which regulate the ATP/ADP exchange. This miRNA may contribute to the energy deprivation in mitochondrial dysfunction. Finally, also the donwregulation of IMMT, caused by an unknown mechanism, may contribute to the alteration of mitochondrial function.

AIMS OF THE STUDY

The aim of this study was to characterize functional alterations of mitochondria in human fetal fibroblasts trisomic for Hsa21 with a special focus to Hsa21 transcripts possibly responsible for that. The mitochondrial dysfunction in DS was characterized investigating respiratory activity and oxidative distress. Oxygen consumption, OXPHOS complex activities, ROS production, membrane potential, $mtCa^{2+}$ and mtDNA copy number were compared between trisomic and euploid fibroblasts. Mitochondrial ultrastructure was also analyzed on fibroblasts in order to define morphological alterations associated to mitochondrial dysfunction. According to literature and previous results, an Hsa21 gene (RIP140) and an Hsa21 miR (miR-let7c) were chosen for further investigations. They were both upregulated in DS-HFF as result of primary dosage effect. RIP140 is a corepressor deeply involved in mitochondrial pathways. The gene was transiently silenced in this study to verify its possible implication in mitochondrial dysfunction and in the regulation of PGC-1α expression. The aim of silencing experiments was also to verify whether RIP140 inhibition in DS cells is able to rescue the mitochondrial function. The role of Hsa21 miRNA Let-7c was investigated for its possible influence on the ANT1 translocator, a gene downregulated in TS21 tissues and possibly involved in DS mitochondrial dysfunction. Our hypothesis is that the upregulation of a miRNA let-7c may contribute to mitochondrial dysfunction in DS, in particular to the alteration of ADP/ATP exchange as a consequence of the downregulation of ANT1, as secondary dosage effect. So the overexpression of let-7c as a primary gene dosage effect could cause the downregulation of ANT1 as a secondary effect in DS and therefore the dysregulation of OXPHOS genes and the alteration of ADP/ATP exchange in the mitochondria. This phenomenon may contribute to mitochondrial dysfunction that we found in DS-HFF. ANT1 is a predicted let-7c target. Transfection experiments of a let-7c miRNA mimic were used to investigate the role of this miRNA on ANT1 regulation.

MATERIALS AND METHODS

Functional analysis that are present in this study and that were published in Piccoli et al. 2013 was performed in collaboration with Professor Nazareno Capitanio and Dr. Claudia Piccoli from the Department of Biochemical Science, University of Foggia. The $mtCa^{2+}$ was assessed with Aequorin in collaboration with Professor Paolo Pinton from the Signal Transduction Lab, University of Ferrara. Morphological analyses were performed in collaboration with Dr. Marina Prisco from the Center of Electronic Microscopy, University of Naples Federico II.

Samples

Primary lines of fetal fibroblasts were used for this study. All samples derived from fetal heart tissues used in Conti et al. (2007) that were explanted from fetuses after therapeutic abortion. HFF were obtained from the Telethon Bank of Fetal Biological Samples at the University of Naples. According to protocols approved by our Institutional Ethics. For this study were used a cellular model of fetal fibroblasts (HFF) from normal fetuses, 5 from euploid fetuses (N-HFF) and 8 from fetuses with Down Syndrome (DS-HFF) with and without cardiophaty (CDS-HFF and NCDS-HFF respectively) (**Table 3**). For silencing experiments 4 DS-HFF (BIO37, BIO55, BIO44 and BIO48) samples were used. For let-7c miRNA mimic transfection all N-HFF samples were used.

Table 3. Primary lines of fetal fibroblasts used in the study

	DS-HFF	
N-HFF	**NCDS-HFF**	**CDS-HFF**
BIO-21	BIO-24	BIO-22
BIO-23	BIO-37	BIO-36
BIO-27	BIO-45	BIO-44
BIO-29	BIO-48	BIO-55
BIO-30		

RNA extraction and Quantitative Real-time PCR

Total RNA from each sample was extracted using TRIzol reagent (Gibco/BRL Life Technologies, Inc., Gaithersburg, MD) and was reverse-

transcribed using iScript cDNA Synthesis kit (Biorad). For miRNA reverse-transcription miScript II RT Kit (Qiagen) was used. Real-time PCR was performed using iQ Supermix SYBR Green 2X on the Bio-Rad iCycler (www.bio-rad.com) according to the manufacturer's protocols. For miRNA dosage miScript SYBR Green PCR Kit (Qiagen) was used. PCR reactions were performed in triplicate. The primers (MWG Biotech, Ebersberg, Germany) used for amplification are listed in **Table 4**. Primer pairs were designed using the Primer 3 software (http://frodo.wi.mit.edu/cgi-bin/primer3/primer3_www.cgi/) to obtain amplicons ranging from 100 to 150 base pairs. In order to test primer efficiency, serial dilutions of cDNAs generated from selected samples, that expressed target genes at a suitable level, were used to generate standard curves for each gene. GAPDH, RPL13A and ABELSON housekeeping genes were chosen as reference genes.

Table 4. Primer sequences of genes analyzed by qRT-PCR.

GENE NAME	PRIMER SEQUENCES
BTG3	**LEFT:** GAGGCAGTTGAGAGGTTTGC **RIGHT:** GAGTGAGCTCCTTTGGCAAG
ITSN1	**LEFT:** GTGAGCGGCACTGATTTGT **RIGHT:** GATCATGCTTCGCTCTTTCC
DYRK1A	**LEFT:** GATATCATATGGGTCAGGTCATTTT **RIGHT:** CTGGACTGTAACATAACACAGTATGC
SOD1	**LEFT:** GCATCATCAATTTCGAGCAG **RIGHT:** CAGCCTCTGTATTATCTCCAA
NRF1	**LEFT**: AAACGGAAACGGCCTCAT **RIGHT**: CTTGCTGTCCCACACGAGTA
IMMT	**LEFT**: AGTTTGTCCTCCGTCCATTG **RIGHT**: CCACCAATACCTCCACCAAC
PGC1α	**LEFT**: ACAGAACTGAGGGACCGTTTT **RIGHT**: TTTCAAGAGCAGCAAAAGCA
NRF2	**LEFT**: CCTGAACTGGTTGCACAGAA **RIGHT**: ACAAATCATGTCCCCATCGT
RIP140	**LEFT**: TGCCGTTGACAAAAAGTCTG **RIGHT**: CTTTGACAGGTGGGAAATGC
NDUFA1	**LEFT**: CTGGCTACTGCGTACATCCA **RIGHT**: TGCGCCTATCTCTTTCCATC
NDUFA8	**LEFT**: GTCATGCCGGGGATAGTG **RIGHT**:TTAAGCACAGCAGAACTAATTTTCA
NDUFB8	**LEFT**: GCCAAGAAGTATAATATGCGTGTG **RIGHT**: GTCAGGGAGCTTCGGGTAG
NDUFS2	**LEFT**: GAATGGGCACAGGAGTTTG

	RIGHT: GGCCCAAAGTTCAGGGTAAT
NDUFS6	**LEFT**: AGAAGGTCACGCACACTGG **RIGHT**: CACGGGCTGCTCTGCTAT
RCAN1	**LEFT:** TTTGCTCAGACCTTACACATAGGA **RIGHT:** GGGAGGGGAGATCAGAAACT
NFATC2	**LEFT:** GAGTTCACATCCCAGAGTCCA **RIGHT:** GAGCACTCGATGGGGTTAGA
NFATC3	**LEFT:** CTTTGCAATGGCAAGAGGA **RIGHT:** GATGAGGCACAGGCAAAGAT
NFATC4	**LEFT:** GTGAGATCATTGGCCGAGAC **RIGHT**: CCAGGTGATGACAGTTCACG
ANT1	**LEFT:** GGGTTTCAACGTCTCTGTCC **RIGHT**: TCCAGCTCACAAAAATGTGC
DICER	**LEFT:** CTGATGGAATTAGAAGAAGCACTTAAT **RIGHT**: ACCAGGGTCCCAGAACTACC
GAPDH	**LEFT:** TGCACCACCAACTGCTTAGC **RIGHT:** GGCATGGACTGTGGTCATGAG
RPL13A	**LEFT:** CCTGGAGGAGAAGAGGAAAGAGA **LEFT:** TTGAGGACCTCTGTGTATTTGTCA
ABELSON	**LEFT:** TGGAGATAACACTCTAAGCATAACTAAAGG **LEFT:** GATGTAGTTGCTTGGGACCCA

Left and Right primer sequences, obtained from Primer 3 software, are indicated for each analyzed gene.

Measurement of the respiratory activity in intact cells

The OCR (oxygen consumption rate) was assessed in intact cells relying on endogenous respiratory substrates and corrected for the residual KCN-sensitive OCR and, therefore, attributable to mitochondrial respiratory chain dependent activity. Cultured cells were gently detached from the dish by tripsinization, washed in PBS, harvested by centrifugation at 500g for 5 min and immediately assessed for O_2 consumption with a high resolution oxymeter (Oxygraph-2k, Oroboros Instruments). About $5x10^6$ viable cells/ml were assayed in 50 mM KPi, 10 mM Hepes, 1 mM EDTA, pH 7.4 at 37°C; after attainment of a stationary endogenous substrate-sustained respiratory rate, 2 µg/ml of oligomycin was added followed by addition of 0.5 mM of the uncoupler carbonilcyanide ptriflouromethoxyphenylhydrazone (FCCP) a potent reversible inhibitor of mitochondrial oxidative phosphorylation able to depolarize mitochondrial membrane potential abolishing the obligatory linkage between the respiratory chain and the phosphorylation system which is observed with intact mitochondria. The rates of oxygen consumption were

corrected for 2 mM KCN-insensitive respiration. The respiratory control ratio (RCR) was obtained dividing the rates of oxygen consumption achieved before and after the addition of oligomycin and the protonophoric uncoupler FCCP (Piccoli et al. 2007).

Measurement of the mitochondrial respiratory chain complexes activity

The specific activities of NADH: ubiquinone oxidoreductase (complex I) and cytochrome c oxidase (complex IV) were assayed spectrophotometrically on frozen–thawn and ultrasound-treated cells in 10 mM Tris, 1 mg/ml serum albumin, pH 8.0. Complex I was assayed (in the presence of 1 µg/ml of antymicin A plus 2 mM KCN) by following the initial 2 µg/ml rotenone-sensitive rate of 50 µM NADH oxidation (ε340nm = 6.22 mM^{-1} cm^{-1}) in the presence of 200 µM decylubiquinone (dUQ) as electron acceptor; the NADH-ferricyanide reductase activity of complex I was measured in the presence of rotenone, antimycin A and KCN with 200 µM potassium ferricyanide from the oxidation of NADH. Complex IV was assayed by following (in the presence of antymicin A) the initial 2 mM KCN-sensitive rate of 20 µM ferro-cytochrome c oxidation under aerobic conditions. The activities were normalized to the initial cell number and to cellular protein content (Cela et al. 2010).
Citrate synthase catalyzes the reaction between acetyl coenzyme A (acetyl CoA) and oxaloacetic acid (OAA) to form citric acid. Citrate synthase activity was assayed spectrophotometrically measuring the reaction between CoA-SH (CoA with a thiol group) and DTNB (5,5′-dithiobis(2-nitrobenzoic acid)) to form 5-thio-2-nitrobenzoic acid (TNB) that absorbs at 412 nm.

Laser scanning confocal microscopy imaging of mitochondrial membrane potential, ROS, Ca^{2+} and mitochondrial activity in live cells

Cells cultured at low density on fibronectin-coated 35-mm glassbottom dishes were incubated for 20 min at 37°C with the either of the following probes: 2µM tetramethylrhodamine ethyl ester (TMRE, a fluorescent lipophilic cation that accumulates in mitochondria electrophoretically) to monitor mitochondrial membrane potential (_Ψm); 10µM 2,7-dichlorofluorescin diacetate (DCF-DA a fluorescent probe H_2O_2sensible that selectively accumulates in mitochondria), which is converted to dichlorofluorescein by intracellular esterases (the acetate group of DCF-DA is removed by intracellular esterases and in the presence of superoxide ion the fluorescent is emitted), for detection of H2O2; 5 µM X-Rhod-1 AM for mitochondrial Ca^{2+}. All probes were from Molecular Probes (Eugene, OR). Stained cells were washed with PBS and examined with a Nikon TE 2000 microscope (images collected using a 60x objective [1.4 NA]) coupled to a Radiance 2100 dual-

laser LSCM system (Bio-Rad). TMRE and Rhod-1 red fluorescence was elicited by exciting with the He-Ne laser beam (λex 543 nm); whereas, dichlorofluorescein green fluorescence was elicited with the Ar-Kr laser beam (λex 488 nm). Acquisition, storage, and analysis of data were performed with LaserSharp and LaserPix software from Bio-Rad or ImageJ version 1.37. Superimposed confocal planes were analyzed by means of the "stack" function of the LCS-Analysis Tools, which produced an ax intensity profile of the average value of the pixels within marked edges, including a single cell, as a function of each focal plane. The integrated value of the xz profile was taken as a measure of the fluorescence intensity of that individual cell relative to the selected emission channel. Correction was made for the minimal background by repeating the procedure in a cell-free field. About one hundred single cells were analyzed for each imaging analysis (Cela et al. 2010). For the evaluation of ROS after RIP140 siRNA transfection 50000 cells were plated on 35-mm well plates (BD Falcon) on 20×20 mm slides (Delchimica). Twenty-Four hours later cells were incubated for 10 minutes at 37°C with 5nM of DCF-DA (Molecular Probes) and then washed three times with PBS 1X. Treated cells were observed using the confocal microscopy Zeiss Axiophot LSM 510 and DCF was elicited with the Ar laser (λex 488 nm). The images were acquiring using a 63X objective and then were analyzed using the ImageJ version 1.37 as previously described. For the evaluation of mitochondrial activity by Mitotracker Red (Molecular Probes). Mithotracker are a group of fluorescent probes that contain chloromethyl moieties that are thought to react with free sulfhydryls within the cell. Since the complexes of the respiratory chain are embedded in the inner mitochondrial membrane and mitochondrial activity is an index of mitochondrial respiration. MitoTracker Red, a selective mitochondrial probe, which accumulates in actively respiring mitochondria was chosen. Three-thousand cells were plated on 24 well plates on 12×12mm slides and then incubated with 150nM of Mitotracker Red for 30 minutes. After incubation cells were fixed with 4% of Paraformaldehyde for 20 minutes and then washed ones with PBS 1X. also for Mitotracker Red analysis confocal microscopy Zeiss Axiophot LSM 510 was used. Mitotracker was elicited with the He-Ne laser (λex 581 nm) . The images were acquiring using a 63X objective and then were analyzed using the ImageJ version 1.37 as previously described.

Mitochondrial calcium measurement using aequorin

Aequorin is a 21-kDa protein from various *Aequorea species* (Shimomura 1986) which, in the active form, consists of an apoprotein and a covalently bound prosthetic group (coelenterazine). When Ca^{2+} ions bind to three high-affinity sites (EF-hand type), aequorin undergoes an irreversible reaction in which a photon is emitted.

Mitochondrial Calcium was measured by the method described by Pinton et al. (2007). Cells were cultured on 13 mm-diameter coverslips in Chang medium B+C (Irvine scientific) at 37 °C and 5% CO_2 for 24 h and then infected with an adenoviral vector containing the plasmid with the cDNA coding for a mitochondrial-matrix addressed mutant form of aequorin. This construct includes the mitochondrial-targeting presequence of subunit VIII of human cytochrome c oxidase fused to the aequorin cDNA. Forty-eight hours after transfection, the cells were incubated for 1.5 h with 5 μM coelenterazine in Chang medium in a 5% CO_2 atmosphere. Coverslips with the transfected cells was placed in a saline solution-perfused chamber at 37 °C, and the number of emitted photons per second was measured after the stimulation with histamine using a photomultiplier with amplifier-discriminator. The output of the amplifier-discriminator was captured by a photon-counting board in a microcomputer and stored for further analysis. In order to calibrate the row luminescent signal in terms of $[Ca^{2+}]$ an algorithm has been developed that takes into account the instant rate of photon emission and the total number of photons that can be emitted by the aequorin of the sample. To obtain the latter parameter, at the end of each experiment the cells were lysed by a hyposmotic medium containing 10 mM $CaCl_2$ and 0,1% Triton X-100 in order to discharge all the aequorin that was not consumed during the experiment.

Morphological analysis and stereological investigation

Fibroblasts from trisomic and euploid fetuses were fixed and embedded for the electron microscope, using agarose as an intermediate embedding medium (Hayat 1981; Kerstens et al. 2000). In the petri dishes the cells were fixed with 4% paraformaldehyde and 5% glutaraldehyde in PBS buffer (0.1M, pH7,3) for 30' at room temperature, then washed in buffer, scraped from culture plates and pelleted by centrifugation for 10 min at 2000g; the supernatant was discarded and the cells were resuspended in 1 ml of 2% liquid agarose at 65°C. Again, the reaction tube was centrifuged for 5 min at 1000g to concentrate the cells in agarose. The agarose-cell pellet was solidified in ice for 30 min, then the agarose cone was carefully taken out of the reaction tube and divided in small pieces (1 mm^3). The agarose-cell blocks was post-fixed in osmium tetroxide (1% in PBS buffer) for 1 h at 4°C, dehydrated and transferred first in propylene oxide, then in a mixture of propylene oxide-Epon 1:1 and finally embedded in Epon resin. The Epon blocks were polymerized for two days at 60°C and then sectioned with a diamond knife to give thin sections, 70-80 nm each; the sections were picked up on 200 mesh copper grids, stained with uranyl acetate (5% in 50% methanol) and Reynolds lead citrate (Reynolds 1963) and observed by transmission electron microscope Philips 208S. Micrographs were acquired with a Mega View II Soft Imaging System camera.

For stereological investigations we used a stereological estimator, the "fractionator" method, to obtain a systematic and uniformly random sampling, which ensures that even for relatively small samples the error is so small that it may safely be ignored (Gundersen 2002).
Fifty cells per sample were analyzed and for each cell the percentages of broken and branched mitochondria and mitochondria with concentric or longitudinal cristae were determined. Furthermore, for each sample 25 micrographs were collected to evaluate the mitochondrial volume density (Vmt, relative volume of mitochondria on cell volume) and mitochondrial cristae volume density (Vmc, relative volume of mitochondrial cristae on mitochondria volume) (Weibel et al. 1966). To this end, a regular point lattice was placed random on each micrograph, by using ImageJ 1.43 software: the Vmt is obtained by differential counting of the points lying on mitochondrial surface and the total points lying on the micrograph; Vmc is obtained by differential counting of the points lying on mitochondrial cristae surface and the total points lying on the mitochondria surface.

Western Blot of PGC-1α

For Western Blot of PGC-1α cells were washed twice with ice-cold PBS and lysed in RIPA buffer (NaCl 154mM; Deoxicolic Acid 12 mM; NaF 0.95 mM; Triton X-100 1%; SDS 2%; PMSF 2 mM) in phosphate buffer in the presence of protease inhibitors. The protein concentration was determined using the Bio-Rad protein assay (Bio-Rad Laboratories Inc., Hercules, CA, USA). For western blot analysis, total lysates were boiled for 5 min in Laemmli sample buffer and analyzed on 7.5% SDSPAGE. Gels were then blotted onto nitrocellulose transfer membranes (Schleicher and Shuell GmbH, Dassel, Germany) using a Bio-Rad apparatus. After transfer, the filters were blocked at room temperature for 1 h with 5% BSA in TTBS (150 mM NaCl, 20 mM Tris-HCl pH 7.5). After washing twice with TTBS (150 mM NaCl, 20 mM Tris-HCl pH 7.5, 0.1% Tween 20), filters were incubated overnight at 4°C with rabbit polyclonal primary antibody to PGC-1α (1:1000, Abcam, Cambridge Science Park, Cambridge, UK). The filters were washed extensively with TTBS and incubated for 1 h at room temperature with anti-rabbit peroxidase-conjugated secondary antibody (Amersham, Little Chalfont, Buckinghamshire, UK) diluted 1:1000 in TTBS. The filters were then washed six times with TTBS and once with TBS and developed using an ECL Western Blotting Substrate detection method (Pierce, Rockford, IL, USA). For reprobing, the nitrocellulose filters were rehydrated and stripped for 30 min at 37°C in restore Western blotting stripping buffer (Pierce) and washed extensively with TTBS. Results were standardized to alpha tubulin and analyzed using NIH Image J (Rasband, W.S., ImageJ, U. S. National Institutes of Health, Bethesda, Maryland, USA, http://imagej.nih.gov/ij/, 1997-2012.).

Transfection protocol

RIP140 was transiently silenced in 4 DS-HFF (BIO48, BIO44, BIO45 and BIO37, see Table 4) using a pool of specific RIP140-siRNAs (ON-TARGETplus SMARTpool, Dharmacon), with negative (ON-TARGETplus SMARTpool Non targeting siRNAs control, Dharmacon) and positive controls (ON-TARGETplus SMARTpool, GAPD siRNAs, Dharmacon) and the Interferin transfection reagent (Polyplus^{TM}) . Cells were plated on 12well plates in a concentration of 50000 cell/well, on 35well plates with 20mm slides (Delchimica) in a concentration of 50000 cell/well, on 24 well plates in a concentration of 30000 cells/well (BD Falcon), in order to asses respectively RIP140 and PGC-1α expression, ROS production, mitochondrial activity. DS-HFF were transfected with RIP-140 siRNAs, non-targeting siRNAs and GAPD siRNAs by Interferin (Polyplus TransfectionTM) using 2 concentrations of siRNAs, 5nM and 20nM, in order to identify an appropriate protocol to inhibit RIP140 expression in DS-HFF. Seventy-two hours after transfection cells were harvested and the effects of RIP140 silencing were evaluated using RT-PCR, DCF and Mitotracker probes.
For miRNA let-7c upregulation a let-7c miRNA mimic by Qiagene (miScript miRNA Mimics) was used. Cells were plated in a concentration of 70000/well on 24well plates (BD Falcon) and after 24 hours were transfected with a miRNA mimic using the Interferin transfection reagent (Polyplus^{TM}). Forty-eight hours after transfection cells were harvested and ANT1 and DICER expression was evaluated.

Bionformatic analysis

TargetScan, Pita, Miranda, Microcosm, microRNA.org and Pictar databases were used for let-7c target prediction. Targets in common between at least 2 databases were chosen. Differential expression of targets in fetal heart samples was analyzed using Gene Spring software v12. Metanalysis of GSE 19836 series (De Cegli et al. 2010) from GEO repository was performed using Gene Spring software v12, followed by Gene Ontology functional scoring by Webgestalt tool (http://bioinfo.vanderbilt.edu/wegestalt/).

Statistics

The Student's t-test was applied to evaluate the statistical significance of data in this study. The significance of the differences between DS-HFF and N-HFF, between CDS-HFF and NCDS-HFF, and between transfected and non transfected cells was determined. For stereological investigations, the data obtained from each samples were averaged per group (DS-HFF and N-HFF; CDS-HFF and NCDS-HFF) and statistical evaluation was performed by two

non-parametric statistical tests, the Kolmogorov-Smirnov and the Kruskal-Wallis tests. The threshold for statistical significance (p-value) was set to 0.05.

RESULTS

In my PhD project the molecular, morphological and functional analyses were combined to study mitochondria function in DS using primary cultures of fetal fibroblasts (HFF) as cellular model. Part of this study was recently published in a paper in which we demonstrated the alteration of mitochondrial function and the dysregulation of some genes that control mitochondrial biogenesis and function in DS-HFF (Piccoli et al. 2013). The results of this published study are briefly reported here.

Based on the notion that NEMG are downregulated in fetal heart tissues trisomic for Hsa21 (Conti et al. 2007), we investigated the molecular basis of this dysregulation and determined whether NEMG downregulation was correlated to abnormal mitochondrial function.

To this aim we collected fetal fibroblasts (HFF) from non trisomic fetuses (N-HFF) and from fetuses with Down Syndrome (DS-HFF) with and without cardiophaty (named CDS-HFF and NCDS-HFF respectively). In all HFF we verified by standard G-banding technique that no changes in chromosome number and structure had occurred in cells after thawing and culture passages.

Hsa21 genes and NEMG are dysregulated in DS-HFF

The expression of Hsa21 and nuclear mitochondrial genes was analyzed in DS-HFF, by qRT-PCR. All Hsa21 genes analyzed were upregulated in DS-HFF confirming the gene dosage effect previously demonstrated in DS tissues (Mao et al. 2005; Conti et al. 2007) (**Figure 1A**). For NEMG we focused to genes involved in mitochondrial biogenesis (NRF1 and PGC-1α) and morphology (IMMT), mitochondrial complex subunit genes (NDUFs) and genes affecting mitochondrial function through the calcineurin pathway (NFATc genes)**.** Most of the investigated genes were downregulated (**Figure 1B**) indicating that the NEMG dysregulation observed in DS fetal hearts (Conti et al. 2007) is similarly found in fibroblasts. We also demonstrated that NFATc3 and NFATc4 were significantly downregulated and inversely correlated to DYRK1A and RCAN1 in trisomic fibroblasts (**Figure 2**) as well as in fetal hearts (Conti et al. 2007).

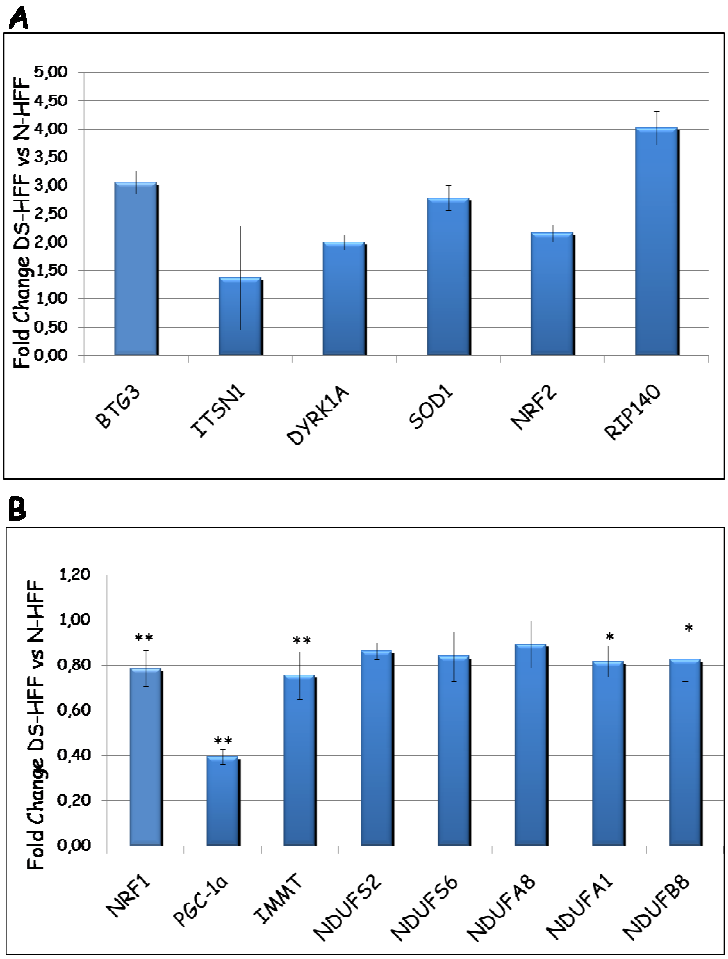

Figure 1. **Dysregulation of gene expression in DS-HFF.** Hsa21 (A) and nuclear-encoded mitochondrial gene expression (B) in DS-HFF versus N-HFF samples, obtained by qRT-PCR. Values represent the mean of three replicates ± standard error of the mean (SEM). * = $p<0.05$, ** = $p<0.01$, # = Not significant; N-HFF = Euploid fibroblasts, DS-HFF = Hsa21 trisomic fibroblasts.

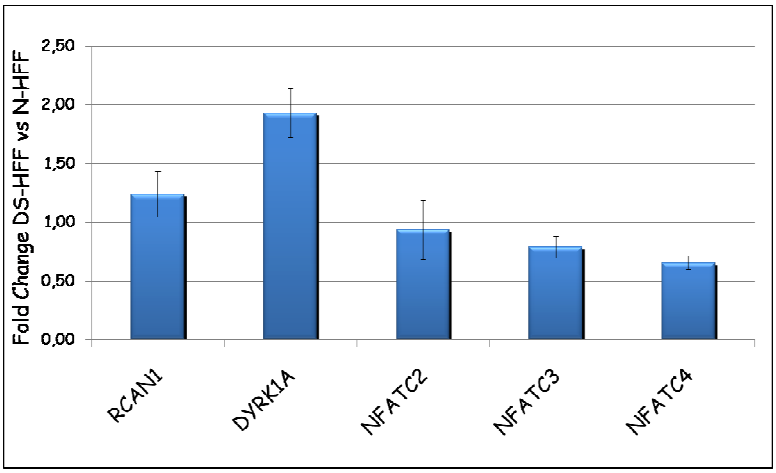

Figure 2. DYRK1A, RCAN/DSCR1 and NFAT gene expression. The kinases DYRK1A and RCAN/DSCR1 are upregulated while NFATc3 and NFATc4 are downregulated in trisomic fibroblasts.

The mitochondrial function is altered in DS-HFF

After assessing NEMG global downregulation in DS-HFF, a mitochondrial functional analysis was carried out in the same cell lines. The respiratory activity of N-HFF and DS-HFF samples was compared by high-resolution oxymetry. The OCR (oxygen consumption rate) was assessed in HFF samples. Although an inter-individual variability was observed, on an average basis, the resting respiration of DS-HFF showed a significant decrease that was more evident in CDS-HFF (≈43% inhibition) when compared to controls (**Figure 3**). Conversely DS-HFF showed a slight increase in the OCR in the presence of the FoF1-ATP synthase inhibitor, the oligomycin; whereas, in the presence of the protonophoric uncoupler FCCP, a slight, albeit significant, decrease (≈27% inhibition) in the OCR was observed. These results indicate that the reduction of OCR in DS-HFF is dependent on the alteration of the electron transporting chain.

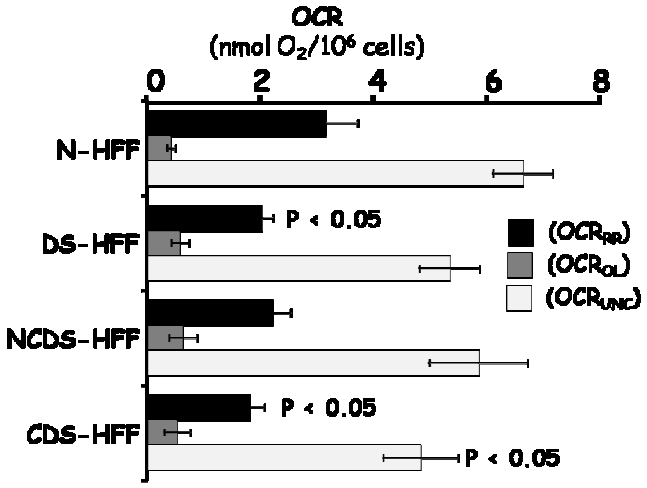

Figure 3. Respirometric analysis in DS fibroblasts. The OCR (normalized to cell number) was assessed by high-resolution oxymetry in intact cells as described in Materials and Methods. A comparative analysis between five different euploid (N-HFF) and eight different DS-HFF samples (NCD-HFF and CDS-HFF) is shown. The endogenous OCR was measured under resting conditions (OCRRR), in the presence of oligomycin (OCROL), and in the uncoupled state in the presence of FCCP (OCRUNC).

To assess whether the observed respiratory deficit resulted from a specific defect in one of the respiratory chain complexes we measured the activity of the complexes I (NADH-dehydrogenase), complex III (cytochrome c reductase) and complex IV (cytochrome c reductase) in DS-HFF. The activity of complex I was significantly reduced (by about 50%) in DS-HFF, both in NCDS-HFF and CDS-HFF as compared to N-HFF (**Figure 4**). No significant differences in activities of complexes III and IV in DS-HFF versus N-HFF were found. Complex I activity was normalized to the activity of citrate synthase, which is an index of mitochondrial mass, and to total protein level per cell. The results after normalization were unchanged.

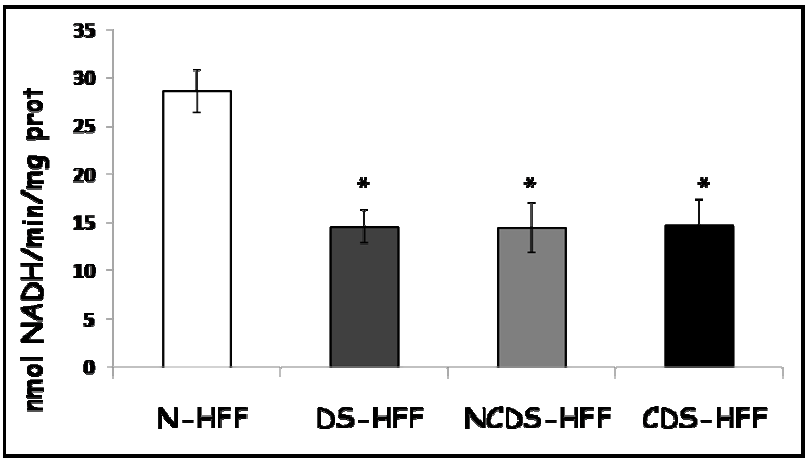

Figure 4. Enzymatic activities of the mitochondrial respiratory chain complex I of DS fibroblasts. The specific activities of complex I (NADH-dehydrogenase) was measured in cell lysates under conditions of saturating substrate as described in Materials and Methods. Dark grey histogram shows that the activity of complex I is significantly reduced in DS-HFF with and without cardiophaty (light grey bar and black bar) compared to N-HFF (white bar). * = $p<0.05$.

We used TMRE to measure the mitochondrial membrane potential (mt$\Delta\psi$) by confocal microscopy imaging. TMRE is a specific mitotropic probe. The fluorescent signal, due to accumulation of the probe in response to membrane potential, was not significantly different among the samples, but the fluorescent signal revealed less inter-digitated mitochondrial network morphology in DS-HFF (**Figure 5**).

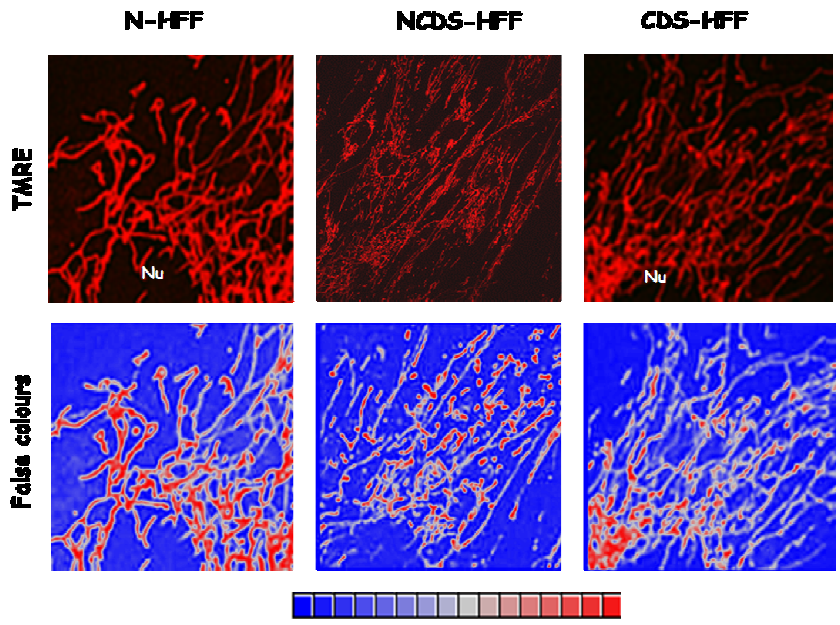

Figure 5. Confocal microscopy analysis of mtΔΨ in DS live fibroblasts compared to N-HFF. Magnifications of intracellular details showing the mitochondrial functional network in samples N-HFF, NCDS- and CDS-HFF. A false-colours rendering of the TMRE-related fluorescence imaging is also shown.

Mitochondria are the major source of ROS as a consequence of mitochondrial activity. In particular complex I is considered one of the sites of generation of superoxide radicals (Li and Trush 1998; Kussmaul and Hirst 2006). The intracellular redox state was assessed by confocal microscopy in order to evaluate any alterations in ROS production possibly correlated to the electron transporting chain anomalies and NEMG dysregulation using the 2'-7'-dichloro fluorescein diacetate (DCFA-DA) probe, a H_2O_2 sensitive fluorescent probe that selectively accumulates in mitochondria. The analysis demonstrated that DS-HFF samples produced more ROS compared to N-HFF with a larger redox imbalance in CDS-HFF (**Figure 6A and 6B**). As shown by the enlargement "a", the brighter signal of the DCF-DA related fluorescence is compartmentalized.

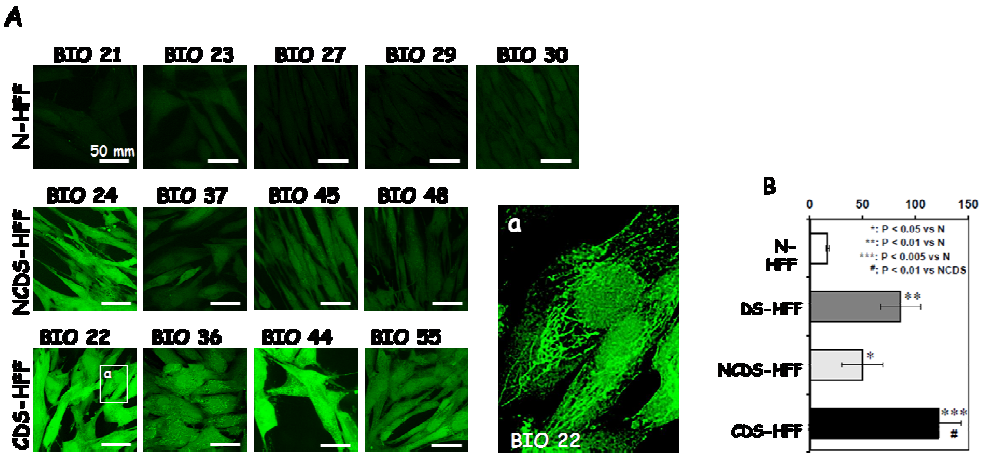

Figure 6. ROS production in DS-HFF versus N-HFF. (A). Confocal microscopy images of DCF-H_2O_2 indicating mitochondrial localization of superoxide radicals (green signals). (B). Representation of DCF-DA pixel intensity in DS-HFF versus N-HFF. Both in NCDS-HFF and in CDS-HFF pixel intensity of DCFA-DA is increased, most in CDS-HFF.in N-HFF (BIO21, BIO23, BIO27, BIO29, BIO30 white bar) (dark gray bar) and DS-HFF (NCDS-HFF-BIO24, BIO37, BIO45, BIO48-light gray bar and DS-HFF- BIO22, BIO36, BIO44, BIO55-black bar). Statistical analysis of the fluorescence intensity per cell as resulting from the averaged values ± SEM of about one hundred randomly selected different cells for each sample from at least in-duplicate experiments; statistical analysis of the differences is also shown.

In order to investigate calcium signaling alterations due to the abnormalities of mitochondrial function and gene dysregulation, we evaluated the intramitochondrial calcium level ($mtCa^{2+}$) using the specific probe Rhod-1, which is a red fluorescent probe. DS-HFF displayed a statistically significant more intense Rhod-1-related fluorescence signal as compared to N-HFF. The compartmentalization of the brighter signal reveals steady-state $mtCa^{2+}$ level (**Figure 7**).

To verify the specific mitochondrial derivation of $mtCa^{2+}$ we used a different method based on a calcium-sensitive photoprotein, the Aequorin. Also Aequorin results revealed the increased concentration of mt Ca^{2+} in DS-HFF, with and without cardiophaty (**Figure 8**). We found a significative 40% calcium overload in DS-HFF samples.

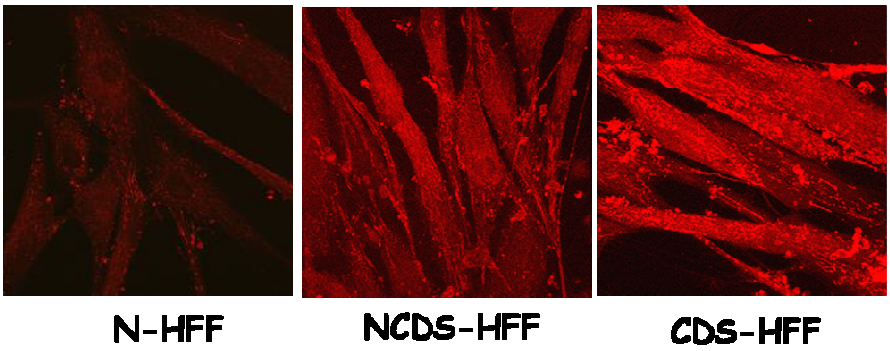

Figure 7. Confocal microscopy analysis of Rhod-1 fluorescence. Confocal microscopy analysis reveals the increase of Ca^{2+} in DS-HFF with and without cardiophaty compared to N-HFF.

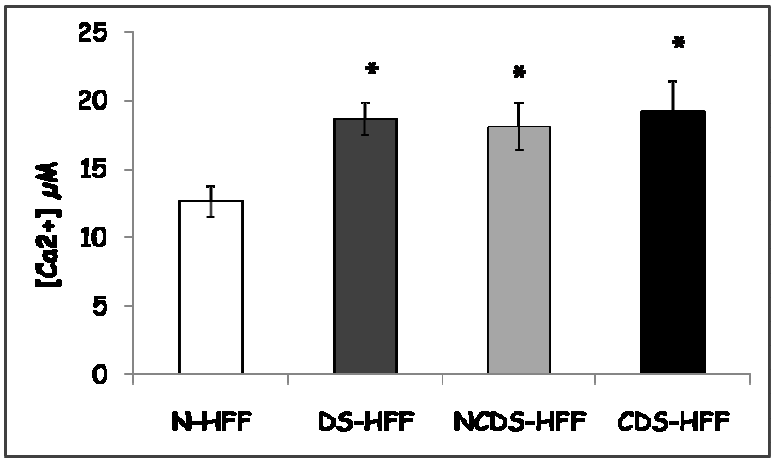

Figure 8. Intramitochondrial calcium measurements in DS-HFF samples with Aequorin. Representation of Aequorin result shows a significative 40% calcium overload in DS-HFF samples (dark bar), with and without cardiophaty (light gray bar and black bar respectively) when compared to N-HFF (white bar). Results are shown as mean of the determinations in each group ± SEM. *=p<0.01.

We blocked the entry of Ca^{2+} in the mitochondria using a specific inhibitor, the ruthenium red (RR), which inhibits the mitochondrial calcium uniporter (MCU) (De Stefani et al. 2011; Drago et al. 2011). We found that the inhibition of the mitochondrial Ca^{2+} by RR caused a substantial inhibition of ROS production suggesting that the entry of Ca^{2+} in the mitochondrial compartment was at least partially responsible for the redox imbalance in trisomic cell samples (**Figure 9A and 9B**). Moreover, treatment with RR resulted in enhancement of the respiratory activity in DS-HFF to the level of N-HFF (**Figure 10**).

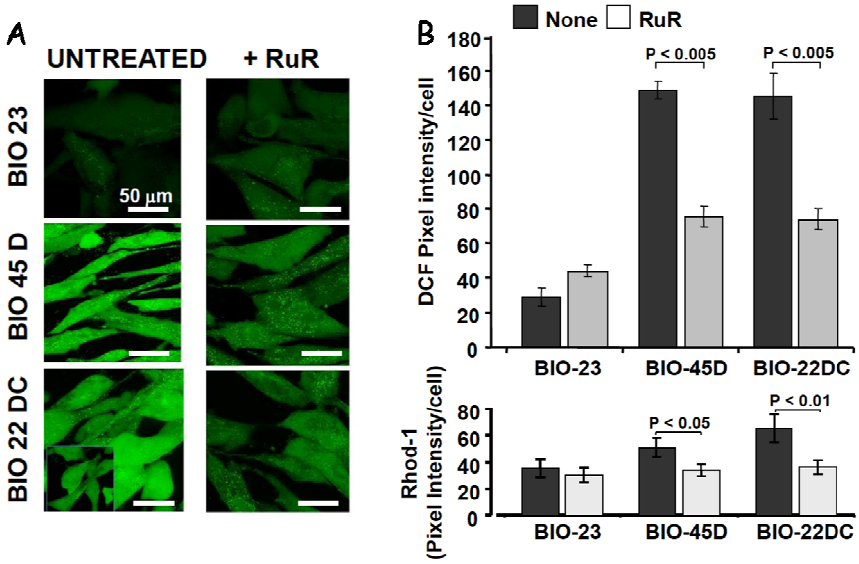

Figure 9. Effect of ruthenium red on ROS production in DS-HFF. Cultured fetus-derived fibroblasts representative of euploid (BIO23) and DS noncardiophatic (BIO45) or cardiopathic (BIO22) samples were treated with RR and then assessed by confocal microscopy for ROS production and $mtCa^{2+}$ by DCF and Rhod-1, respectively. (A) DCF-related fluorescence imaging of untreated and RR-treated fibroblasts (representative of 3 different experiments). (B) Statistical analysis of the DCF-related (upper histogram) and Rhod-1-related (lower histogram) fluorescence intensity per cell. In the graph is represented the average value ±SEM of about one hundred cells for each sample from three different experiments.

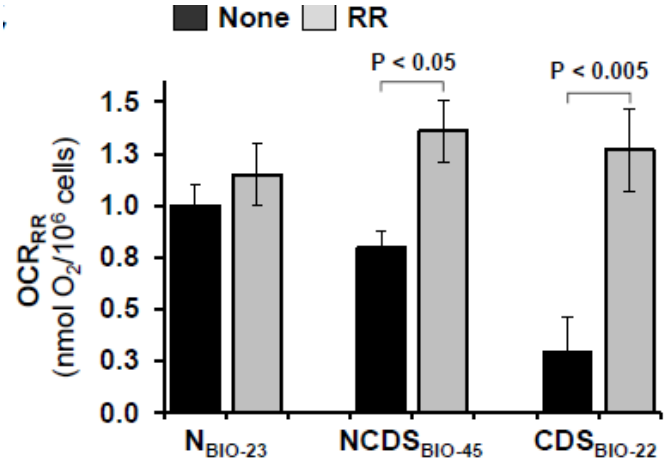

Figure 10. Effect of RR on the respiratory activity of DS-HFF. The OCR was measured in NCDS- and CDS-HFF (BIO45 and BIO22 respectively) with and without RR compared to N-HFF (BIO23). The bars are means ±SEM of the average determinations for each sample (untreated and RR-treated) carried out in triplicate.

A normal mitochondrial morphology is necessary for mitochondrial function as the mitochondrial cristae represent the subcellular localization of the oxidative phosphorylation coupled to the respiratory chain. Electron microscopy (EM) of trisomic fibroblasts revealed an abnormal morphology in a significant number of mitochondria showing an increased size, irregular shape, evident breaks, in particular in the inner membrane. In addition, the mitochondria show alterations in the pattern of cristae: broadened and arranged concentrically or oriented parallel to the long axis of the organelle (longitudinal cristae) (**Figure 11A**). Broken mitochondria and mitochondria with concentric and longitudinal cristae were significantly more abundant in trisomic samples than in the euploid ones with a $p<0.05$ (**Figure 11B**). Stereological analysis demonstrated that the mitochondrial volume density was similar in euploid and trisomic samples (**Figure 11C**) while the cristae volume density was significantly reduced in DS-HFF samples with a $p<0.05$ (**Figure 11D**).

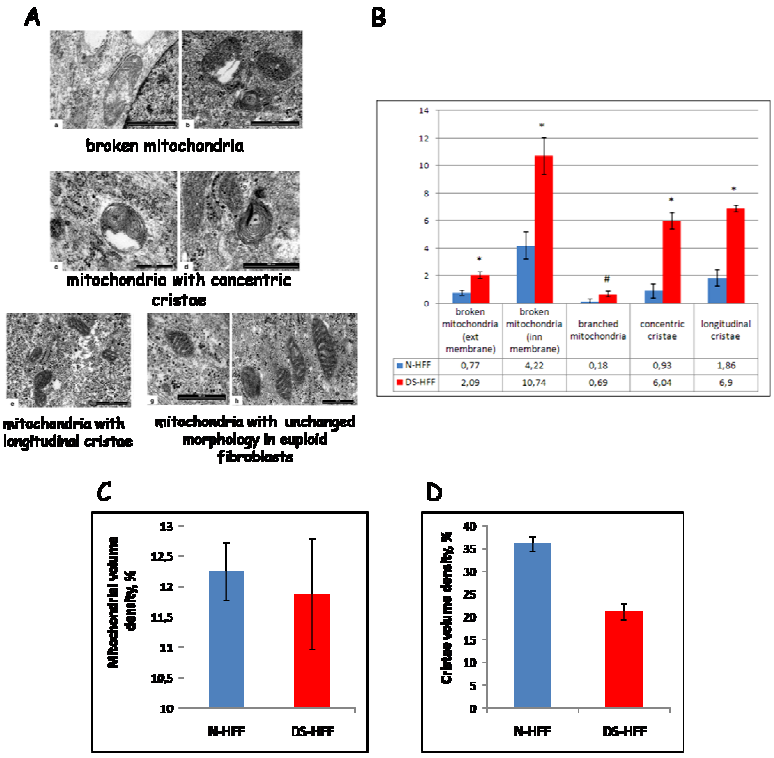

Figure 11. Mitochondria of DS fibroblasts show morphological abnormalities. (A) Electron micrographs of mitochondria in DS-HFF (a-f) and in N-HFF (g, h) Scale bars: 500 nm. (B) The percentage of anomalous mitochondria is significantly higher in trisomic samples (DS-HFF). (C) The mitochondrial volume density is not significantly different between trisomic and euploid fibroblasts. (D) The mitochondrial cristae volume density is almost 50% lower in DS-HFF than in the euploid samples. In all the graphs mean values ± SEM are shown. *=p<.05 #=not significant

The assessment of mtDNA copy number is usually proportional to mitochondria cellular content. In DS-HFF, mtDNA copy number, measured by RT-PCR against nuclear DNA (nDNA) copy number, was reduced by about 40%, if compared to N-HFF (**Figure 12**).

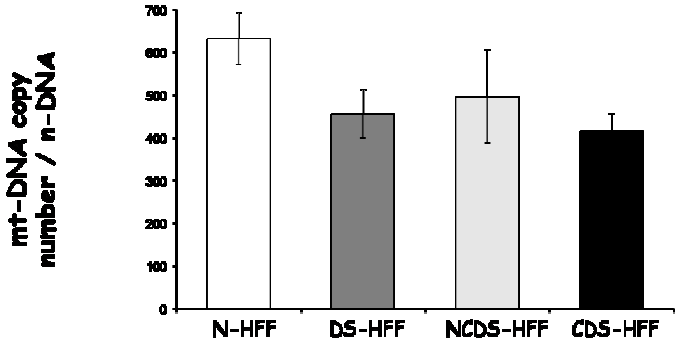

Figure 12. mtDNA copy number determination: mtDNA copy number of single sample and as mean are shown. In DS-HFF (dark gray bar) are reduced, both in NCDS-HFF (light gray bar) and in CDS-HFF (black bar), compared to N-HFF (white bar).

Which Hsa21 gene or transcript might be responsible for mitochondrial dysfunction in DS?

This study focused on the role of chromosome 21 in mitochondrial dynsfuction. According to our working hypothesis in the introduction (**Figure 9**) and based on literature and bioinformatics investigations, we have chosen for our studies the Hsa21 gene, RIP140/NRIP1 (Receptor Interacting Protein 1/Nuclear Receptor Interacting Protein 1), and the Hsa21 miRNA let-7c. We were interested on RIP140 because this corepressor possibly regulates the expression of some mitochondrial genes and functions, and on the microRNA let-7c which may contribute to mitochondrial dysfunction through the downregulation of ANT1 (Adenine Nucleotide Translocator 1) gene expression.

Meta-analysis of public expression data strongly suggests that RIP140 affects mitochondrial function

In order to investigate which overexpressed Hsa21 gene might dysregulate mitochondrial gene expression, we performed a meta-analysis of gene expression data from Gene Expression Omnibus repository (http://www.ncbi.nlm.nih.gov/geo), followed by Gene Ontology functional class scoring (http://bioinfo.vanderbilt.edu/webgestalt/) of all the lists of significantly dysregulated genes in DS subjects or models, putting attention to mitochondrial related categories and pathways. We first demonstrated that an enrichment of NEMG was observed in the lists of downregulated genes in microarray data of brain and astrocytes from DS fetuses (Mao et al. 2005, GSE 1397 series). An interesting result cames from the analysis of the GSE 19836

series (De Cegli et al. 2010) derived from a mouse embryonic stem cell bank in which 32 orthologs of human chromosome 21 genes were individually overexpressed in an inducible manner. Each clone was transcriptionally profiled in inducing versus non-inducing conditions by Affymetrix Gene Chip Mouse 430_2 (RNAs were from 3 induced mouse ESCs and 3 not induced controls, for each Hsa21 gene). The overexpression of a corepressor gene mapping to Hsa21, RIP140, in mouse ESCs model causes NEMG downregulation as main consequence, being the mitochondria one of the most affected Cell Component GO category, with $p<0.005$ (**Figure 13**). The analysis of these 2 sets of data together with our previous findings in TS21 hearts demonstrated that downregulation of NEMG is a costant finding in TS21 fetal tissues and that the Hsa21 gene RIP140 is involved in this effect.

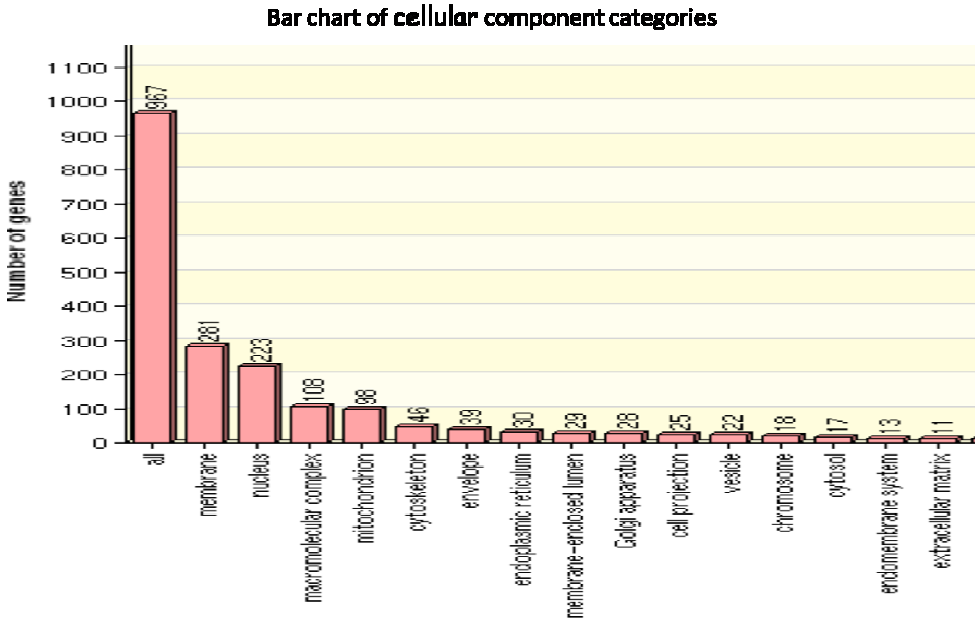

Figure 13. Cellular component categories influenced by RIP140 upregulation in mES (De Cegli et al. 2010). Bar chart showing that mitochondrion category (the fourth bar) is one of the most influenced by RIP140 upregulation(enrichment = 98 observed genes instead of 66 expected genes with $p< 0.005$).

The Hsa21 gene RIP140 is a major regulator of PGC-1α

As the expression and function of PGC-1α, a master regulator of mitochondrial biogenesis and function, is regulated by RIP140 (**Figure 7** in Introduction), we analyzed this 2 genes in DS-HFF by qRT-PCR demonstrating that PGC-1α is significantly downregulated, when RIP140 is significantly upregulated in DS-HFF compared to N-HFF (**Figure 14**). PGC-1α was downregulated also at the protein level (**Figure 15A and 15B**).

To investigate the direct effects of RIP140 modifications on PGC-1α expression we silenced RIP140 with a specific SMART pool of siRNA in 4 lines of DS-HFF. qRT-PCR, performed 72h after transfection, demonstrated a significant inverse correlation between RIP140 silencing and PGC-1α upregulation in a siRNA dosage-dependent way (**Figure 16**).

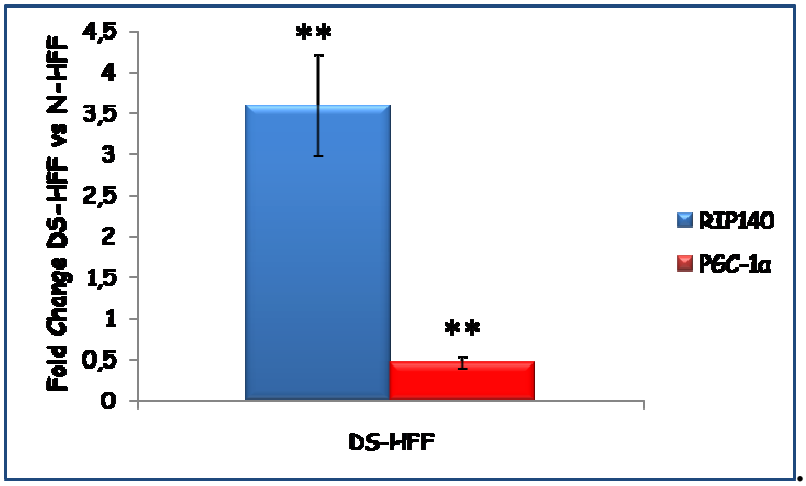

Figure 14. Gene expression of RIP140 and PGC-1α in DS-HFF versus N-HFF. Values represent the average determination for 5 DS-HFF samples carried out in triplicate. ** = p<0.02. P-values express significance for DS-HFF vs N-HFF comparisons

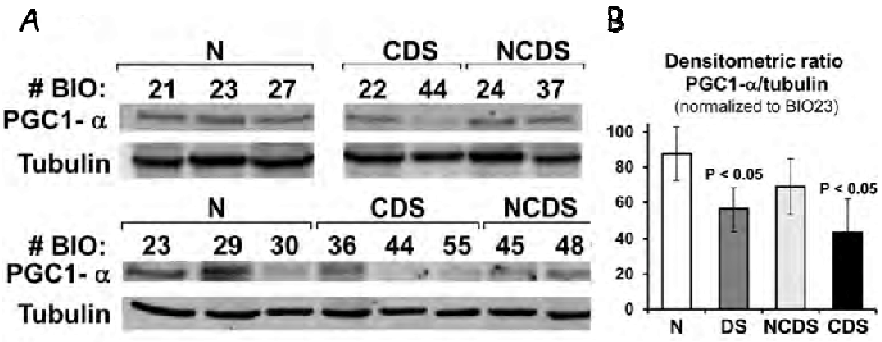

Figure 15. PGC-1α protein expression in DS fibroblasts. (A) Western Blot analysis of PGC-1α protein in NCDS-HFF and CDS-HFF vs euploid samples. (B) Densitometric analysis of PGC-1α protein expression compared to tubulin expression and normalized to BIO23 (N-HFF).

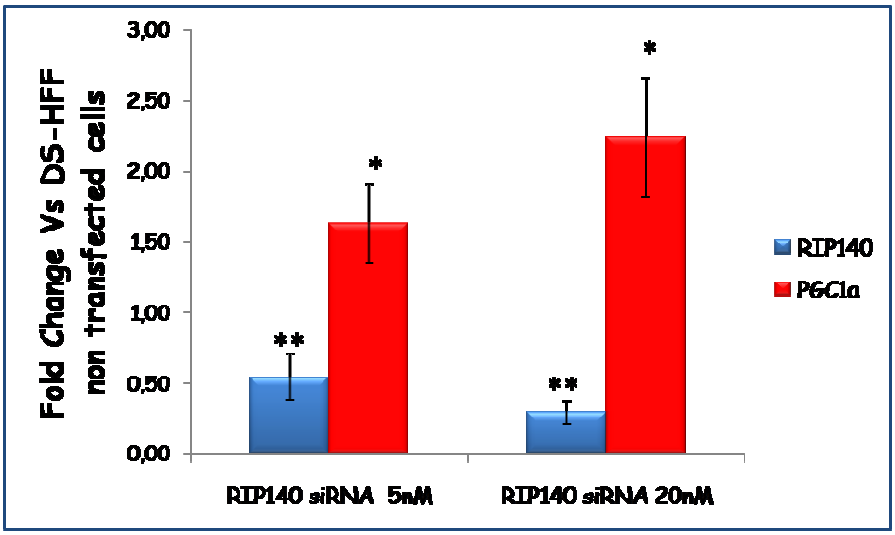

Figure 16. RIP140 and PGC-1α expression in RIP140-silenced DS-HFF. RIP140 and PGC-1α expression level in non-transfected (NT) and in DS-HFF transfected with 5nM and 20nM of RIP140 siRNA dosage. Values represent the average determination for 4 RIP140-silenced trisomic samples carried out in triplicate ± SEM. * = $p<0.05$, ** = $p<0.02$.

RIP140 silencing affects mitochondrial function in DS-HFF

To investigate whether RIP140 affects mitochondrial dysfunction in DS through the downregulation of PGC-1α and other NEMG, we evaluated functional parameters in DS-HFF after RIP140 silencing compared to non silenced cells. We evaluated redox state of DS-HFF silenced cells measuring ROS production by confocal microscopy using a DCF probe as previously described. The intensity of DCF was measured in 4 silenced DS-HFF compared to non transfected DS-HFF samples and N-HFF samples. The fluorescent signal of DCF was up to 50% decreased in silenced DS-HFF in a siRNA-dosage dependent way (**Figure 17A**). Pixel intensity was measured in about 50 cells after RIP140 silencing (**Figure 17B**).

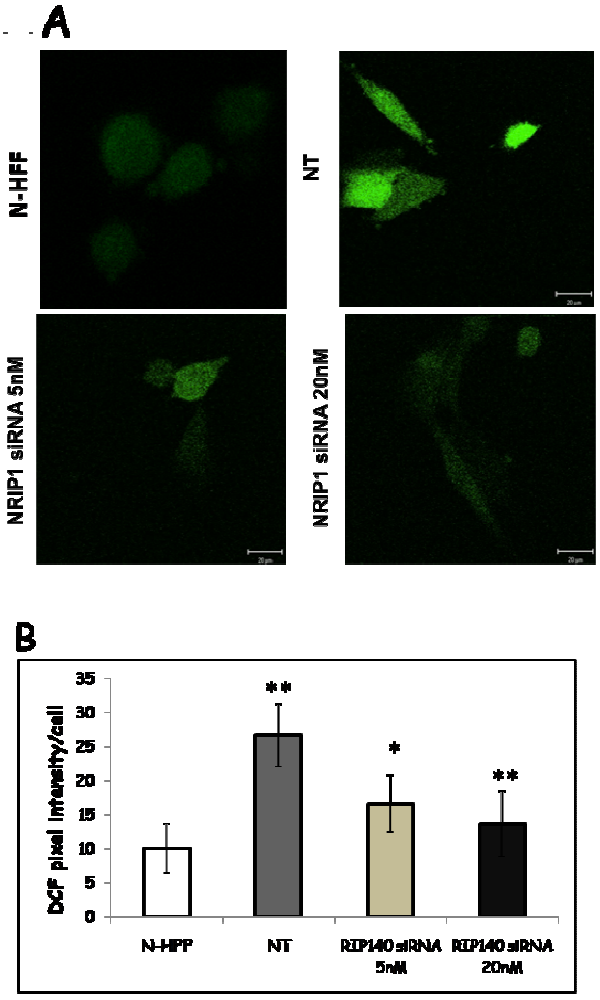

Figure 17. ROS analysis in RIP140-silenced DS-HFF. (A) Representative live cell imaging and statistical analysis of the DCF fluorescence intensity of N-HFF cells, non-transfected trisomic cells (NT) and trisomic cells with 5nM and 20nM RIP140 siRNA dosage (green signal). (B) Measurement of DCF pixel intensity per cell. Values represent the average determination for 4 RIP140-silenced trisomic samples (at least 50 randomly selected different cells per sample/experimental condition). * = $p<10^{-4}$, ** = $p<10^{-6}$.

Mitochondrial activity was also evaluated by confocal microscopy using a MitoTracker dye. MitoTracker Red, a selective mitochondrial probe was chosen. Its accumulation is dependent upon membrane potential. Our aim was to investigate whether this parameter is correlated to RIP140 expression. Mitotracker fluorescent intensity was increased in DS-HFF silenced cells in a siRNA concentration dependent way (**Figure 18A**). This result was confirmed by the pixel intensity analysis in about 50 cells (**Figure 18B**).

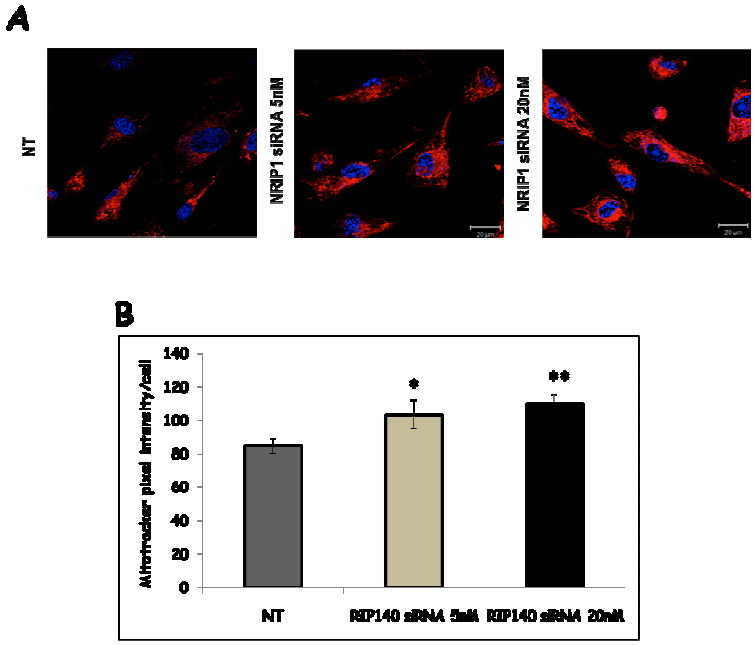

Figure 18. Mitochondrial activity in RIP140-silenced DS-HFF. (A) Representative live cell imaging and statistical analysis of the Mitotracker fluorescence intensity of nontransfected trisomic cells (NT) and of trisomic cells with 5nM and 20nM RIP1140 siRNA dosage (red signal). (B) Measurement of Mitotracker pixel intensity per cell. Values represent the average determination for 4 RIP140-silenced trisomic samples (at least 50 randomly selected different cells per sample/experimental condition). * = $p<0.005$, ** = $p<0.05$.

Hsa21 MiRNA let-7c may negatively regulate mitochondrial energy mobilization thorough the downregulation of ANT1

Non coding Hsa21 transcripts were also evaluated. The expression of 5 Hsa21 miRNAs, miR-99a, miR-125b, let-7c, miR-155 and miR-802 (**Figure 19**) were evaluated by RT-PCR in fetal hearts demonstrating that miR-99a, miR-125b, miR-let-7c and miR-155 were expressed in 18-22 weeks fetal hearts and miR-802 was not expressed.

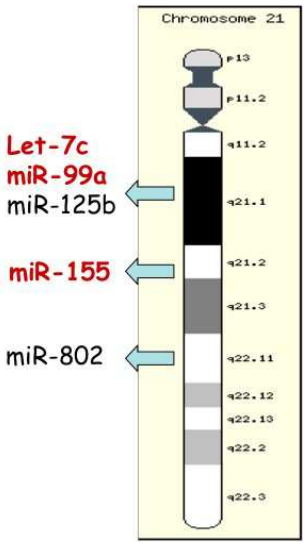

Figure 19. Analyzed Hsa21 miRNAs. Localization on chromosome 21 of analyzed miRNAs in DS fetal hearts. Overexpressed miRNAs are red, miR-125b (normoregulated miRNA) and miR-802 (not expressed miRNA) are black.

Comparing DS heart tissue to controls, we found that miR-let-7c, miR-99a and miR-155 were overexpressed in trisomic hearts, whereas miR-125b was expressed with high variability (**Figure 20**).

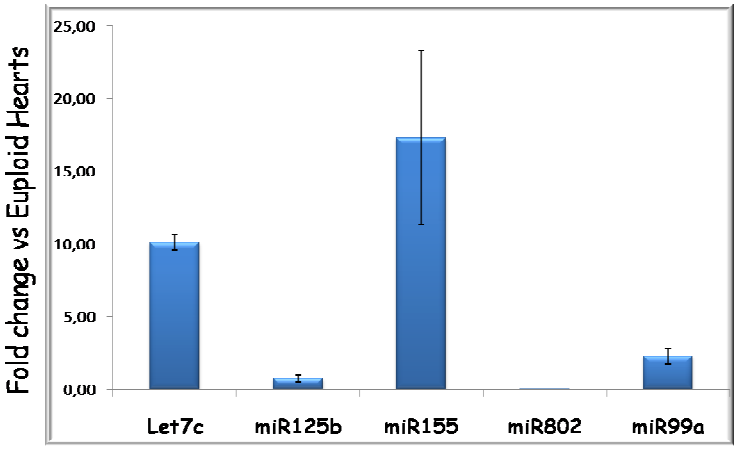

Figure 20. Hsa21 microRNAs expression. Hsa21 miRNas expression in 6 DS fetal hearts. from 6 DS individuals, 3 with CHD (CHD samples) and 3 without CHD (DH samples), and 3 non-trisomic controls (NH samples). Values represent the average determination in 6 DS fetal hearts compared to 3 euploid hearts.

As miRNAs could affect protein expression by either interfering with RNA translation or promoting mRNA degradation, we evaluated the mRNA expression of target genes of overexpressed miRNAs by using the data set of our previous study (Conti et al. 2007). We have analyzed target prediction by 6

different softwares (TargetScan, Pita, Miranda, Microcosm, microRNA.org and Pictar) filtering target genes according to microarray results. Seventeen targets of miR-99a, 12 of miR-155 and 15 of let-7c were expressed in fetal heart and downregulated in trisomic samples. Based on the notion that overexpression of Hsa21 miRNAs can result in downregulation of specific target genes possibly involved in DS phenotype, we considered only the list of genes downregulated in DS fetal hearts. We focused the analysis on the miRNA let-7c. We found 4583 genes possibly targeted by this miRNA. Forty-four genes were downregulated in trisomic hearts with a Fold Change>1,3 and p<0,05. We were interested to let-7c because 9 NEMG were predicted targets of this miRNA and downregulated in trisomic samples (**Table 5**). Notably, one of this genes was ANT1.

Table 5. Let-7c target genes downregulated in DS fetal hearts.

Probe Set	Fold Change	p-value	Gene Name	Database
205295_at	0,668	0,000318	CKMT2	Microcosm
203858_s_at	0,765	0,0101	COX10	Pita
215210_s_at	0,58	0,0138	E2k	Pictar
201226_at	0,651	0,016	NDUFB8	TargetScan
211715_s_at	0,554	0,0201	BDH1	Pita
202825_at	**0,645**	**0,0263**	**ANT1**	**Pictar;TargetScan;Pita**
203781_at	0,75	0,0318	MRPL33	Microcosm
211150_s_at	0,596	0,0377	DLAT	Pita
217961_at	0,754	0,0423	FLJ20551	Pita

Nine let-7c mitochondrial target genes downregulated in DS fetal hearts including ANT1 (in red).

ANT1 is predicted by 3 out of 6 databases that we used (Pictar, TargetScan and Pita). Since ANT1 has a central role in OXPHOS, our hypothesis was that the ANT1 downregulation could be an effect of the specific interaction between let-7c and this gene at the seed sequence. To validate this hypothesis we performed a transfection experiment of a let-7c mimic miRNA in normal fibroblasts in which ANT1 is expressed. Forty-eight hours after transfection at 25nM dosage, ANT1 was about 1.7 fold downregulated (**Figure 21**)**.** DICER expression was evaluated as a control, since DICER is a let-7c validated target (Tokumaru et al. 2008). DICER was indeed downregulated in cells transfected with the let-7c mimic. This result is the first confirmation of our hypothesis, but other experiments will be necessary to definitely validate that ANT1 is a let-7c target. We plan to perform the reverse experiment using miRNA inhibitor and a Luciferase assay.

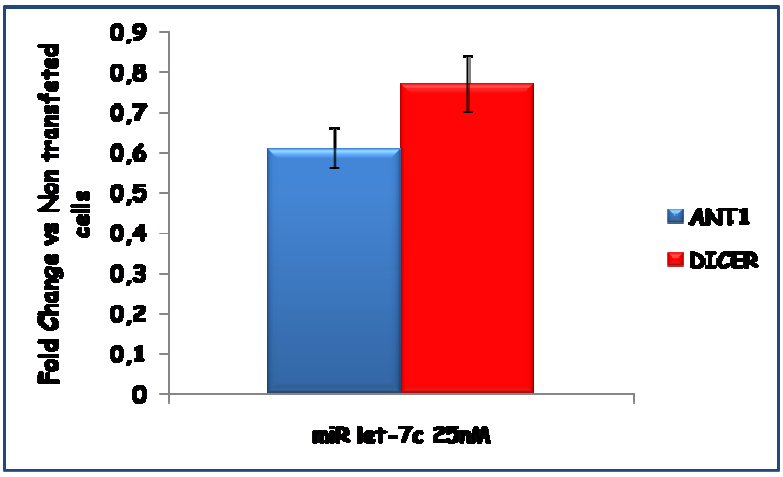

Figure 24. ANT1 and DICER expression in silenced fibroblasts. ANT1 (blue bar) and DICER (red bar) expression after miRNA let-7c upregulation by miRNA mimic at 25nM. Values represent the average determination for 5 transfected samples versus non transfected samples.

DISCUSSION

Possible causes of mitochondrial dysfunction in DS-HFF

In this study we investigated the molecular mechanisms leading to mitochondrial alterations in fibroblasts derived from fetuses with trisomy of Hsa21. These fibroblasts were from the same fetuses in which Conti et al. (2007) determined heart gene expression profile. Fibroblasts from trisomic fetuses were named DS-HFF and were divided in 2 groups according to presence or absence of cardiopathy, CDS-HFF and NCDS-HFF, respectively.
First of all, NEMG expression was evaluated in DS-HFF, focusing on genes involved in mitochondrial biogenesis (NRF-1 and PGC-1α), mitochondrial morphology (IMMT), and genes of the respiratory complexes (NDUFS2, NDUFS6, NDUFA8, NDUFA1 and NDUFB8). These genes were downregulated in agreement with the results obtained by Conti et al. (2007) in DS fetal hearts and by Mao et al. (2005) in DS fetal brain.
To test the hypothesis that the decreased NEMG expression might determine mitochondrial dysfunction, a survey of mitochondrial activity was performed in DS-HFF vs. control N-HFF. First of all, oxygen consumption rate was measured and it was demonstrated that the oxygen consumption was significantly reduced in basal, uncoupled and ATP-synthase-dependent respiratory conditions in DS-HFF. Noticeably, the decrease was more pronounced in DS fibroblasts from cardiopathic fetuses. The activity of complex I, complex III and complex IV was thereafter evaluated. Only the activity of complex I was reduced by about 50% in DS-HFF, both in NCDS-HFF and CDS-HFF if compared to N-HFF. A complex I deficiency is characteristic of other mitochondrial diseases. It was also found in mouse models with trisomy of chromosome 16 as well as in models of Parkinson's disease, suggesting that different neurodegenerative diseases may be associated to the same mitochondrial dysfunction (Bambrick et al. 2008).
It is known that the activity of the complexes produces in the mitochondria the electric potential, $\Delta\psi$. We found that $\Delta\psi$ was not particularly affected by trisomy 21, but a more detailed analysis of the fluorescent signal revealed an alteration of the mitochondrial network. This alteration might contribute to mitochondrial dysfunction because the normal mitochondrial function requires the conservation of fusion and fission events.
Mitochondria have a key role in oxygen metabolism and are the major source of ROS formation. Complex I, in particular, controls ROS production. In order to investigate the possible unbalance of redox homeostasis as a consequence of the alteration of respiratory complexes chain in DS-HFF, ROS production was evaluated. DCF signal revealed the increase of ROS in DS-HFF which localized to an intracellular compartment resembling the mitochondrial network. Schuchmann (2000) and Heinemann (2000) also demonstrated that a Ts16 mouse model had an increased $O^{2-}\bullet$ basal generation, possibly attributed

to a complex I deficiency. The brightness of DCF was much increased in CDS-HFF and this result is in accordance with the oxygen consumption rate results, that showed a more pronounced reduction of oxygen consumption in CDS-HFF. The mechanism underling this phenomenon will be the subject for future investigations.

As ROS production is also correlated to the overload of Ca^{2+} into mitochondria (Adam-Vizi and Starkov 2010; Feissner et al. 2009) we evaluated the intramitochondrial Ca^{2+} level in DS-HFF, using two different probes, Rhod-1 and Aequorin. Both methods revealed an increase of Ca^{2+} level in DS-HFF compared to N-HFF with a linear positive correlation between Ca^{2+} and ROS generation in trisomic samples. Notably, blockage of the major mitochondrial Ca^{2+} transporting system resulted in substantial depression of ROS overproduction in DS-HFF, whereas it was ineffective in N-HFF. Moreover, ruthenium red treatment resulted in full recovery of the respiratory activity in DS-HFF. The aequorin method specifically confirmed the intramitochondrial localization of the increased Ca^{2+} level. All together, these observations would argue for a linkage between chronic intramitochondrial Ca^{2+} levels, inhibition of complex I and mitochondrial ROS production. Even though the causes of the $mtCa^{2+}$ homeostasis deregulation in trisomic cells have not yet been completely identified, literature suggests that Ca^{2+} mobilization/signalling is correlated to PPARγ (Bush et al. 2007). This correlation might link $mtCa^{2+}$ to PGC-1α, which is an important coactivator of the PPARs transcription factor family including PPARγ.

Also the 40% decrease of mtDNA copy number that we demonstrated in DS-HFF might be correlated to the downregulation of PGC-1α, a master regulator of mitochondrial biogenesis and function (Scarpulla 2011; Scarpulla 1012). Druzhyna et al. (2008) demonstrated a similar mtDNA copy number decrease in fibroblasts from DS patients due to a defective repair of oxidative damage. PGC1α coactivates numerous transcription factors, including nuclear receptors such as PPARγ and PPARα and estrogen receptor α, exerting the final effect of promoting mitochondrial biogenesis and regulating mitochondrial respiratory capacity (Leone et al. 2005; Scarpulla 2011; Scarpulla 2012). A key role of PGC-1α in the regulation of mitochondrial biogenesis and function is demonstrated by PGC-1α knockout mice, that show decreased mitochondrial number and respiratory capacity in skeletal muscle (Leone et al. 2005).

Lastly, we must also consider that the redox imbalance demonstrated in DS cells might also be furtherly affected by the overexpression of the HSA21 gene copper-zinc superoxide dismutase (SOD1), that we found overexpressed in trisomic fibroblasts. Neuronal death in DS has been associated to the triplicated expression of SOD1, which was suggested to be involved in the oxidative damage of neurons (Lee et al. 2001).

As already mentioned, normal mitochondrial morphology is necessary for mitochondrial function. Bersu et al. (1998) and Shukkur et al. (2006) described a number of alterations of the mitochondrial structure, like an unusual branched morphology of mitochondria, in cultured cerebellar neurons from Ts16 mice,

and an increased number of abnormal mitochondria, especially with broken cristae, in brain tissues of Ts1Cje mice.
In this study alterations of mitochondrial morphology were demonstrated. In particular abnormal mitochondrial cristae were increased in DS-HFF that showed broken mitochondria, mitochondria with concentric and longitudinal cristae and decreased cristae volume density. Our hypothesis is that these abnormalities might be correlated to the IMMT downregulation that we found in DS cells and tissues. IMMT downregulation was demonstrated to cause a drastic change in the organization of the inner membrane, that formed concentric layers instead of being organized into tubular cristae (John et al. 2005), leading to cristae patterns similar to those observed in DS samples.
The conclusion of the published part of my PhD project (Piccoli et al. 2013) was that NEMG downregulation is demonstrated in fibroblasts from DS fetuses and that it is associated to global mitochondrial dysfunction and oxidative distress, more pronounced in cells derived from DS fetuses with CHD. PGC-1α might be a possible candidate gene responsible for the altered mitochondrial phenotype. PGC-1α transcription and activity are positively regulated by Ca^{2+} signaling and negatively regulated by the corepressor RIP140 (Scarpulla 2011). Based on these findings we formulated the hypothesis that this Hsa21 gene plays an important role in mitochondrial dysfunction in DS. This hypothesis was demonstrated in the second part of my project.

Hsa21 gene RIP140 affects mitochondrial dysfunctionin DS

A high number of NEMG was found to be downregulated in the heart (Conti ate al. 2007), in the brain (Mao et al. 2005) as well as in fibroblasts (Piccoli et al. 2013) from human fetuses. This poses the question of whether several NEMG might be under the control of the same regulatory gene and how this gene is affected by trisomy of Hsa21. We focused on RIP140, a gene mapping to Hsa21, that codes for a corepressor protein. Literature on RIP140 function and modulation in mouse models strongly supports this hypothesis. Indeed, RIP140 gene expression deeply affects the oxidative metabolism and mitochondrial biogenesis (Powelka et al. 2006; Seth et al. 2007; Fritah et al. 2010; Chen et al. 2012). Genes upregulated by RIP140 silencing are downregulated by its overexpression (Seth et al. 2007). We formulated the hypothesis that the overexpression of RIP140 might contribute to the dowregulation of NEMG and, therefore, to mitochondrial dysfunction. RIP140 is overexpressed in DS hearts and fibroblasts and the upregulation of RIP140 protein was also demonstrated in DS hippocampus (Gardiner 2006) together with the upregulation of SUMO3, another gene mapping to Hsa21, which modulates RIP140 activity (Rytinki and Palvimo 2009). The simultaneous upregulation of both Hsa21 genes, RIP140 and SUMO3, might exert a synergistic effect on mitochondrial dysfunction.
The PGC-1α protein, that plays a central role in regulating mitochondrial biogenesis and respiratory function through the interaction with transcriptional

partners, like NRF1, ERRα, PPARs and YY1, is negatively controlled by the co-repressor RIP140 (Scarpulla 2011). PGC-1α null mice (Leone et al. 2005; Mitra et al. 2012), as well as knock-in RIP140 mice (Seth et al. 2007), show reduced expression of mitochondrial genes in multiple tissues. Also the transcription factors NRF-1 and ERRα and their targets are repressed by RIP140 and induced by PGC-1α in a dose dependent manner, in neonatal rat cardiomyocytes (Chen et al. 2012).

In the present study we observed that NRF1 and PGC-1α are significantly downregulated in DS-HFF while RIP140 is upregulated supporting the hypothesis that RIP140 controls the expression of PGC-1α in DS-HFF. The result of this analysis is in agreement with Powelka et al. (2006). By comparing the list of NEMG downregulated in DS fetal hearts (Conti et al. 2007) to RIP140 target genes (Seth et al. 2007) we found an overlapping higher than 60%, being 40 genes in common between the 2 lists (**Figure 1**). Almost all these genes belong to the respiratory chain complexes **(Figure 2**).

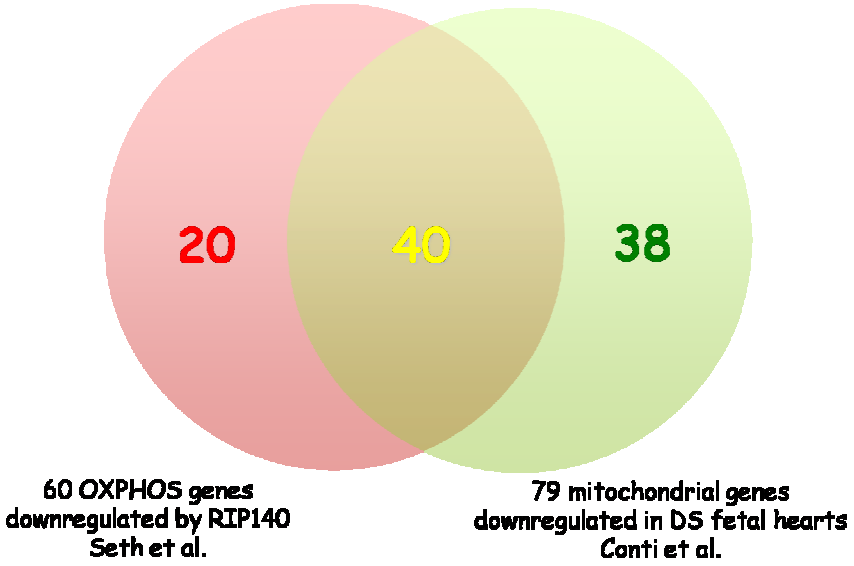

Figure 1. Venn Diagram of the lists of NEMG affected by RIP140 upregulation (Seth et al., 2007) and of NEMG dowregulated in DS fetal heart tissue (Conti et al., 2007) demonstrates an overlap higher than 60%.

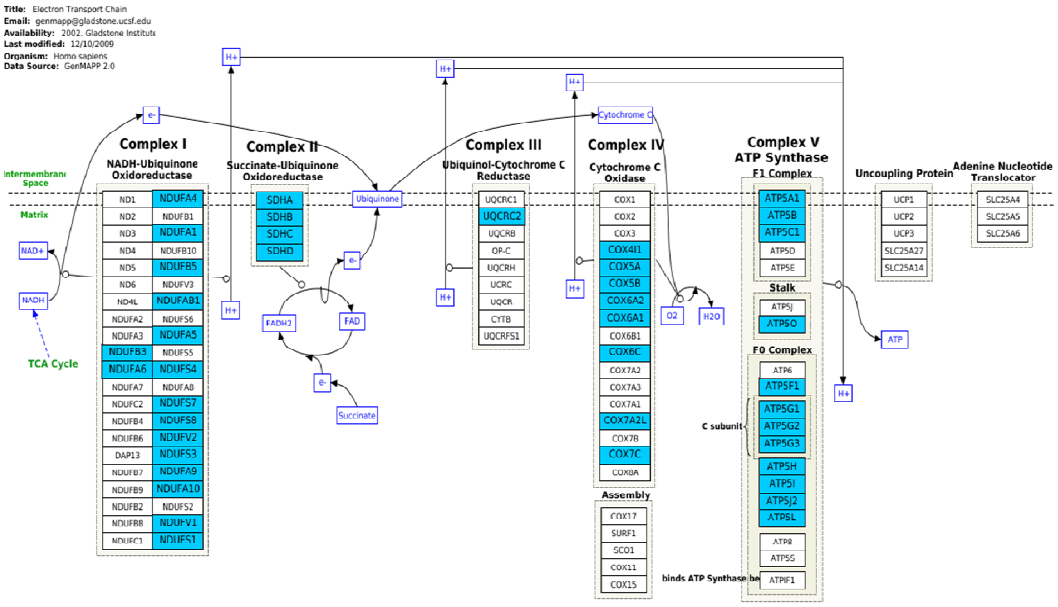

Figure 2. Most of the overlapping genes from the Venn Diagram shown in Figure 14 are included in all the respiratory chain complexes (blue boxes).

To validate the hypotheses we formulated about RIP140 role, we transiently silenced the gene in trisomic fibroblasts. Silencing experiments demonstrated an inverse correlation between RIP140 and PGC-1α also in trisomic cells. Furthermore, ROS production was decreased and mitochondrial activity was increased in silenced DS-HFF, demonstrating that RIP140 inhibition is able not only to increase PGC-1α, but also to promote at least a partial rescue of mitochondrial function

All these data reinforce the hypothesis that RIP140 plays a key role in DS mitochondrial dysfunction.

Hsa21 MicroRNA let-7c may contribute to mitochondrial dysfunction in DS

The adenine nucleotide translocator-1 plays an important role in the regulation of the intracellular energetic balance by facilitating the exchange of extramitochondrial ADP and intramitochondrial ATP. There are 4 isoforms of this gene, but only the isoform 1, mainly expressed in the heart, is a predicted target of the Hsa21 miRNA let-7c, as resulted by interrogating 6 miRNA prediction databases. ANT1 is downregulated in DS fetal heart and fibroblasts, in which Let-7c is upregulated.

qRT-PCR after let-7c upregulation showed an inverse relationship as ANT1 was downregulated. Based on this finding the reverse experiment using the let-7c miRNA inhibitor is ongoing. Furthermore, a luciferase assay experiment

will be performed to validate the specific interaction between ANT1 3' UTR and miRNA let-7c using. HeLa cells will be co-transfected with let-7c mimic and a vector containing the ANT1 3' UTR downstream of the Luc gene.
In conclusion we have demonstrated that RIP140 silencing is responsible for the upregulation of PGC-1α and for the partial rescue of mitochondrial function in DS-HFF, in particular for the reduction of ROS production and the increase of mitochondrial activity. We have also demonstrated that let-7c upregulation causes the downregulation of ANT1 so it is possibly responsible for the alteration of mitochondrial energy production in DS.
Our results suggest that the upregulation of RIP140 together with the upregulation of let-7c, DYRK1A and RCAN1, according to our working hypothesis (**Figure 9** in Introduction), might represent the molecular alterations leading to mitochondrial dysfunction in DS.

The results of this study might be translated in DS therapy

This study provides the basis for clinical trials aimed to restore mitochondrial function in DS subjects to counteract specific phenotypic features such as the neurodegeneration. So far, few therapeutic approaches have been undertaken in this direction mainly based on the use of antioxidants and nutraceutics with poor results. New therapies could be based either on inhibition of RIP140 by specific RNAi or on the use of drugs affecting genes involved in the same dysregulated pathways.
Gene therapy in DS is opening new scenarios using RNAi as a tool to silence specific genes in biological systems. A first approach might be to silence RIP140 in a Dp(16)1Yey/+, a mouse model of DS with 3 copies of RIP140, using a non viral systems, based on cationic lipids, polymers, dendrimers or different types of nanoparticles. These vectors have been demonstrated to be non immunogenic, easy to prepare and non expensive (Alvarez-Erviti et al. 2011). The siRNA of interest may be complexed to liposomes and to the rabies virus glycoprotein (RVG) (Kumar et al. 2007) that enables transvascular delivery of siRNAs into the brain across the blood brain barrier and binds specifically toacetylcholine receptors (AchRs) on neural cells. New improvements are continuously proposed for these techniques (Zabel 2013; Pulford et al. 2010; Tao et al. 2012).
The other possible therapeutical approach to counteract mitochondrial dysfunction in DS might be based on drugs such as PGC-1α activators and PPARγ agonists. These drugs are already routinely used in clinical practice for treatment of metabolic syndromes, Type 2 Diabetes, and neurodegenerative diseases such as Alzheimer disease. Pharmacological activators of PGC-1α, such as metformin, via AMPK induction, as well as resveratrol, via SIRT1 induction (Rodgers et al. 2005), have been tested in other disease mouse models (Dong et al. 2007; Lagouge et al. 2006; Jager et al. 2007). On the other hand thiazolidinediones, such as pioglitazone and rosiglitazone, selectively

stimulate PPARγ. In Alzheimer disease mouse models this drugs demonstrated to attenuate mitochondrial dysfunction, as well as bezafibrate, another PPARγ agonist (Bastin et al. 2008; Nicolakakis et al. 2008; Escribano et al. 2009; Johri et al. 2011; Sauerbeck et al. 2011; Yamaguchi et al., 2012).
We expect that therapeutic interventions based on these assumptions might improve the life quality and expectancy of DS subjects.

ACKNOWLEDGEMENTS

Foremost, I would like to express my sincere gratitude to my Professor Lucio Nitsch, thanks to him for his continuous support, his advices and suggestions that helped me in all the time of my research. I could not imagine having a better mentor for my PhD.

My sincere appreciation goes to Dr. Anna Conti for all I have learned from her and for her continuous help and support in all stages of this thesis. I would also like to thank her for being an open person to ideas, and for encouraging and helping me to shape my interest and ideas.

Special thanks go to Dr. Antonella Izzo, I would like to express my deep gratitude and respect to her. Her teachings and her attitude to research inspired me during my PhD work. I would not have been able to complete this journey without her moral and professional support.

I would like to thank also Dr. Ferdinando Bonfiglio for his special support and friendship.

Thanks to all people of my laboratory and to everyone that have contributed to my PhD project, in particular to Dr. Nazzareno Capitanio, Dr. Claudia Piccoli, Dr. Rosella Scrima, Dr. Olga Cela, Dr. Marina Prisco, Dr. Paolo Pinton, Dr. Mariastella Zannini, Dr. Tiziana de Cristofaro and Dr. Tina Di Palma.

I would also like to thank my family and Albert for the support they always provided me.

REFERENCES

Adam-Vizi V, Starkov AA. Calcium and mitochondrial reactive oxygen species generation: how to read the facts. J Alzheimers Dis. 2010;20 Suppl 2:S413-26.

Alvarez-Erviti L, Seow Y, Yin H, Betts C, Lakhal S, Wood MJ. Delivery of siRNA to the mouse brain by systemic injection of targeted exosomes. Nat Biotechnol 2011; 29:341-345.

Amano K, Sago H, Uchikawa C, Suzuki T, Kotliarova SE, Nukina N, Epstein CJ, Yamakawa K. Dosage-dependent over-expression of genes in the trisomic region of Ts1Cje mouse model for Down syndrome. Hum Mol Genet 2004, 13(13):1333-1340.

Arbuzova S, Hutchin T, Cuckle H. Mitochondrial dysfunction and Down's syndrome. Bioessays 2002, 24(8):681-684.

Arron JR, Winslow MM, Polleri A, Chang CP, Wu H, Gao X, Neilson JR, Chen L, Heit JJ, Kim SK, Yamasaki N, Miyakawa T, Francke U, Graef IA, Crabtree GR. NFAT dysregulation by increased dosage of DSCR1 and DYRK1A on chromosome 21. Nature 2006, 441(7093):595-600.

Bambrick LL, Fiskum G. Mitochondrial dysfunction in mouse trisomy 16 brain. Brain Res. 2008 Jan 10;1188:9-16.

Bastin J, Aubey F, Rötig A, Munnich A, Djouadi F. Activation of peroxisome proliferator-activated receptor pathway stimulates the mitochondrial respiratory chain and can correct deficiencies in patients' cells lacking its components. J Clin Endocrinol Metab. 2008 Apr;93(4):1433-41.

Bauer MK, Schubert A, Rocks O, Grimm S. Adenine nucleotide translocase-1, a component of the permeability transition pore, can dominantly induce apoptosis. J Cell Biol. 1999 Dec 27;147(7):1493-502.

Bersu ET, Ahmad FJ, Schwei MJ, Baas PW. Cytoplasmic abnormalities in cultured cerebellar neurons from the trisomy 16 mouse.Brain Res Dev Brain Res. 1998 Jul 1;109(1):115-20.

Busciglio J, Yankner BA. Apoptosis and increased generation of reactive oxygen species Down’s syndrome neurons in vitro. Nature 1995;378:776–779.

Busciglio J, Pelsman A, Wong C, Pigino G, Yuan M, Mori H, Yankner BA. Altered metabolism of the amyloid beta precursor protein is associated with mitochondrial dysfunction in Down's syndrome. Neuron 2002, 33(5):677-688.

Bush CR, Havens JM, Necela BM, Su W, Chen L, Yanagisawa M, Anastasiadis PZ, Guerra R, Luxon BA, Thompson EA. Functional genomic analysis reveals cross-talk between peroxisome proliferator-activated receptor gamma and calcium signaling in human colorectal cancer cells. J Biol Chem. 2007 Aug 10;282(32):23387-401.

Bushdid PB, Osinska H, Waclaw RR, Molkentin JD, Yutzey KE. NFATc3 and NFATc4 are required for cardiac development and mitochondrial function. Circ Res 2003, 92(12):1305-1313.

Camello-Almaraz MC, Gomez-Pinilla PJ, Pozo MJ and Camello PJ. Mitochondrial reactive oxygen species and Ca^{2+} signaling. Am J Physiol Cell Physiol 2006, 291: C1082–C1088.

Caviedes P, Caviedes R and Rapoport SI. Altered calcium currents in cultured sensory neurons of normal and trisomy 16 mouse fetuses, an animal model for human trisomy 21 (Down syndrome). Biol Res. 2006;39(3):471-81.

Cela O, Piccoli C, Scrima R, Quarato G, Marolla A, Cinnella G, Dambrosio M, Capitanio N. Bupivacaine uncouples the mitochondrial oxidative phosphorylation, inhibits respiratory chain complexes I and III and enhances ROS production: Results of a study on cell cultures. Mitochondrion 2010 Aug;10(5):487-96.

Chen Q, Vazquez EJ, Moghaddas S, Hoppel CL, and Lesnefsky EJ. Production of reactive oxygen species by mitochondria: central role of complex III. J Biol Chem 2003, 278: 36027–36031.

Chen XJ. Induction of an unregulated channel by mutations in adenine nucleotide translocase suggests an explanation for human ophthalmoplegia. Hum Mol Genet. 2002 Aug 1;11(16):1835-43.

Chen Y, Wang Y, Chen J, Chen X, Cao W, Chen S, Xu S, Huang H. and Liu P. Roles of transcriptional corepressor RIP140 and coactivator PGC-1alpha in energy state of chronically infarcted rat hearts and mitochondrial function of cardiomyocytes. Mol Cell Endocrinol. 2012 Oct 15;362(1-2):11-8.

Conti A, Fabbrini F, D'Agostino P, Negri R, Greco D, Genesio R, D'Armiento M, Olla C, Paladini D, Zannini M, Nitsch L. Altered expression of mitochondrial and extracellular matrix genes in the heart of human fetuses with chromosome 21 trisomy. BMC Genomics. 2007;8:268.

Cork LC. Neuropathology of Down Syndrome and Alzheimer Disease. Am J Med Genet Suppl. 1990;7:282.

Dauphinot L, Lyle R, Rivals I, Dang MT, Moldrich RX, Golfier G, Ettwiller L, Toyama K, Rossier J, Personnaz L, Antonarakis SE, Epstein CJ, Sinet PM, Potier MC. The cerebellar transcriptome during postnatal development of the Ts1Cje mouse, a segmental trisomy model for Down syndrome. Hum Mol Genet. 2005;14(3):373-84.

De Cegli R, Romito A, Iacobacci S, Mao L, Lauria M, Fedele AO, Klose J, Borel C, Descombes P, Antonarakis SE, di Bernardo D, Banfi S, Ballabio A, Cobellis G. A mouse embryonic stem cell bank for inducible overexpression of human chromosome 21 genes. Genome Biol. 2010;11(6):R64.

De Giorgi F, Lartigue L, Ichas F. Electrical coupling and plasticity of the mitochondrial network. Cell Calcium. 2000 Nov-Dec;28(5-6):365-70.

De Stefani D, Raffaello A, Teardo E, Szabo I, Rizzuto R. A forty-kilodalton protein of the inner membrane is the mitochondrial calcium uniporter. Nature. 2011 Jun 19;476(7360):336-40.

Dong W, Gao D, Zhang X. Mitochondria biogenesis induced by resveratrol against brain ischemic stroke. Med Hypotheses. 2007;69(3):700-1.

Drago I, Pizzo P, Pozzan T. After half a century mitochondrial calcium in- and efflux machineries reveal themselves. EMBO J. 2011 Sep 20;30(20):4119-25.

Druzhyna NM, Wilson GL, LeDoux SP. Mitochondrial DNA repair in ageing and disease. Mech Ageing Dev. 2008 Jul-Aug; 129(7-8):383-90.

Epstein CJ, Korenberg JR, Anneren G, Antonarakis SE, Ayme S, Courchesne E, Epstein LB, Fowler A, Groner Y, Huret JL et al. Protocols to establish genotype-phenotype correlations in Down syndrome. Am J Hum Genet 1991, 49(1):207-235.

Epstein CJ, Takashima A and Yamakawa K. Mitochondrial dysfunction and tau hyperphosphorylation in Ts1Cje, a mouse model for Down syndrome. Hum Mol Genet 2006, 15(18):2752-2762.

Escribano L, Simón AM, Pérez-Mediavilla A, Salazar-Colocho P, Del Río J, Frechilla D. Rosiglitazone reverses memory decline and hippocampal glucocorticoid receptor down-regulation in an Alzheimer's disease mouse model. Biochem Biophys Res Commun. 2009 Feb 6;379(2):406-10.

Feissner RF, Skalska J, Gaum WE, Sheu SS. Crosstalk signaling between mitochondrial Ca^{2+} and ROS.Front Biosci. 2009 Jan 1;14:1197-218. Review.

Ferencz C, Neill CA, Boughman JA, Rubin JD, Brenner JI, Perry LW. Congenital cardiovascular malformations associated with chromosome abnormalities: an epidemiologic study. J Pediatr 1989, 114(1):79-86.

Fiore C, Trézéguet V, Le Saux A, Roux P, Schwimmer C, Dianoux AC, Noél F, Lauquin GJ, Brandolin G. and Vignais PV. The mitochondrial ADP/ATP carrier: structural, physiological and pathological aspects. Biochimie. 1998 Feb;80(2):137-50.

FitzPatrick DR, Ramsay J, McGill NI, Shade M, Carothers AD, Hastie ND. Transcriptome analysis of human autosomal trisomy. Hum Mol Genet. 2002;11(26):3249-56.

Fritah A, Steel JH, Nichol D, Parker N, Williams S, Price A, Strauss L, Ryder TA, Mobberley MA, Poutanen M, Parker M, White R. Elevated expression of the metabolic regulator receptor-interacting protein 140 results in cardiac hypertrophy and impaired cardiac function. Cardiovasc Res. 2010 Jun 1;86(3):443-51.

Gardiner K: Predicting pathway perturbations in Down syndrome. J Neural Transm Suppl 2003(67):21-37.

Gardiner K. Transcriptional dysregulation in Down syndrome: predictions for altered protein complex stoichiometries and post-translational modifications, and consequences for learning/behavior genes ELK, CREB, and the estrogen and glucocorticoid receptors. Behav Genet. 2006 May;36(3):439-53.

Graham BH, Waymire KG, Cottrell B, Trounce IA, MacGregor GR, Wallace DC. A mouse model for mitochondrial myopathy and cardiomyopathy resulting from a deficiency in the heart/muscle isoform of the adenine nucleotide translocator. Nat Genet. 1997 Jul;16(3):226-34.

Gundersen HJG. The smooth fractionator. Journal of Microscopy 2002; 207, 191–210

Gwack Y, Sharma S, Nardone J, Tanasa B, Iuga A, Srikanth S, Okamura H, Bolton D, Feske S, Hogan PG, Rao A. A genome-wide Drosophila RNAi screen identifies DYRK-family kinases as regulators of NFAT. Nature 2006 Jun 1;441(7093):646-50.

Haworth RA, Hunter DR. Control of the mitochondrial permeability transition pore by high-affinity ADP binding at the ADP/ATP translocase in permeabilized mitochondria. J Bioenerg Biomembr. 2000 Feb;32(1):91-6.

Hayat MA. Principles and Techniques of Electron Microscopy: Biological Applications. Fourth Edition. 2000, Cambridge University Press.

Huo L, Scarpulla RC. Mitochondrial DNA instability and peri-implantation lethality associated with targeted disruption of nuclear respiratory factor 1 in mice. Mol Cell Biol. 2001 Jan;21(2):644-54.

Jager S, Handschin C, St-Pierre J and Spiegelman BM. AMP-activated protein kinase (AMPK) action in skeletal muscle via direct phosphorylation of PGC-1a. Proc Natl Acad Sci U S A. 2007 Jul 17;104(29):12017-22.

John JB, Shang Y, Li L, Renken C, Mannella CA, Selker JML, Rangell L, Bennett MJ, Zha J. The mitochondrial inner membrane protein Mitofilin controls cristae morphology. Mol Biol of the Cell 2005;16:1543-1554.

Johri A, Calingasan NY, Hennessey TM, Sharma A, Yang L, Wille E, Chandra A, Beal MF. Pharmacologic activation of mitochondrial biogenesis exerts widespread beneficial effects in a transgenic mouse model of Huntington's disease. Hum Mol Genet. 2012 Mar 1;21(5):1124-37.

Kahlem P, Sultan M, Herwig R, Steinfath M, Balzereit D, Eppens B, Saran NG, Pletcher MT, South ST, Stetten G, Lehrach H, Reeves RH, Yaspo ML. Transcript level alterations reflect gene dosage effects across multiple tissues in a mouse model of down syndrome. Genome Res 2004, 14(7):1258-1267.

Kerstens HM, Robben JC, Poddighe PJ, Melchers WJ, Boonstra H, de Wilde PC, Macville MV, Hanselaar AG. AgarCyto: a novel cell-processing method for multiple molecular diagnostic analyses of the uterine cervix. J Histochem Cytochem. 2000 May;48(5):709-18.

Klingenberg M. Molecular aspects of the adenine nucleotide carrier from mitochondria.Arch Biochem Biophys. 1989 Apr;270(1):1-14.

Kumar P, Wu H, McBride JL, Jung KE, Kim MH, Davidson BL, Lee SK, Shankar P, Manjunath N. Transvascular delivery of small interfering RNA to the central nervous system. Nature. 2007 Jul 5;448(7149):39-43.

Kussmaul L and Hirst J. The mechanism of superoxide production by NADH:ubiquinone oxidoreductase (complex I) from bovine heart mitochondria. Proc Natl Acad Sci USA 2006; 103, 7607–7612.

Lagouge M, Argmann C, Gerhart-Hines Z, Meziane H, Lerin C, Daussin F, Messadeq N, Milne J, Lambert P, Elliott P, Geny B, Laakso M, Puigserver P and Auwerx J. Resveratrol Improves Mitochondrial Function and Protects

against Metabolic Disease by Activating SIRT1 and PGC-1a. Cell. 2006 Dec 15;127(6):1109-22.

Lee M, Hyun D, Jenner P and Halliwell B. Effect of overexpression of wild-type and mutant Cu/Zn-superoxide dismutases on oxidative damage and antioxidant defences: relevance to Down's syndrome and familial amyotrophic lateral sclerosis. J. Neurochem. 2001, 76, 957–965.

Leone TC, Lehman JJ, Finck BN., Schaeffer PJ, Wende AR, Boudina S, Courtois M, Wozniak DF, Sambandam N, Bernal-Mizrachi C, Chen Z, Holloszy JO,Medeiros DM, Schmidt RE, Saffitz JE, Abel ED, Semenkovich CF, Kelly DP. PGC-1alpha deficiency causes multi-system energy metabolic derangements: muscle dysfunction, abnormal weight control and hepatic steatosis. PLoS Biol. 2005 Apr;3(4):e101.

Li CM, Guo M, Salas M, Schupf N, Silverman W, Zigman WB, Husain S, Warburton D, Thaker H, Tycko B. Cell type-specific over-expression of chromosome 21 genes in fibroblasts and fetal hearts with trisomy 21. BMC Med Genet. 2006;7:24.

Li Y and Trush MA. Diphenyleneiodonium, an NAD(P)H oxidase inhibitor, also potently inhibits mitochondrial reactive oxygen species production. Biochem Biophys Res Commun 1998; 253, 295–299.

Lyle R, Gehrig C, Neergaard-Henrichsen C, Deutsch S, Antonarakis SE. Gene expression from the aneuploid chromosome in a trisomy mouse model of down syndrome. Genome Res 2004, 14(7):1268-1274.

Mao R, Wang X, Spitznagel EL Jr, Frelin LP, Ting JC, Ding H, Kim JW, Ruczinski I, Downey TJ, Pevsner J. Primary and secondary transcriptional effects in the developing human Down syndrome brain and heart. Genome Biol 2005, 6(13):R107.

Mitra R, Nogee DP, Zechner JF, Yea K, Gierasch CM, Kovacs A, Medeiros DM, Kelly DP, Duncan JG. The transcriptional coactivators, PGC-1alpha and beta, cooperate to maintain cardiac mitochondrial function during the early stages of insulin resistance. J Mol Cell Cardiol. 2012 Mar;52(3):701-10.

Nicolakakis N, Aboulkassim T, Ongali B, Lecrux C, Fernandes P, Rosa-Neto P, Tong XK, Hamel E. Complete rescue of cerebrovascular function in aged Alzheimer's disease transgenic mice by antioxidants and pioglitazone, a peroxisome proliferator-activated receptor gamma agonist. J Neurosci. 2008 Sep 10;28(37):9287-96.

Palmieri L, Alberio S, Pisano I, Lodi T, Meznaric-Petrusa M, Zidar J, Santoro A, Scarcia P, Fontanesi F, Lamantea E, Ferrero I, Zeviani M. Complete loss-of-function of the heart/muscle-specific adenine nucleotide translocator is associated with mitochondrial myopathy and cardiomyopathy. Hum Mol Genet. 2005 Oct 15;14(20):3079-88.

Park SC, Mathews RA, Zuberbuhler JR, Rowe RD, Neches WH, Lenox CC. Down syndrome with congenital heart malformation. Am J Dis Child 1977, 131(1):29-33.

Piccoli C, Scrima R, Quarato G, D'Aprile A, Ripoli M, Lecce L, Boffoli D, Moradpour D, Capitanio N. Hepatitis C virus protein expression causes calcium-mediated mitochondrial bioenergetic dysfunction and nitro-oxidative stress. Hepatology 2007; 46(1): 58-65.

Piccoli C, Izzo A, Scrima R, Bonfiglio F, Manco R, Negri R, Quarato G, Cela O, Ripoli M, Prisco M, Gentile F, Calì G, Pinton P, Conti A, Nitsch L, Capitanio N. Chronic pro-oxidative state and mitochondrial dysfunctions are more pronounced in fibroblasts from Down syndrome foeti with congenital heart defects. Hum Mol Genet. 2013 Mar 15;22(6):1218-32.

Pinton P, Rimessi A, Romagnoli A, Prandini A, Rizzuto R Biosensors for the detection of calcium and pH. Methods in cell biology 2007 80: 297-325.

Powelka, A.M., Seth, A., Virbasius, J.V., Kiskinis, E., Nicoloro, S.M., Guilherme, A., Tang,X., Straubhaar, J., Cherniack, A.D., Parker, M.G. et al. Suppression of oxidative metabolism and mitochondrial biogenesis by the transcriptional corepressor RIP140 in mouse adipocytes. J Clin Invest. 2006 Jan;116(1):125-36.

Pulford B, Reim N, Bell A, Veatch J, Forster G, Bender H, Meyerett C, Hafeman S, Michel B, Johnson T, Wyckoff AC, Miele G, Julius C, Kranich J, Schenkel A, Dow S, Zabel MD. Liposome-siRNA-peptide complexes cross the blood-brain barrier and significantly decrease PrP on neuronal cells and PrP in infected cell cultures.PLoS One. 2010 Jun 14;5(6):e11085.

Reynolds ES. The use of lead citrate at high pH as an electron-opaque stain in electron microscopy. J Cell Biol 1963;17, 208-228.

Roat E, Prada N, Ferraresi R, Giovenzana C, Nasi M, Troiano L, Pinti M, Nemes E, Lugli E, Biagioni O, Mariotti M, Ciacci L, Consolo U, Balli F, Cossarizza A. Mitochondrial alterations and tendency to apoptosis in peripheral blood cells from children with Down syndrome. FEBS letters 581(2007): 521-525.

Rodgers JT, Lerin C, Haas W, Gygi SP, Spiegelman BM, Puigserver P. Nutrient control of glucose homeostasis through a complex of PGC-1alpha and SIRT1. Nature. 2005 Mar 3;434(7029):113-8.

Rytinki MM. and Palvimo JJ. SUMOylation attenuates the function of PGC-1alpha. J Biol Chem. 2009 Sep 18;284(38):26184-93.

Sauerbeck A, Gao J, Readnower R, Liu M, Pauly JR, Bing G, Sullivan PG. Pioglitazone attenuates mitochondrial dysfunction, cognitive impairment, cortical tissue loss, and inflammation following traumatic brain injury. Exp Neurol. 2011 Jan;227(1):128-35.

Scarpulla RC. Nuclear control of respiratory chain expression in mammalian cells. J Bioenerg Biomembr. 1997 Apr;29(2):109-19. Review.

Scarpulla, RC. Metabolic control of mitochondrial biogenesis through the PGC-1 family regulatory network. Biochim Biophys Acta. 2011 Jul;1813(7):1269-78.

Scarpulla RC, Vega RB, Kelly DP. Transcriptional integration of mitochondrial biogenesis. Trends Endocrinol Metab. 2012 Sep;23(9):459-66.

Schuchmann S and Heinemann U. Increased mitochondrial superoxide generation in neurons from trisomy 16 mice: a model of Down's syndrome. Free Radic Biol Med. 2000 Jan 15; 28(2):235-50.

Seth A, Steel JH, Nichol D, Pocock V, Kumaran MK, Fritah A, Mobberley M, Ryder TA, Rowlerson A, Scott J, Poutanen M, White R, Parker M. The transcriptional corepressor RIP140 regulates oxidative metabolism in skeletal muscle. Cell Metab. 2007 Sep;6(3):236-45

Shimomura O. Isolation and properties of various molecular forms of aequorin. The Biochemical journal 1986 234: 271-277.

Shukkur EA, Shimohata A, Akagi T, Yu W, Yamaguchi M, Murayama M, Chui D, Takeuchi T, Amano K, Subramhanya KH, Hashikawa T, Sago H, Epstein CJ, Takashima A and Yamakawa K. Mitochondrial dysfunction and tau hyperphosphorylation in Ts1Cje, a mouse model for Down syndrome. Hum Mol Genet 2006, 15(18):2752-2762.

Skulachev VP. Mitochondrial filaments and clusters as intracellular power-transmitting cables. Trends Biochem Sci. 2001 Jan;26(1):23-9. Review.

Sommer CA and Henrique-Silva F. Trisomy 21 and Down syndrome Braz. J. Biol. 2008; 68(2): 447-452, 449.

Subramanian V, Golik P, Murdock DG, Levy S, Kerstann KW, Coskun PE, Melkonian GA, Wallace DC. MITOCHIP assessment of differential gene expression in the skeletal muscle of Ant1 knockout mice: coordinate regulation of OXPHOS, antioxidant, and apoptotic genes. Biochim Biophys Acta. 2008 Jul-Aug;1777(7-8):666-75.

Tao Y, Han J and Dou H. 2012. Brain-targeting gene delivery using a rabies virus glycoprotein peptide modulated hollow liposome: bio-behavioral study. J Mater Chem 2012;22:11808-11815.

Tokumaru S, Suzuki M, Yamada H, Nagino M, Takahashi T. let-7 regulates Dicer expression and constitutes a negative feedback loop. Carcinogenesis. 2008 Nov;29(11):2073-7.

Valenti D, Tullo A, Caratozzolo MF, Merafina RS, Scartezzini P, Marra E and Vacca RA. Impairment of F1F0-ATPase, adenine nucleotide translocator and adenylate kinase causes mitochondrial energy deficit in human skin fibroblasts with chromosome 21 trisomy. Biochem J. 2010 Oct 15;431(2):299-310.

Valenti D, Manente GA., Moro L, Marra E and Vacca RA. Deficit of complex I activity in human skin fibroblasts with chromosome 21 trisomy and overproduction of reactive oxygen species by mitochondria: involvement of the cAMP/PKA signaling pathway. Biochem J. 2011 May 1;435(3):679-88.

Vo N, Fjeld C, Goodman RH. Acetylation of nuclear hormone receptor-interacting protein RIP140 regulates binding of the transcriptional corepressor CtBP. Mol Cell Biol. 2001 Sep;21(18):6181-8.

Weibel ER, Kistler GS, Scherle WF. Practical stereological methods for morphometric cytology. J Cell Biol. 1966 Jul;30(1):23-38.

White R, Morganstein D, Christian M, Seth A, Herzog B, Parker MG. Role of RIP140 in metabolic tissues: connections to disease. FEBS Lett. 2008 Jan 9;582(1):39-45.

Yamaguchi S, Li H, Purevsuren J, Yamada K, Furui M, Takahashi T, Mushimoto Y, Kobayashi H, Hasegawa Y, Taketani T, Fukao T, Fukuda S. Bezafibrate can be a new treatment option for mitochondrial fatty acid oxidation disorders: evaluation by in vitro probe acylcarnitine assay. Mol Genet Metab. 2012 Sep;107(1-2):87-91.

Yamato F, Takaya J, Yasuhara A, Teraguchi M, Ikemoto Y and Kaneko K. Elevated intracellular calcium in neutrophils in patients with Down syndrome. Pediatr Int. 2009 Aug;51(4):474-7.

Zabel MD. Lipopeptide Delivery of siRNA to the Central Nervous System; Nanotechnology for Nucleic Acid Delivery. Methods in Molecular Biology 2013;948:251-262.

Zoratti M, Szabò I. The mitochondrial permeability transition. Biochim Biophys Acta. 1995 Jul 17;1241(2):139-76. Review.

Human Molecular Genetics, 2013, Vol. 22, No. 6 ***1218–1232***
doi:10.1093/hmg/dds529
Advance Access published on December 20, 2012

Chronic pro-oxidative state and mitochondrial dysfunctions are more pronounced in fibroblasts from Down syndrome foeti with congenital heart defects

Claudia Piccoli[1,†], Antonella Izzo[2,†], Rosella Scrima[1], Ferdinando Bonfiglio[2], Rosanna Manco[2], Rosa Negri[2], Giovanni Quarato[1], Olga Cela[1], Maria Ripoli[1], Marina Prisco[3], Flaviana Gentile[4], Gaetano Calì[4], Paolo Pinton[5], Anna Conti[2], Lucio Nitsch[2,†] and Nazzareno Capitanio[1,*,†]

[1]Department of Clinical and Experimental Medicine, University of Foggia, Foggia 71100, Italy, [2]Department of Cellular and Molecular Biology and Pathology and [3]Department of Biological Sciences, University of Naples Federico II, Naples 80131, Italy, [4]Institute of Experimental Endocrinology and Oncology, National Research Council, Naples 80131, Italy and [5]Department of Experimental and Diagnostic Medicine, University of Ferrara, Ferrara 44100, Italy

Received October 27, 2012; Revised and Accepted December 12, 2012

Trisomy of chromosome 21 is associated to congenital heart defects in ∼50% of affected newborns. Transcriptome analysis of hearts from trisomic human foeti demonstrated that genes involved in mitochondrial function are globally downregulated with respect to controls, suggesting an impairment of mitochondrial function. We investigated here the properties of mitochondria in fibroblasts from trisomic foeti with and without cardiac defects. Together with the upregulation of Hsa21 genes and the downregulation of nuclear encoded mitochondrial genes, an abnormal mitochondrial cristae morphology was observed in trisomic samples. Furthermore, impairment of mitochondrial respiratory activity, specific inhibition of complex I, enhanced reactive oxygen species production and increased levels of intra-mitochondrial calcium were demonstrated. Seemingly, mitochondrial dysfunction was more severe in fibroblasts from cardiopathic trisomic foeti that presented a more pronounced pro-oxidative state. The data suggest that an altered bioenergetic background in trisomy 21 foeti might be among the factors responsible for a more severe phenotype. Since the mitochondrial functional alterations might be rescued following pharmacological treatments, these results are of interest in the light of potential therapeutic interventions.

INTRODUCTION

Down syndrome (DS) is characterized by a complex phenotype in which over 80 features occur with various degrees of expression and frequency (1). DS is a major cause of congenital heart defects (CHD) mainly endocardial cushion defects, the most frequent being atrioventricular canal defects followed by ventricular septal defects and tetralogy of Fallot (2). By comparing the gene expression profiles of 10 human hearts from trisomic foeti to five foetal hearts of non-trisomic controls, we previously demonstrated a global upregulation of chromosome 21 (Hsa21) genes and a dysregulation of ∼400 genes localized on other chromosomes (3). Microarray analysis clearly showed the downregulation of genes encoding all five mitochondrial complex subunits and of genes implicated in mitochondrial biogenesis. This suggested that the corresponding proteins and enzymatic activities might be reduced in DS subjects and that mitochondrial function could be consequently impaired.

*To whom correspondence should be addressed at: Department of Clinical and Experimental Medicine, Via Pinto 1 c/o OO.RR., 71100 Foggia, Italy. Tel: +39 881711148; Fax: +39 881714745; Email: n.cap@unifg.it
†The authors wish it to be known that, in their opinion, the first two authors (C.P., A.I.) should be regarded as joint First Authors and that the last two authors (L.N., N.C.) contributed equally to the work.

Trisomy of chromosome 21 has been associated with mitochondrial dysfunction in cells and tissues from DS subjects (4–6) and in mouse models (7,8). These results led to the hypothesis that mitochondrial dysfunction contributes to the DS phenotype. Protein levels of mitochondrial complexes I, III and V were decreased in cerebellar and brain regions of DS subjects (9). Complex I was also deficient in mouse models of trisomy of chromosome 16. The results were similar to those obtained from models of Parkinson's disease, suggesting that different neurodegenerative diseases may be associated with the same mitochondrial dysfunction (10).

Recently, it has been also reported that the mitochondrial energy production apparatus was less efficient in foetal DS fibroblasts, due to the dysregulation of adenine nucleotide translocator, ATP synthase and adenylate kinase, and a selective deficit of complex I, which contributes to reactive oxygen species (ROS) overproduction in DS mitochondria. These events were attributed to changes in the cAMP/PKA signalling pathway (11,12), which is known to affect the abundance of the transcriptional coactivator *PGC-1α* (peroxisome proliferator-activated receptor gamma coactivator 1-alpha). This protein, that plays a central role in regulating mitochondrial biogenesis and respiratory function through the interaction with transcriptional partners, like *NRF1*, *ERRα*, *PPARs* and *YY1*, is negatively controlled by the co-repressor *RIP140*, a gene mapping to Hsa21 (13).

Even though these results are indicative of widespread mitochondrial dysfunction in DS, molecular studies have not yet been performed to investigate the basis of mitochondrial dysfunction at the transcriptional level. Furthermore, no hypotheses have been formulated about the mechanisms by which trisomy of Hsa21 genes might induce such a dysfunction.

The original contribution of the present study consists of a contemporary analysis of mitochondrial features at the molecular, morphological and functional level in 13 human primary lines of foetal fibroblasts (HFF) derived from Hsa21 trisomic foeti, with or without CHD, and from euploid controls. The mitochondrial defects associated with DS were analysed taking into account the regulation of the Hsa21 and mitochondrial-related genes and the cardiac phenotype, in order to identify pathways involved in mitochondrial function and dysrupted by the Hsa21 trisomy. A striking and more severe ROS- and Ca^{2+}-related mitochondrial dysfunction emerged in cardiopathic-derived Hsa21 trisomic fibroblasts, unveiling a more pronounced pro-oxidative state.

RESULTS

The present study combines the molecular, morphological and functional analyses of mitochondria in 13 human primary cultures of HFF. Five were from euploid foeti (N-HFF, N standing for normal), and eight (DS-HFF) were derived from Hsa21 trisomic foeti [four samples from DS foeti with heart defects, named CDS-HFF (CDS standing for Cardiopathic Down Syndrome), and four samples from DS foeti without heart defects, named NCDS-HFF (NCDS standing for Non Cardiopathic Down Syndrome)].

Gene expression is dysregulated in DS-HFF samples

The analysis of HFF karyotypes demonstrated that all trisomic fibroblasts showed three copies of Hsa21 as the only cytogenetic alteration (data not shown). The expression of some Hsa21 genes was determined by quantitative real-time PCR (qRT-PCR) experiments comparing DS-HFF versus N-HFF. In particular, the Hsa21 genes *BTG3*, *SOD1*, *ITSN1*, *DYRK1A*, *NRF2* and *RIP140* were upregulated in trisomic fibroblasts when compared with controls (Fig. 1A), thus confirming the gene dosage effects that was previously demonstrated in human foetal tissues (3,14). We then focused on genes that mapped to chromosomes different from Hsa21 and were involved in multiple mitochondrial functions, such as the respiratory chain, mitochondrial biogenesis and morphology, and genes involved in related pathways, such as the *Calcineurin/NFAT* (Nuclear factor of activated T-cells) axe. Most of the analysed genes were significantly downregulated in trisomic versus euploid fibroblasts (Fig. 1B), demonstrating that trisomy of chromosome 21 perturbs the expression of genes involved in mitochondrial pathways. Moreover, *NFATc3* and *NFATc4* were significantly downregulated while *DYRK1A* and *RCAN1*, two Hsa21 genes involved in regulating the levels of *NFATc* phosphorylation, were upregulated in trisomic versus euploid fibroblasts (Fig. 1C).

Mitochondria of DS-HFF show morphological abnormalities

Electron microscopy (EM) of trisomic fibroblasts revealed that a significant number of mitochondria had an abnormal morphology, showing an increased size, irregular shape, evident breaks, mainly of inner membranes. In addition, the mitochondria showed alterations in the pattern of cristae where some were broadened and arranged concentrically or oriented parallel to the long axis of the organelle (longitudinal cristae) (Fig. 2A). Broken mitochondria and mitochondria with concentric and longitudinal cristae were significantly more abundant in trisomic samples than in the euploid ones ($P < 0.05$) (Fig. 2B). Stereological analysis demonstrated that the mitochondrial volume density, expressed as a percentage of cellular volume, was similar in euploid and trisomic samples while the cristae volume density, expressed as a percentage of mitochondrial volume, was significantly lower in all DS-HFF samples when compared with N-HFF ($P < 0.05$) (Fig. 2C and D).

The functional mitochondrial phenotype is altered in CDS-HFF

Endogenous oxygen consumption rate in intact HFF

The respiratory activity of N-HFF and DS-HFF samples was compared by high-resolution oxymetry. The oxygen consumption rate (OCR) was assessed in intact cells relying on endogenous respiratory substrates and corrected for the residual KCN-sensitive OCR and, therefore, attributable to mitochondrial respiratory chain-dependent activity. Figure 3A shows the results of a systematic analysis whereby the activity of each cellular sample was measured. Although a relatively large inter-individual variability was observed within each of

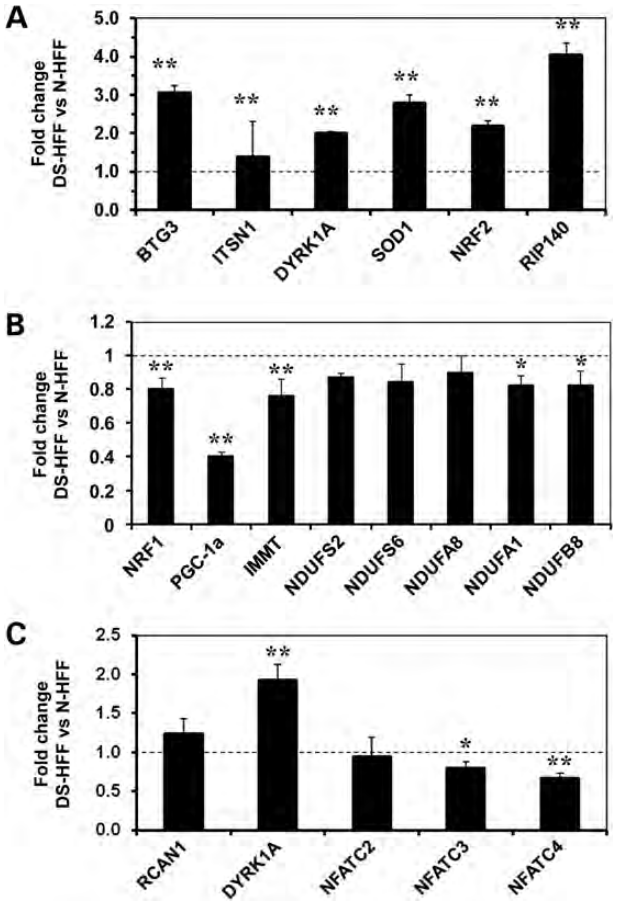

Figure 1. Gene expression is dysregulated in DS fibroblasts. Gene expression fold change in DS-HFF samples versus N-HFF samples for Hsa21 genes (**A**), nuclear-encoded mitochondrial genes (**B**) and calcineurin/NFAT-related genes (**C**) as obtained by qRT-PCR. Values represent the mean of three replicates ± SEM. $^{*}P < 0.05$, $^{**}P < 0.01$, N-HFF, Euploid fibroblasts; DS-HFF, Hsa21 trisomic fibroblasts.

the three groups, on an average basis, the resting respiration of DS-HFF showed a significant decrease that was more evident in CDS-HFF (≈43% inhibition) when compared with N-HFF. Conversely, a slight increase in the OCR in the presence of the FoF1-ATP synthase inhibitor oligomycin was observed in DS-HFF, whereas in the presence of the protonophoric uncoupler FCCP a slight, albeit significant, decrease (≈27% inhibition) in the OCR was observed in CDS-HFF when compared with N-HFF. The respiratory control ratio (RCR), attained by dividing the uncoupled OCR by that in the presence of oligomycin, was as high as 14–16 irrespective of the cell group analysed (Fig. 3B). The ATP-synthase independent OCR (leak) was unchanged between N- and DS-HFF, whereas the oxidative phosphorylation-dependent OCR (OXPHOS) was significantly reduced in DS-HFF, and more specifically in CDS-HFF, by 36% when compared with N-HFF (Fig. 3B). The decrease in OCR_{RR}, observed in DS-HFF, individually correlated to the altered mitochondrial morphology and cristae volume density assessed by EM (Fig. 3C). Next, we measured the mitochondrial membrane potential ($\Delta\Psi_m$) by confocal microscopic imaging using the specific mitotropic probe TMRE. A significant difference was not observed in the TMRE-related fluorescence among N-HFF, NCDS-HFF and CDS-HFF (Fig. 4A), even though a finer analysis of the fluorescent signal revealed a less interdigitated mitochondrial network morphology in DS-HFF (Fig. 4B).

Complex I activity

To assess if the observed respiratory deficit in DS-HFF resulted from a specific defect in one or the other of the respiratory chain complexes, the activity of the protonmotive complexes I, III and IV was measured in cell lysates. The activity of citrate synthase, which is an index of mitochondrial mass, was also measured. Figure 5A shows that the activity of complex I was significantly depressed (by about 50%) in both NCDS-HFF and CDS-HFF when compared with N-HFF. The decreased activity of complex I correlated with the altered mitochondrial cristae morphology. Conversely, significant differences in activities of complexes III and IV were not observed among the three cell groups (Fig. 5B and C). Likewise, the citrate synthase activity was practically unaffected (Fig. 5D); therefore, following normalization to the mitochondrial mass, the selective inhibition of complex I in trisomic cells was confirmed (data not shown). Total protein levels per cell were slightly less in trisomic samples but not to a statistically significance degree compared with N-HFF (Fig. 5E).

Mitochondria-related ROS production

Intracellular ROS level was assessed by confocal microscopy imaging of cells treated with the redox-sensitive fluorescent probe DCF. Every trisomic sample displayed an enhanced ROS production when compared with N-HFF, with a larger redox imbalance in CDS-HFF (Fig. 6A). Enlargement of the confocal images showed a compartmentalized, brighter signal of the DCF-related fluorescence with a very low variability within each group. On an average basis, the ROS-related DCF fluorescence was much larger in CDS-HFF when compared with NCDS-HFF (Fig. 6B). Plotting the DCF fluorescence versus the normalized complex I activity for each individual HFF sample suggested the presence of a threshold value of complex I activity below which extra-ROS production was generated (Fig. 6C). To further ascertain the source of the ROS release in DS-HFF, cells were treated with DPI, which is a pan-inhibitor of flavin-containing oxidases (including complex I). DPI treatment was associated with a marked decrease in the ROS over-production in representative samples of both NCDS- and CDS-HFF, whereas it was ineffective in N-HFF (Fig. 7). Production of ROS by the respiratory chain complex I is fostered by the presence of a $\Delta\Psi_m$ (15). Short-time incubation of cells with the uncoupler FCCP significantly inhibited ROS release both in NCDS- and CDS-HFF with a larger effect in the latter (Fig. 7). It has been recently reported that alteration of PKA-dependent signalling affects functioning of the oxidative phosphorylation (OXPHOS) system (11,16,17). Treatment of cells with the cAMP analogue db-cAMP significantly reduced ROS production in both NCDS- and CDS-HFF although the redox state, especially in CDS-HFF, was not fully renormalized to the level of N-HFF (cf. Fig. 7 with 6B).

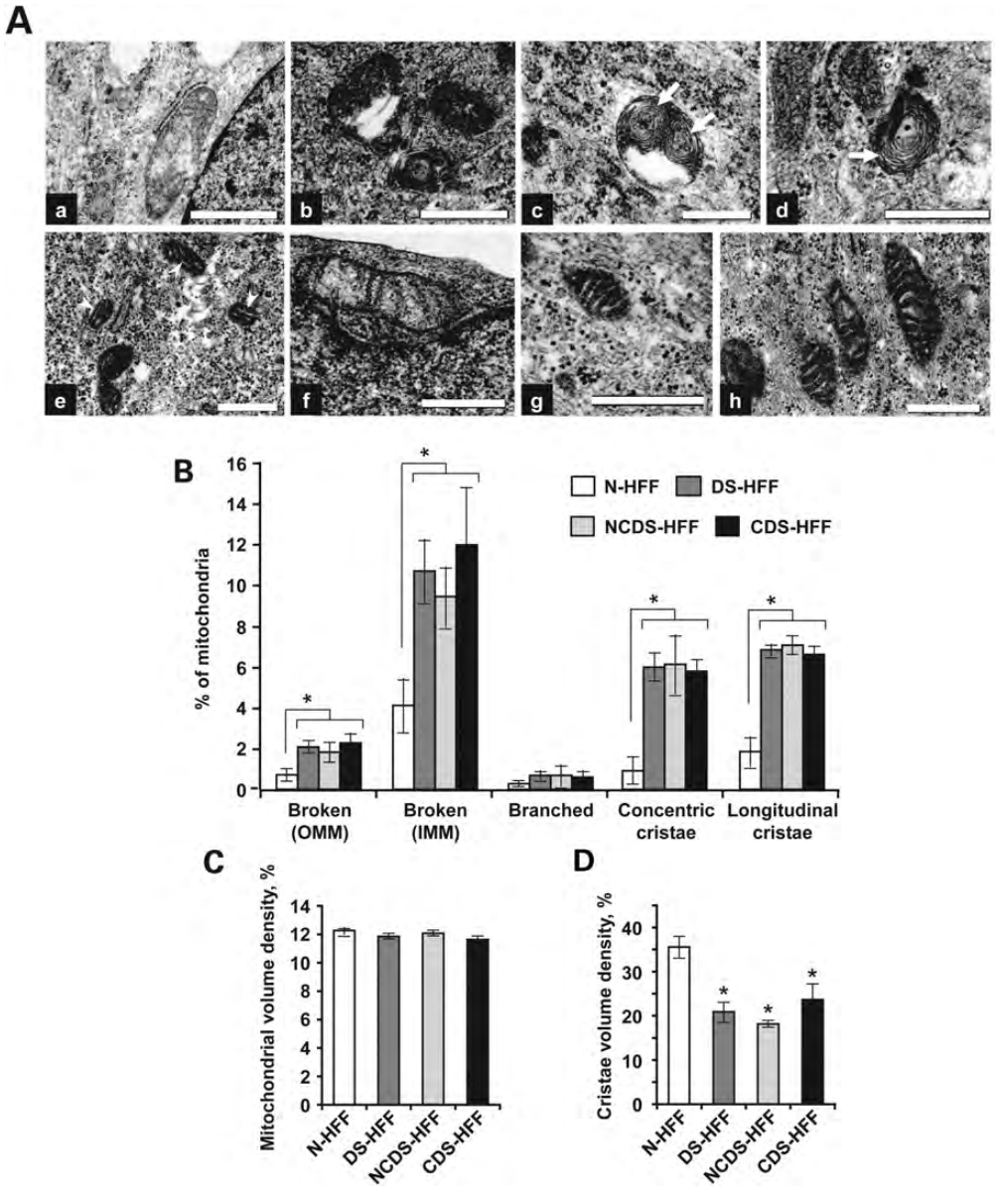

Figure 2. Mitochondria of DS fibroblasts show morphological abnormalities. (**A**) Electron micrographs of morphologically abnormal mitochondria in DS-HFF (a–f) and normal mitochondria in N-HFF (g and h); (a and b) broken mitochondria; (c and d) mitochondria with concentric cristae (arrow); (e) mitochondria with longitudinal cristae (arrow head); (f) mitochondria with significantly reduced cristae; (g and h) mitochondria with unchanged morphology in N-HFF. Scale bars: 500 nm. (**B**) Percentages of mitochondria with abnormal morphology in fibroblasts. (**C**) Mitochondrial volume density relative to cell volume. (**D**) Mitochondrial cristae volume density relative to mitochondrial volume. In (**B**)–(**D**), the mean values ± SEM are shown along with statistical analysis; $^{*}P$ significant cut off < 0.05 Kolmogorov–Smirnov and Kruskall–Wallis tests. N-HFF, euploid fibroblasts; DS-HFF, Hsa21 trisomic fibroblasts; NCDS-HFF, Hsa21 trisomic fibroblasts from DS foeti without heart defects; CDS-HFF, Hsa21 trisomic fibroblasts from DS foeti with heart defects.

Steady-state intra-mitochondrial calcium level

Deregulation of Ca^{2+} homeostasis and Ca^{2+}-mediated signalling has been described in cells derived from trisomic patients or in murine models of DS (18–20). Mitochondria are known to function as a Ca^{2+} buffer by taking up Ca^{2+} mainly via a specific ruthenium red (RR)-inhibitable uniporter (21,22). To verify this point, we evaluated the intramitochondrial level of calcium ($mtCa^{2+}$) using the specific probe Rhod-1. Figure 8A and B shows representative confocal microscopic images of the analysis along with statistical evaluation of the results. It is shown that DS-HFF displayed a statistically significant more intense Rhod-1-related fluorescence signal when compared with N-HFF. However, this was mainly contributed by the CDS-HFF samples. Closer examination of the intracellular fluorescence unveiled a compartmentalization of the brighter signal confirming that it was largely displaying the steady-state $mtCa^{2+}$ level. The enhanced $mtCa^{2+}$ load in DS-HFF correlated positively with the increase in ROS production (Fig. 8C) consistent with the notion that calcium entry in mitochondria induces redox state alterations (23).

To verify the interplay between calcium and ROS, representative trisomic samples were treated with RR and the redox

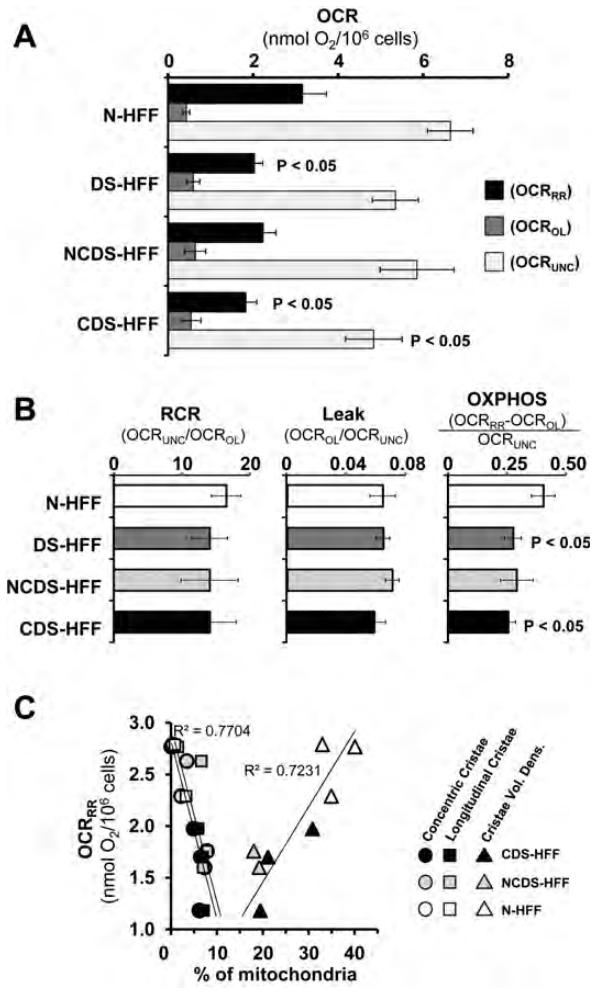

Figure 3. Respirometric analysis in DS fibroblasts. (**A**) OCRs normalized to cell number were assessed by high-resolution oxymetry in intact cells as described in the Materials and Methods. A comparative analysis between five different euploid (N-HFF) and eight different trisomic (DS-HFF) samples is shown; a distinction of the DS-HFF between non-cardiopathic (NCDS-HFF, $n = 4$) and cardiopathic (CDS-HFF, $n = 4$) foetus-derived fibroblasts is also reported. The endogenous OCR were measured under resting conditions (OCR_{RR}), in the presence of oligomycin (OCR_{OL}) and in the uncoupled state in the presence of FCCP (OCR_{UNC}). (**B**) Respiration-linked bioenergetic parameters computed by the OCR measurements shown in (A). RCR, respiratory control ratio; Leak, non-ATP-synthase-controlled respiratory activity; OXPHOS, ATP-synthase-controlled respiratory activity. The bars in (A) and (B) are means ± SEM of the average determinations for each sample carried out at least in triplicate; when statistically significant, the difference when compared with the euploid samples is shown. (**C**) Correlation plots between respiratory activity under resting conditions (OCR_{RR}) and percentage of concentric or longitudinal cristae or of cristae volume density for individual fibroblast samples (see the symbol legend).

state assessed by DCF. As shown in Figure 9A and B, inhibition of the mitochondrial Ca^{2+} porter by RR caused a substantial inhibition of ROS production, suggesting that the entry of Ca^{2+} in the mitochondrial compartment was at least partially responsible for the redox imbalance in trisomic cell samples. Moreover, treatment with RR resulted in enhancement of the respiratory activity in DS-HFF to the level of N-HFF (Fig. 9C). Similar results were obtained evaluating mitochondrial calcium levels by a different method based on a calcium-sensible photoprotein, the aequorin (see Supplementary Material, Text S1 and Fig. S1).

Mitochondrial biogenesis is affected by Hsa21 trisomy

Lastly, to verify if the observed mitochondrial dysfunction was associated to a decreased mitochondrial biogenesis, we quantified the copy number of mitochondrial DNA by absolute qRT-PCR. There was an average value of ∼600 copies per nuclear genome (i.e. per cell) in N-HFF, 500 in NCDS-HFF and 400 in CDS-HFF (Fig. 10A). A statistical significance was attained only for CDS-HFF.

As the mtDNA replication is controlled by *PGC-1α*, which is a master regulator of mitochondrial biogenesis (13), we analysed the correlation between *PGC-1α* expression and the amount of mtDNA. The amount of *PGC-1α* gene transcripts was reduced by ∼40–50% in trisomic samples versus N-HFF (Fig. 10B). Western blotting of *PGC-1α* confirmed at the protein level a significant decrease in NCDS-HFF and an even more marked decrease in CDS-HFF when compared with N-HFF (Fig. 10C). A direct correlation between *PGC-1α* expression and amount of mtDNA was observed in our samples (Fig. 10D).

DISCUSSION

We previously demonstrated that more than 80 genes, encoding mitochondrial enzymes and respiratory chain subunits, are downregulated in foetal trisomic heart tissues (3). Of these genes, 40 % have consensus DNA binding sites for the nuclear respiratory factor *NRF1* in their 5' flanking regions, and 20 % of them show a high affinity for the oestrogen-related receptor *ERRα* (see Supplementary Material, Text S2 and Tables S3 and S4). It has been recently demonstrated that the transcription factors *NRF1* and *ERRα* and their targets are repressed by Hsa21 gene *RIP140* and induced by *PGC-1α* in a dose dependent manner in neonatal rat cardiomyocytes (24). Our results indicate that *NRF1* and *PGC-1α* are significantly downregulated in DS HFF. Western blotting of *PGC-1α* confirmed the downregulation also at the protein level in trisomic fibroblasts. This downregulation correlated well with the downregulation of complex I activity and with the mtDNA copy number decrease (more evidently in CDS-HFF). *PGC-1α* function has been investigated in several specialized cell types and transgenic mouse models, demonstrating its role in the regulation of mitochondrial oxidative metabolism. *PGC-1α* null mice show reduced expression of mitochondrial genes in multiple tissues (25,26). *PGC-1α* controls the expression of nuclear-encoded mitochondrial genes through interactions with its transcriptional partners *NRF1* and *ERRα*, which are also downregulated in DS samples.

Morphological analysis of mitochondria in trisomic versus euploid samples demonstrated ultrastructural changes in DS-HFF mitochondria. These results provide additional evidence of altered mitochondrial morphology observed in DS brain tissues and mouse models (8,27). Silencing experiments demonstrated that the downregulation of *IMMT* causes a drastic change in the organization of the inner membrane

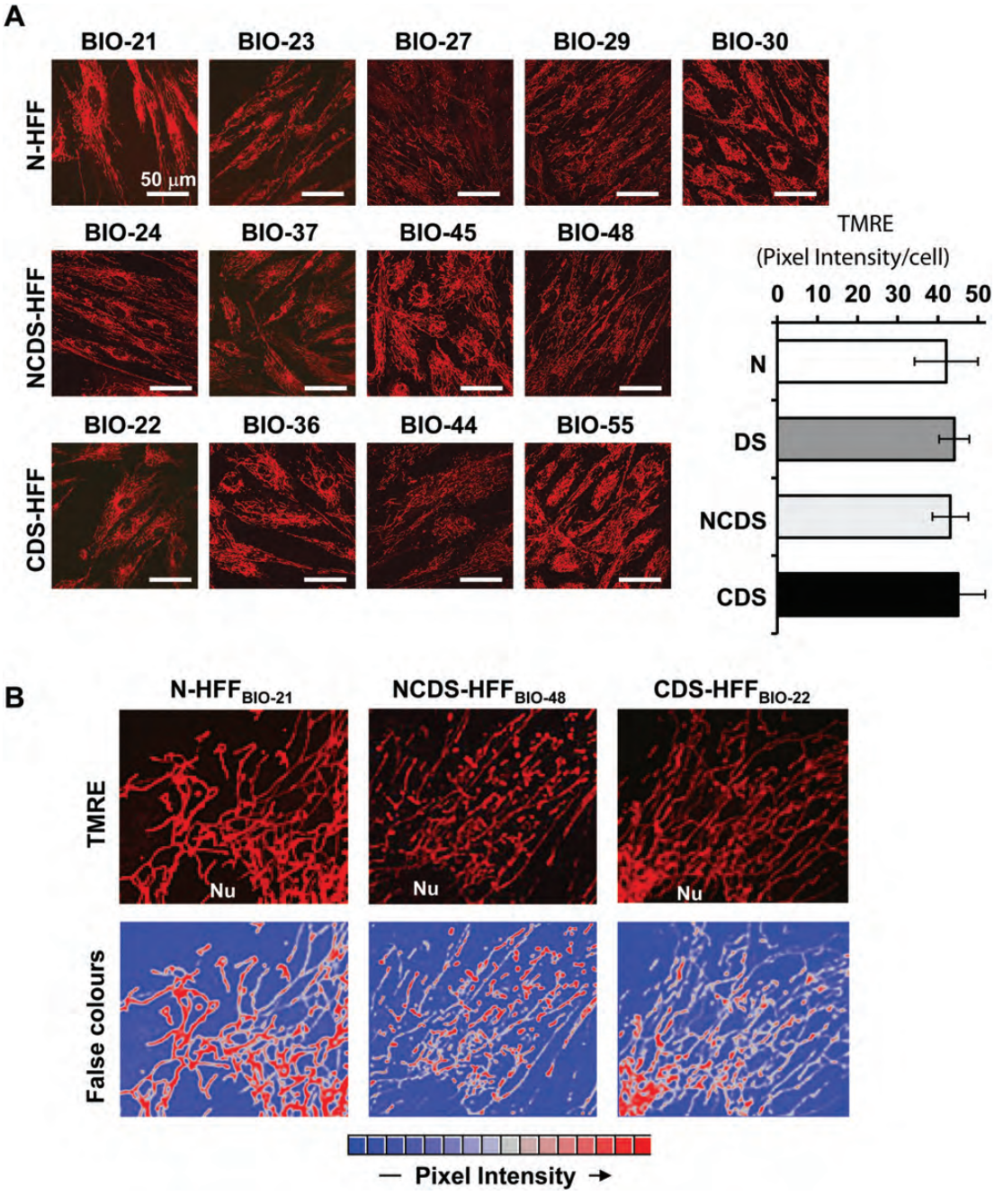

Figure 4. Confocal microscopy analysis of mtΔΨ in DS live fibroblasts. (**A**) Representative LSCM imaging of the TMRE-related fluorescence of euploid (N-HFF) and DS (NCDS-HFF and CDS-HFF) fibroblasts. The horizontal histograms on the right show the statistical analysis of the fluorescence intensity per cell as resulting from the averaged values ± SEM of about 100 randomly selected different cells for each sample from at least in-duplicate experiments. (**B**) Magnifications of intracellular selected details showing the mitochondrial functional network in representative samples of N-, NCDS- and CDS-HFF. A false-colours rendering of the TMRE-related fluorescence imaging is also shown.

that formed concentric layers instead of organizing into tubular cristae (28,29), leading to cristae patterns similar to those observed in DS samples. It is interesting to note that IMMT is significantly downregulated in DS fibroblasts.

Mitochondria have a key role in oxygen metabolism and subsequently they are the major source of ROS formation. Respirometry experiments conducted in this study demonstrated that in DS fibroblasts the OCR was significantly reduced in basal, uncoupled and ATP-synthase-dependent respiratory conditions, thus suggesting an impairment in oxidative phosphorylation competence, especially pronounced in DS fibroblasts from cardiopathic foeti. A correlation between the reduced respiratory activity and the morphological alterations in DS-HFF mitochondria indicates that the occurrence of de-structured cristae might partly account for the dysfunctioning oxidative phosphorylation in trisomic

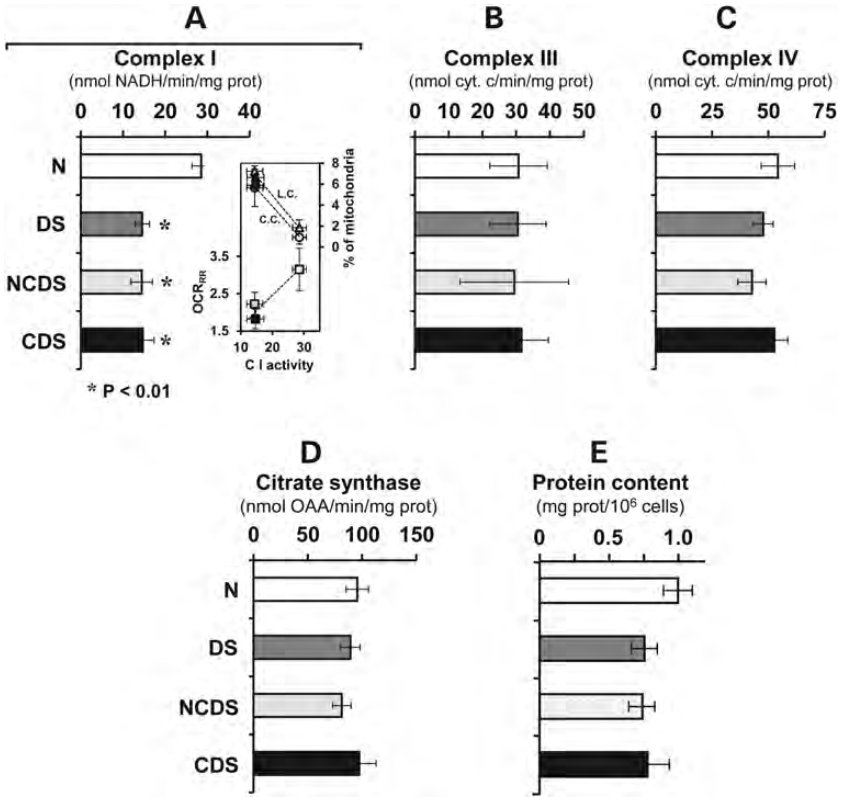

Figure 5. Enzymatic activities of the mitochondrial respiratory chain complexes of DS fibroblasts. The specific activities of (**A**) complex I (NADH-dehydrogenase), (**B**) complex III (cytochrome c reductase), (**C**) complex IV (cytochrome c reductase) were measured in cell lysates under conditions of saturating substrate as described in the Materials and Methods. The inset in (A) shows the correlation plot of the complex I activity versus either the OCR_{RR} (left Y axe) and the cristae morphological features (right Y axe; L.C., longitudinal cristae; C.C., concentric cristae); the values are means ± SEM of the clustered N-, NCDS- and CDS-HFF (same colour as the horizontal bars of the histogram). The citrate synthase activity, a marker of the mitochondrial content and the amount of protein per cell number are also shown in (**D**) and (**E**), respectively. N, DS, NCDS and CDS refer to the fibroblast sampling described in the legend of Figure 3; the bars are means ± SEM of the average determinations for each sample carried out in triplicate; when statistically significant, the difference when compared with the euploid samples is shown.

samples as also suggested by other authors (30,31). The analysis of individual complexes in the mitochondrial respiratory chain showed a strong reduction in the activity of complex I in DS fibroblasts irrespective of whether they were derived from cardiopathic trisomic foeti. Similar results have been recently reported (11). The authors attributed the reduced activity of complex I to defective cAMP/PKA-dependent phosphorylation. The impact of the OXPHOS decrease observed in DS fibroblasts did not result, however, in a severe bioenergetic failure compromising cell growth. This could be explained by an adaptive compensatory increase in the glycolytic flux, as shown in ref. (12), and by the gene-dosage effect of the Hsa21-harbored regulatory glycolytic enzyme phosphofructokinase PFKL (32).

In the present study, we observed a remarkable alteration in the redox homeostasis in DS-HFF highlighted by an increased production of ROS, which localized to an intracellular compartment resembling the mitochondrial network and was sensitive to the FCCP uncoupler and to the complex I inhibitor DPI. These two features would point to complex I as a major ROS generator in DS-HFF sustained by a 'forward electron transfer' mechanism (33,34). ROS production in DS-HFF was substantially suppressed by db-cAMP treatment, supporting the hypothesis that deregulation of post-translational modification of complex I is involved in the redox imbalance observed in DS-HFF.

A feature emerging from the present study is that the redox imbalance observed in DS-HFF was much larger in fibroblasts from cardiopathic foeti irrespective of the similar degree of inhibition of complex I in NCDS- and CDS-HFF. Release of ROS has been repetitively reported to be associated with an overload of Ca^{2+} into the mitochondria, although the mechanism remains to be satisfactorily explained (35,36). Consistent with this notion, we observed that DS-HFF displayed a higher steady level of intramitochondrial Ca^{2+} when compared with N-HFF, with the CDS-HFF exhibiting the highest $mtCa^{2+}$. A linear positive correlation was found between $mtCa^{2+}$ and ROS generation in the three cytotype samples. Most notably, blockage of the major mitochondrial Ca^{2+}-transporting system resulted in substantial depression of ROS overproduction in DS-HFF, whereas it was ineffective in N-HFF. Moreover, ruthenium red treatment resulted in full recovery of the respiratory activity in DS-HFF. All together, these observations would argue for a linkage between chronic intramitochondrial Ca^{2+} levels, inhibition of complex I and mitochondrial ROS production. Although

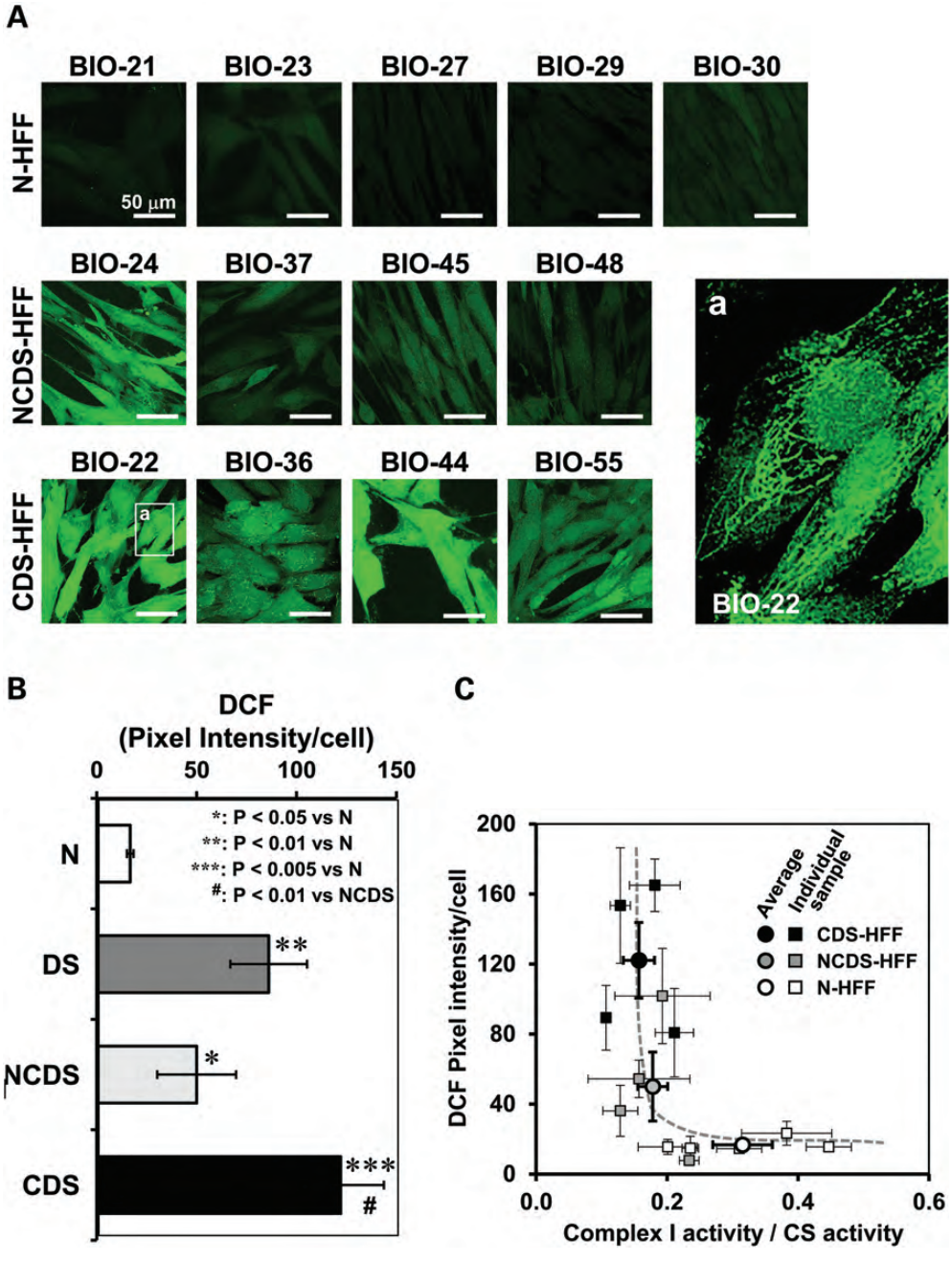

Figure 6. Confocal microscopy analysis of ROS production in DS live fibroblasts. (**A**) Representative LSCM imaging of the DCF-related fluorescence of euploid (N-HFF) and DS (NCDS-HFF and CDS-HFF) fibroblasts. A representative magnification of an intracellular selected detail (white rectangle) of the indicated CDS sample is shown displaying compartmentalization of the brighter DCF fluorescence signal. (**B**) Statistical analysis of the fluorescence intensity per cell as resulting from the averaged values ± SEM of about 100 randomly selected different cells for each sample from at least in-duplicate experiments; statistical analysis of the differences is also shown. (**C**) Correlation plot between the complex I activity normalized to the CS activity and the DCF-related fluorescence signal/cell for individual and averaged fibroblast samples (see symbol legend, means ± SEM).

we have not specifically addressed the cause of the Ca^{2+} homeostasis deregulation in trisomic cells, a survey of the literature suggests that cross-talk between PPARγ and Ca^{2+} mobilization/signalling (37) may be likely in this case. *PGC-1α* is an important coactivator of the *PPARs* transcription factor family, mainly *PPARγ* (38,39). Depression of *PGC-1α* activity, observed in DS-HFF samples, would consequently affect the transcriptional efficiency of *PPARs*-controlled genes.

PGC-1α function is both antagonized and regulated by a gene mapping to Hsa21, the nuclear receptor interacting protein *RIP140*. This highly conserved gene shows a 1.5- to 4-fold upregulation both in the heart and fibroblasts from DS subjects. The upregulation of *RIP140* protein was also demonstrated in the DS hippocampus (40). In the same experiment, the authors demonstrated that *SUMO3* (another gene mapping to Hsa21) is also upregulated in these cells. It was

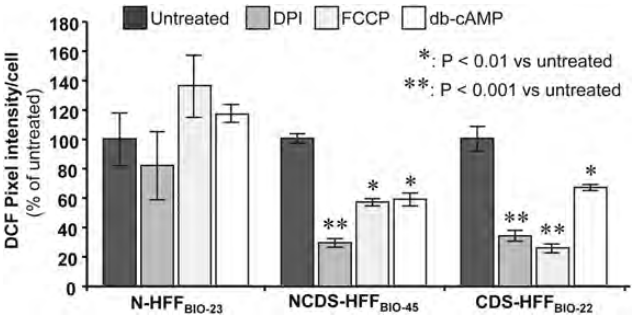

Figure 7. Effect of FCCP, DPI and db-cAMP on ROS production in DS fibroblasts. Cultured foetus-derived fibroblasts representative of euploid (BIO23) and DS non-cardiopathic (BIO45) or cardiopathic (BIO22) samples were treated for 2 h with either of 0.5 μM FCCP, 100 μM DPI or 100 μM db-cAMP and then assessed by LSCM for ROS production by DCF. The values shown are means ± SEM ($n = 3$ under each condition) of the DCF-related fluorescence intensity/cell normalized for each fibroblast sample to untreated cells. When statistically significant, the difference between untreated and compound-treated cells is reported.

demonstrated that the sumoylation of *RIP140* modulates its repressive activity (41). The simultaneous upregulation of both the Hsa21 genes, due to the primary dosage effect, might exert a synergistic effect. Silencing and re-expression experiments showed that *RIP140* expression significantly affects oxidative metabolism and mitochondrial biogenesis (42). Even mild *RIP140* overexpression repressed nuclear mitochondrial genes involved in all the respiratory chain complexes (43). We previously demonstrated that the same genes were repressed in DS foetal hearts (3).

Two other genes mapping to Hsa21, the kinase *DYRK1A* and the regulator of calcineurin 1 (*DSCR1/RCAN1*), were demonstrated to control *PGC-1α* via the *Calcineurin/NFAT* pathway, largely through the binding of *NFATc* to the *PGC-1α* promoter (44). The concurrent overexpression of the Hsa21 genes RIP140, SUMO3, *RCAN1* and *DYRK1A* and the downregulation of NFATc genes (45), observed in DS samples, is expected to result in the depression of *PGC-1α* expression.

In this study, we have demonstrated that some mitochondrial alterations are more pronounced in fibroblasts derived from DS foeti with heart defects. It must be pointed out that not all the subjects with trisomy 21 develop congenital cardiopathies, even though a heart developmental delay has been demonstrated in all DS human embryos at 8–10 gestational weeks (46). This suggests that a different inter-individual genetic background may affect the severity of the cardiopathic outcome in DS patients by impairing the oxidative metabolism. Assuming that altered cardiovascular development in DS likely originates from the trisomy of a critical Hsa21 region between *Tiam1* and *Kcnj6* (47), a more severe cardiac phenotype might be associated with different bioenergetic phenotypes characterized, at the cellular level, by a larger mitochondrial Ca^{2+} load and related ROS generation, as observed in CDS-HFF. Interesting is the evidence that the induction of oxidative stress in pregnant mice on day 7.5 disrupts cardiac neural crest migration and causes outflow tract defects like that observed in DS, and that antioxidant administration before the induction prevents the heart defects (48). Implications of our findings have a potential therapeutic value, as a number of drugs are becoming available to specifically inhibit the observed mitochondrial alterations. Some protocols are being developed to improve oxidative imbalance in DS using antioxidants such as the coenzyme Q10 (49,50). On the basis of our results, we also plan to investigate the effects of PPARγ agonists and/or of PGC-1α activators. The combination of these pharmacologically active compounds might correct mitochondria-related dysfunctions in trisomic foeti/patients.

MATERIALS AND METHODS

Ethics Statement

Human primary lines of HFF used in this study were obtained from the 'Telethon Bank of Fetal Biological Samples' at the University of Naples according to protocols approved by the local Institutional Ethics Committee.

Samples

Skin biopsies were explanted from 13 human foeti after therapeutic abortion at 18–22 gestational weeks and were classified as follows: five euploid human foeti (N-HFF) and eight foeti with trisomy of Hsa21 (DS-HFF) including four foeti with CHD, named CDS-HFF and four foeti without heart defects, named NCDS-HFF (Supplementary Material, Table S1). Fibroblasts from biopsies were cultured in T25 flasks (BD Falcon) with Chang medium B+C (Irvine Scientific) supplemented with 1% penicillin/streptomycin (Gibco) at 37°C in 5% CO_2 atmosphere; all the analyses described throughout this study were carried out at passages 4–5. Karyotype analysis was performed by standard G-banding technique.

The presence of CHD was established by colour Doppler foetal echocardiography followed by direct examination at the time of tissue explantation and dissection.

RNA extraction and quantitative real-time PCR

Total RNA from each sample was extracted using TRIzol reagent (Gibco/BRL Life Technologies, Inc., Gaithersburg, MD, USA) and was reverse-transcribed using the iScript cDNA Synthesis kit (Bio-Rad Laboratories Inc., Hercules, CA, USA). Real-time PCR was performed using iQ Supermix SYBR Green 2X on a Bio-Rad iCycler according to the manufacturer's protocols. PCR reactions were performed in triplicate. Primer pairs (MWG Biotech, Ebersberg, Germany) were designed using the Primer 3 software (http://frodo.wi.mit.edu/primer3) to obtain amplicons ranging from 100 to 150 bp (Supplementary Material, Table S2). *GAPDH* and *RPL13A* housekeeping genes were chosen as reference genes.

Morphological analysis

Fibroblasts from trisomic and euploid foeti were fixed and embedded for the electron microscope, using agarose as an intermediate embedding medium (51). Cells were fixed in petri dishes with 4% paraformaldehyde and 5% glutaraldehyde in PBS buffer (0.1 M, pH 7.3) for 30 min at room temperature,

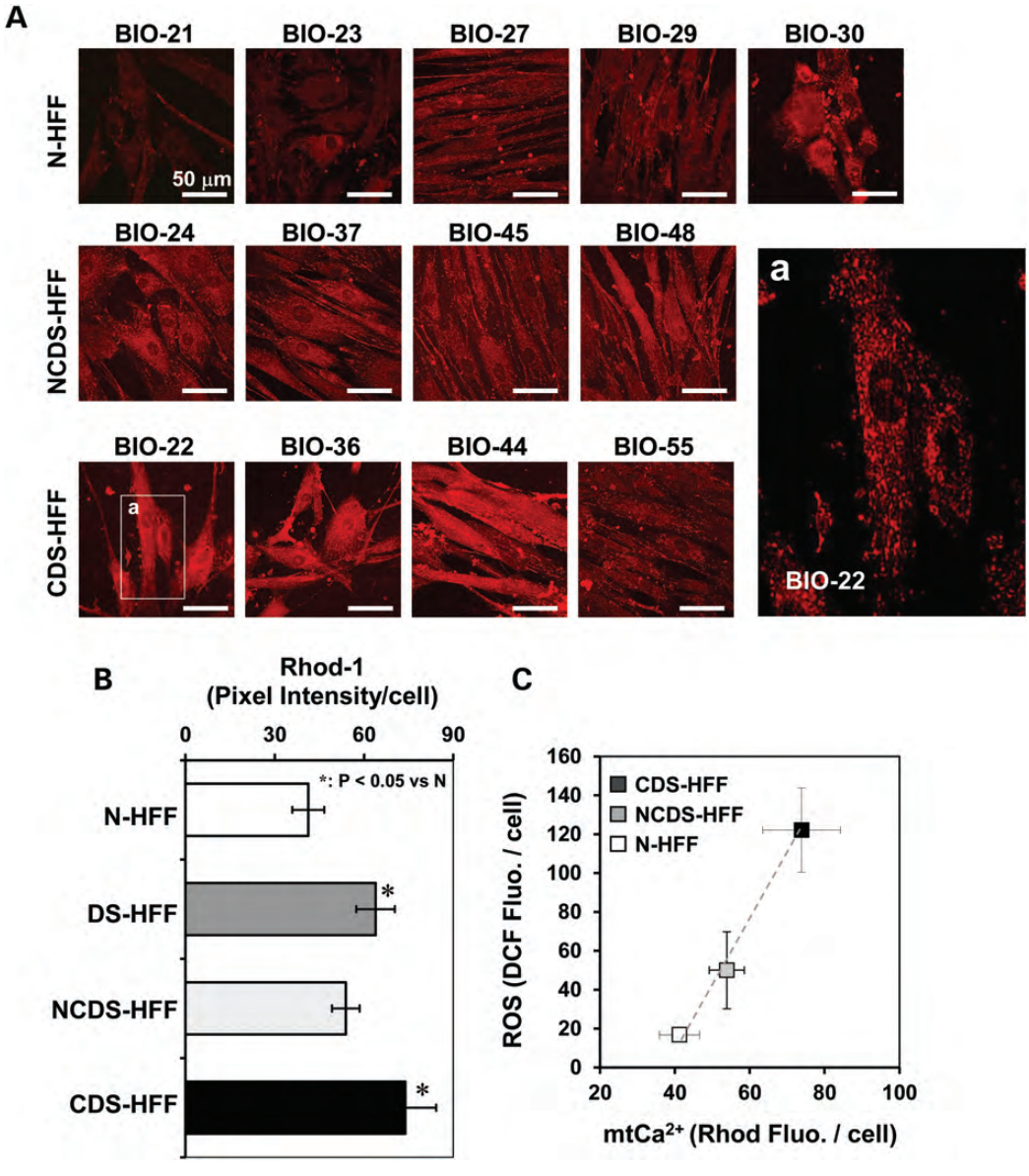

Figure 8. Confocal microscopy analysis of mitochondrial Ca^{2+} in DS live fibroblasts. (**A**) Representative LSCM imaging of the Rhod-1-related fluorescence of euploid (N-HFF) and DS (NCDS-HFF and CDS-HFF) fibroblasts. A representative magnification (white rectangle) of the indicated CDS sample is shown displaying the punctuate compartmentalization of the Rhod-1-fluorescence signal. (**B**) Statistical analysis of the fluorescence intensity per cell as resulting from the averaged values ± SEM of about 100 randomly selected different cells for each sample from at least in-duplicate experiments; when statistically significant, the difference when compared with the euploid samples is shown. (**C**) Correlation plot between the Rhod-1- and DCF-related fluorescence signal/cell for averaged fibroblast samples (see symbol legend, means ± SEM).

then washed in buffer, scraped from culture plates and pelleted by centrifugation for 10 min at 2000*g*; the supernatant was discarded and the cells were resuspended in 1 ml of 2% liquid agarose at 65°C. Again, the reaction tube was centrifuged for 5 min at 1000*g* to concentrate the cells in agarose. The agarose-cell pellet was solidified in ice for 30 min, and then the agarose cone was carefully taken out of the reaction tube and divided into small pieces (1 mm^3). The agarose-cell blocks were post-fixed in osmium tetroxide (1% in PBS buffer) for 1 h at 4°C, dehydrated and transferred first to propylene oxide, then to a mixture of propylene oxide-Epon (1:1) and finally embedded in Epon resin. The Epon blocks were polymerized for 2 days at 60°C and then sectioned with a diamond knife to give thin sections, 70–80 nm each; the sections were picked up on 200 mesh copper grids, stained with uranyl acetate (5% in 50% methanol) and Reynolds lead citrate (52) and observed on a Philips 208S transmission electron microscope. Micrographs were acquired with a Mega View II Soft Imaging System camera. Three N-HFF (BIO-21, BIO-23, BIO-27) and six DS-HFF samples (BIO24, BIO-36, BIO-37, BIO-44, BIO-48 and BIO55) were analysed using the 'fractionator' method to obtain a systematic and uniformly random sampling, which ensures that even for relatively small samples, the error is so small that it may safely be ignored (53). Fifty cells per sample were analysed and for each cell the percentages of inner and outer membrane

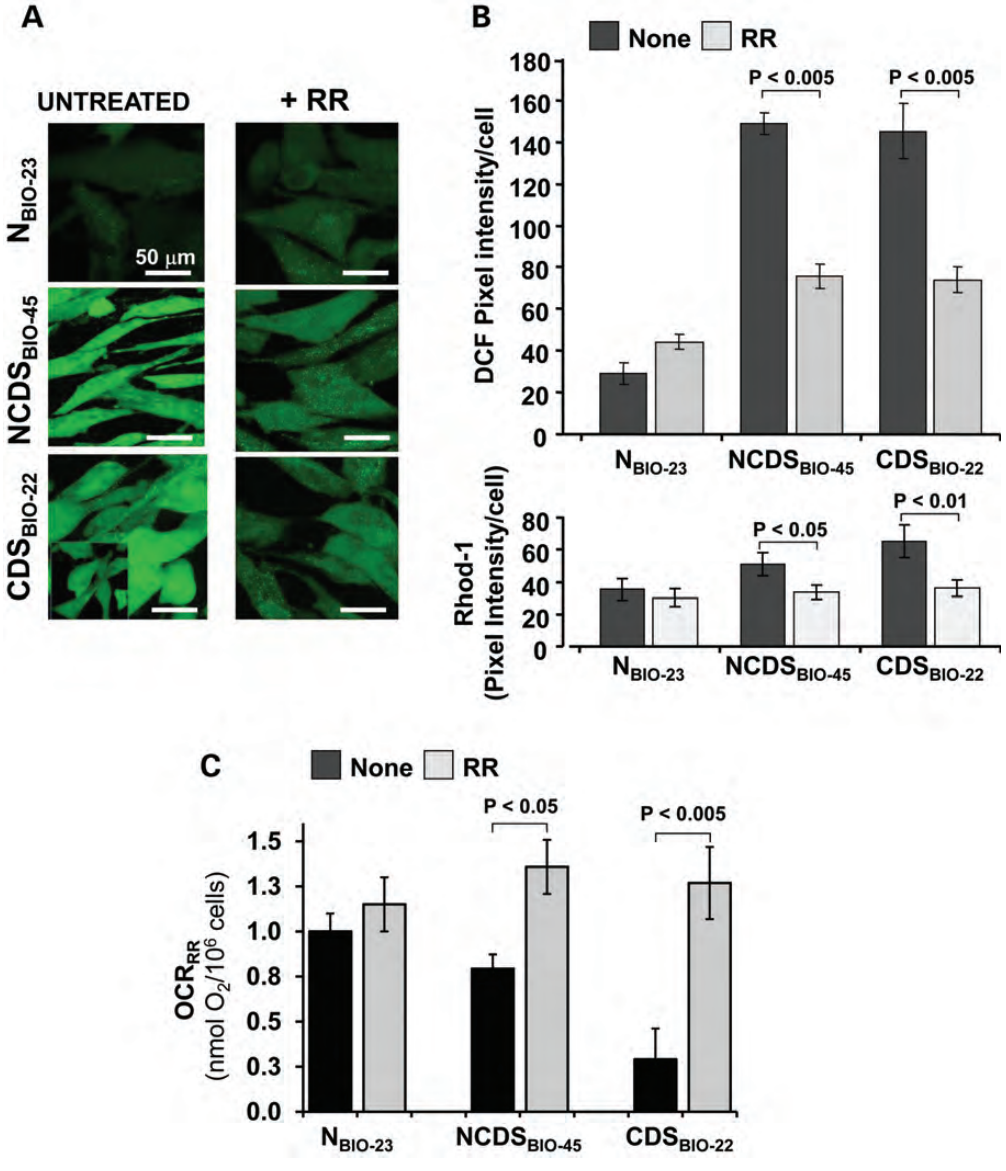

Figure 9. Effect of ruthenium red on ROS production and respiratory activity in DS live fibroblasts. Cultured foetus-derived fibroblasts representative of euploid (BIO23) and DS non-cardiopathic (BIO45) or cardiopathic (BIO22) samples were treated with 10 μM ruthenium red (RR) for 4 h and then assessed by LSCM for ROS production and $mtCa^{2+}$ by DCF and Rhod-1, respectively. (**A**) DCF-related fluorescence imaging of untreated and RR-treated fibroblasts (representative of three different experiments). (**B**) Statistical analysis of the DCF-related (upper histogram) and Rhod-1-related (lower histogram) fluorescence intensity per cell. The average values ± SEM of about 100 randomly selected different cells for each sample from three different experiments are shown. (**C**) Effect of RR on the respiratory activity of the same representative samples of N-, NCDS- and CDS-HFF as in (A). The OCR_{RR} was measured as described in the legend of Figure 3 and treatment with RR as in (A); the bars are means ± SEM of the average determinations for each sample (untreated and RR-treated) carried out in triplicate. When statistically significant, the difference between untreated and RR-treated cells is reported in (B) and (C).

breakages, branched mitochondria and mitochondria with concentric or longitudinal cristae were determined. Furthermore, for each sample, 25 micrographs were collected to evaluate the mitochondrial volume density (Vmt, relative volume of mitochondria on cell volume) and mitochondrial cristae volume density (Vmc, relative volume of mitochondrial cristae on mitochondria volume) (54). The volume density (also named relative volume or volume fraction) is a ratio between volumes. This is an intuitive parameter, unbiasedly estimated by overlaying a test system of points on images and then counting those falling over the objects of interest and those over the reference space. The ratio of points gives the estimation of volume. According to Delesse's principle, the volume fraction of an object varies proportionally to their area fraction as measured in random 2D sections; this means that each point controls an area in a 2D section and is related to a defined volume in the 3D organ (55).

Western blot analysis

Cells were washed twice with ice-cold PBS and lysed in RIPA buffer (NaCl 154 mM; Deoxicolic Acid 12 mM; NaF 0.95 mM;

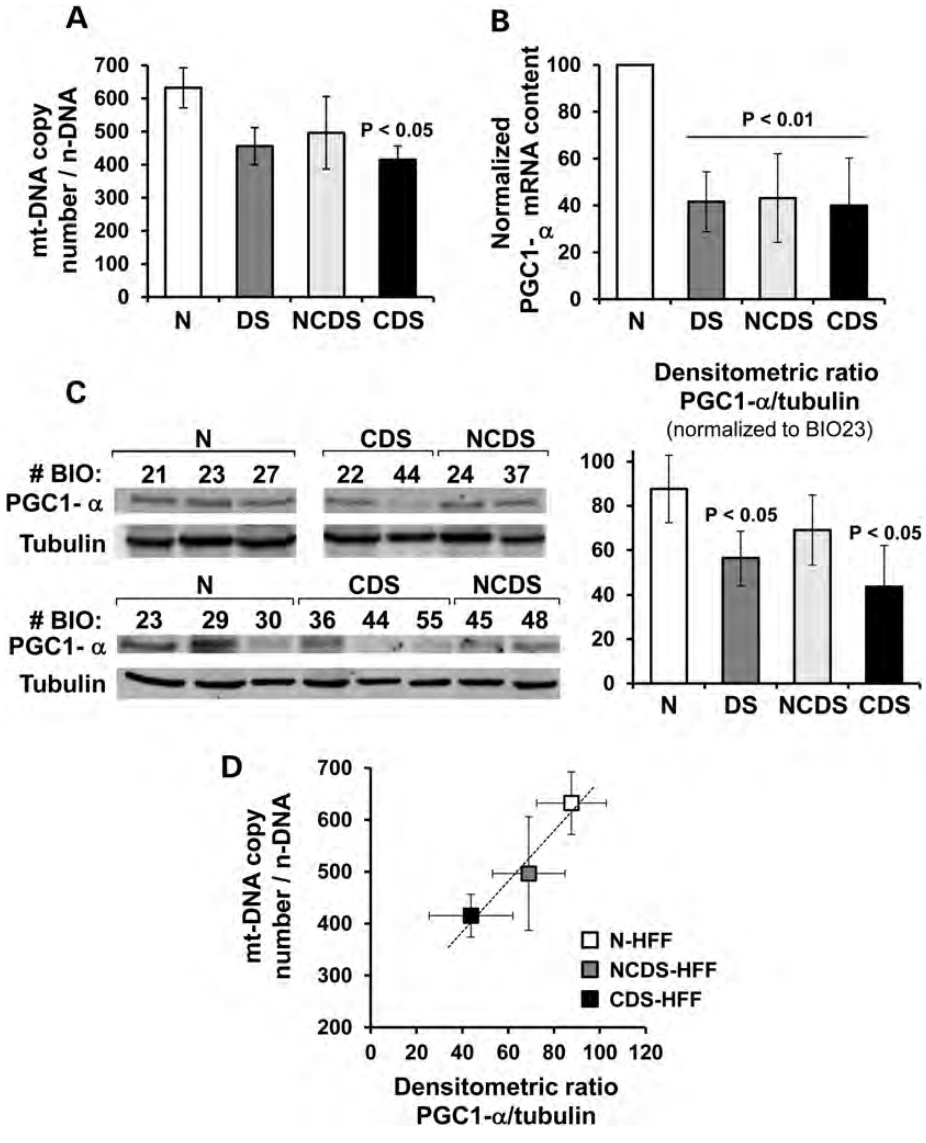

Figure 10. Analysis of the mitochondrial DNA content and expression of PGC-1α in DS fibroblasts. (**A**) Absolute qRT-PCR analysis of mtDNA (see Materials and Methods for details). The bars are means ± SEM from five euploid and eight DS fibroblast samples; a distinction between non-cardiopathic (NCDS, $n = 4$) and cardiopathic (CDS, $n = 4$) foetus-derived fibroblasts is also reported. (**B**) Expression analysis of the PGC-1α by qRT-PCR. The values, means ± SEM, of the DS samples are normalized to that of the euploid fibroblasts. (**C**) Analysis of the PGC-1α protein. (Panel on the left) Western blotting of PGC-1α on total cellular protein extracts from euploid and DS samples (representative of two to three different analyses carried out for each sample). (Panel on the right) Densitometric analysis of the PGC-1α-related immunodetected bands (means ± SEM of two to three assays). To compare different electrophoretic runs, the densitometric value (normalized to tubulin) of the euploid sample BIO-23 was taken as an internal reference. When statistically significant, the *P*-value, when compared with the euploid samples, is shown in (A and B) and (C and **D**) Correlation plot between the normalized PGC-1α protein expression and the mt-DNA copy number for averaged fibroblast samples (see symbol legend, means ± SEM).

Triton X-100 1%; SDS 2%; PMSF 2 mM) in phosphate buffer in the presence of protease inhibitors. The protein concentration was determined using the Bio-Rad protein assay (Bio-Rad Laboratories Inc.). For western blot analysis, total lysates were boiled for 5 min in Laemmli sample buffer and analysed on 7.5% SDS–PAGE. Gels were then blotted onto nitrocellulose transfer membranes (Schleicher and Shuell GmbH, Dassel, Germany) using a Bio-Rad apparatus. After transfer, the filters were blocked at room temperature for 1 h with 5% BSA in TTBS (150 mM NaCl, 20 mM Tris-HCl pH 7.5). After washing twice with TTBS (150 mM NaCl, 20 mM Tris-HCl pH 7.5, 0.1% Tween 20), filters were incubated overnight at 4°C with rabbit polyclonal primary antibody to *PGC-1α* (1:1000, Abcam, Cambridge Science Park, Cambridge, UK). The filters were washed extensively with TTBS and incubated for 1 h at room temperature with anti-rabbit peroxidase-conjugated secondary antibody (Amersham, Little Chalfont, Buckinghamshire, UK) diluted 1:1000 in TTBS. The filters were then washed six times with TTBS and once with TBS and developed using an ECL western blotting substrate detection method (Pierce, Rockford, IL, USA). For reprobing, the nitrocellulose filters were re-hydrated and

stripped for 30 min at 37°C in restore western blotting stripping buffer (Pierce) and washed extensively with TTBS. Results were standardized to alpha tubulin and analysed using NIH Image J (Rasband, W.S., ImageJ, U. S. National Institutes of Health, Bethesda, Maryland, USA, http://imagej.nih.gov/ij/, 1997–2012).

Measurement of the respiratory activity in intact cells

Cultured cells were gently detached from the dish by tripsinization, washed in PBS, harvested by centrifugation at 500*g* for 5 min and immediately assessed for O_2 consumption with a high-resolution oxymeter (Oxygraph-2k, Oroboros Instruments). About 1×10^6 viable cells per ml were assayed in 50 mM KPi, 10 mM Hepes, 1 mM EDTA, pH 7.4 at 37°C; after attainment of a stationary endogenous substrate-sustained resting oxygen consumption rate (OCR_{RR}), 2 μg/ml of the ATP-synthase inhibitor oligomycin was added (OCR_{OL}) followed by addition of 0.5 mM of the uncoupler carbonilcyanide p-triflouromethoxyphenylhydrazone (FCCP) (OCR_{UNC}). The rates of oxygen consumption were corrected for 2 mM KCN-insensitive respiration. The RCR was obtained by the ratio OCR_{UNC}/OCR_{OL}, the leak by the ratio OCR_{OL}/OCR_{UNC} and the ATP-synthesis-linked respiration (OXPHOS) by the ratio $(OCR_{RR}\text{-}OCR_{OL})/OCR_{UNC}$ (56).

Measurement of the activity of mitochondrial respiratory chain complexes

The specific activities of NADH:ubiquinone oxidoreductase (complex I), ubiquinone:cytochrome c oxidoreductase (complex III) and cytochrome c oxidase (complex IV) were assayed spectrophotometrically on frozen-thawn and ultrasound-treated cells in 10 mM Tris, 1 mg/ml serum albumin, pH 8.0. Complex I was assayed (in the presence of 1 μg/ml of antymicin A *plus* 2 mM KCN) by following the initial 2 μg/ml rotenone-sensitive rate of 50 μM NADH oxidation ($\varepsilon_{340nm} = 6.22\ mM^{-1}\ cm^{-1}$) in the presence of 200 μM decylubiquinone (dUQ) as electron acceptor; complex III was assayed (in the presence of rotenone *plus* KCN) by following the initial 1 μg/ml antymicin A-sensitive rate of 50 μM ferri-cytochrome *c* reduction ($\varepsilon_{550nm} = 21.1\ mM^{-1}\ cm^{-1}$) in the presence of 200 μM $dUQH_2$ as electron donor. Complex IV was assayed by following (in the presence of antymicin A) the initial 2 mM KCN-sensitive rate of 20 μM ferro-cytochrome *c* oxidation under aerobic conditions. The activities were normalized to the initial cell number and to cellular protein content (57). Citrate synthase catalyses the reaction between acetyl coenzyme A and oxaloacetic acid to form citric acid. Citrate synthase activity was assayed spectrophotometrically ($\varepsilon_{412nm} = 13.6\ mM^{-1}\ cm^{-1}$) measuring the reaction between CoA-SH and DTNB (5,5′-dithiobis (2-nitrobenzoic acid)) to form 5-thio-2-nitrobenzoic acid (TNB) (58).

Laser scanning confocal microscopy (LSCM) live cell imaging of mitochondrial membrane potential, ROS and $mtCa^{2+}$

Cells cultured at low density on fibronectin-coated 35-mm glass-bottom dishes were incubated for 20 min at 37°C with the either of the following probes: 2 μM tetramethylrhodamine ethyl ester (TMRE) to monitor mitochondrial membrane potential ($\Delta\Psi_m$); 10 μM 2,7-dichlorofluorescin diacetate, which is converted to dichlorofluorescein by intracellular esterases, for detection of H_2O_2; 5 μM X-Rhod-1 AM for mitochondrial Ca^{2+}. All probes were from Molecular Probes (Eugene, OR). Stained cells were washed with PBS and examined with a Nikon TE 2000 microscope [images collected using a ×60 objective (1.4 NA)] coupled to a Radiance 2100 dual-laser LSCM system (Bio-Rad). TMRE and Rhod-1 red fluorescence were elicited by exciting with the He–Ne laser beam (λex 543 nm), whereas dichlorofluorescein green fluorescence was elicited with the Ar–Kr laser beam (λex 488 nm). Acquisition, storage and analysis of data were performed with LaserSharp and LaserPix software from Bio-Rad or ImageJ version 1.37. Superimposed confocal planes were analysed by means of the 'stack' function of the LCS-Analysis Tools, which produced an *xz* intensity profile of the average value of the pixels within marked edges, including a single cell, as a function of each focal plane. The integrated value of the *xz* profile was taken as a measure of the fluorescence intensity of that individual cell relative to the selected emission channel. Correction was made for the minimal background by repeating the procedure in a cell-free field. About 100 single cells were analysed for each imaging analysis (57).

Statistics

The ANOVA test with Bonferroni *post hoc* correction was applied to evaluate the statistical significance of differences measured throughout the data sets presented. Concerning stereological investigations, the data obtained from each sample were averaged per group (N-HFF, DS-HFF, NCDS-HFF and CDS-HFF) and statistical evaluations were performed by using two nonparametric statistical tests, the Kolmogorov–Smirnov and the Kruskal–Wallis tests. The threshold for statistical significance (*P*-value) was set to 0.05.

SUPPLEMENTARY MATERIAL

Supplementary Material is available at *HMG* online.

Conflict of Interest statement. None declared.

FUNDING

This work was supported by grants from Campania Region (POR CREME to L.N.) and from the Italian Ministry of University and Research (PRIN-2008FJJHKM_001 to N.C.).

REFERENCES

1. Epstein, C.J., Korenberg, J.R., Anneren, G., Antonarakis, S.E., Ayme, S., Courchesne, E., Epstein, L.B., Fowler, A., Groner, Y., Huret, J.L *et al.* (1991) Protocols to establish genotype-phenotype correlations in Down syndrome. *Am. J. Hum. Genet.*, **49**, 207–235.
2. Park, S.C., Mathews, R.A., Zuberbuhler, J.R., Rowe, R.D., Neches, W.H. and Lenox, C.C. (1977) Down syndrome with congenital heart malformation. *Am. J. Dis. Child*, **131**, 29–33.

3. Conti, A., Fabbrini, F., D'Agostino, P., Negri, R., Greco, D., Genesio, R., D'Armiento, M., Olla, C., Paladini, D., Zannini, M *et al.* (2007) Altered expression of mitochondrial and extracellular matrix genes in the heart of human fetuses with chromosome 21 trisomy. *BMC Genomics*, **8**, 268.
4. Busciglio, J. and Yankner, B.A. (1995) Apoptosis and increased generation of reactive oxygen species in Down's syndrome neurons in vitro. *Nature*, **378**, 776–779.
5. Busciglio, J., Pelsman, A., Wong, C., Pigino, G., Yuan, M., Mori, H. and Yankner, B.A. (2002) Altered metabolism of the amyloid beta precursor protein is associated with mitochondrial dysfunction in Down's syndrome. *Neuron*, **33**, 677–688.
6. Roat, E., Prada, N., Ferraresi, R., Giovenzana, C., Nasi, M., Troiano, L., Pinti, M., Nemes, E., Lugli, E., Biagioni, O *et al.* (2007) Mitochondrial alterations and tendency to apoptosis in peripheral blood cells from children with Down syndrome. *FEBS Lett.*, **581**, 521–525.
7. Schuchmann, S. and Heinemann, U. (2000) Increased mitochondrial superoxide generation in neurons from trisomy 16 mice: a model of Down's syndrome. *Free Radic. Biol. Med.*, **28**, 235–250.
8. Shukkur, E.A., Shimohata, A., Akagi, T., Yu, W., Yamaguchi, M., Murayama, M., Chui, D., Takeuchi, T., Amano, K., Subramhanya, K.H *et al.* (2006) Mitochondrial dysfunction and tau hyperphosphorylation in Ts1Cje, a mouse model for Down syndrome. *Hum. Mol. Genet.*, **15**, 2752–2762.
9. Kim, S.H., Vlkolinsky, R., Cairns, N., Fountoulakis, M. and Lubec, G. (2001) The reduction of NADH ubiquinone oxidoreductase 24- and 75-kDa subunits in brains of patients with Down syndrome and Alzheimer's disease. *Life Sci.*, **68**, 2741–2750.
10. Bambrick, L.L. and Fiskum, G. (2008) Mitochondrial dysfunction in mouse trisomy 16 brain. *Brain Res.*, **1188**, 9–16.
11. Valenti, D., Manente, G.A., Moro, L., Marra, E. and Vacca, R.A. (2011) Deficit of complex I activity in human skin fibroblasts with chromosome 21 trisomy and overproduction of reactive oxygen species by mitochondria: involvement of the cAMP/PKA signalling pathway. *Biochem. J.*, **435**, 679–688.
12. Valenti, D., Tullo, A., Caratozzolo, M.F., Merafina, R.S., Scartezzini, P., Marra, E. and Vacca, R.A. (2010) Impairment of F1F0-ATPase, adenine nucleotide translocator and adenylate kinase causes mitochondrial energy deficit in human skin fibroblasts with chromosome 21 trisomy. *Biochem. J.*, **431**, 299–310.
13. Scarpulla, R.C. (2011) Metabolic control of mitochondrial biogenesis through the PGC-1 family regulatory network. *Biochim. Biophys. Acta*, **1813**, 1269–1278.
14. Mao, R., Wang, X., Spitznagel, E.L. Jr, Frelin, L.P., Ting, J.C., Ding, H., Kim, J.W., Ruczinski, I., Downey, T.J. and Pevsner, J. (2005) Primary and secondary transcriptional effects in the developing human Down syndrome brain and heart. *Genome Biol.*, **6**, R107.
15. Sharma, L.K., Lu, J. and Bai, Y. (2009) Mitochondrial respiratory complex I: structure, function and implication in human diseases. *Curr. Med. Chem.*, **16**, 1266–1277.
16. Bellomo, F., Piccoli, C., Cocco, T., Scacco, S., Papa, F., Gaballo, A., Boffoli, D., Signorile, A., D'Aprile, A., Scrima, R *et al.* (2006) Regulation by the cAMP cascade of oxygen free radical balance in mammalian cells. *Antioxid. Redox Signal*, **8**, 495–502.
17. Papa, S., Rasmo, D.D., Technikova-Dobrova, Z., Panelli, D., Signorile, A., Scacco, S., Petruzzella, V., Papa, F., Palmisano, G., Gnoni, A *et al.* (2012) Respiratory chain complex I, a main regulatory target of the cAMP/PKA pathway is defective in different human diseases. *FEBS Lett.*, **586**, 568–577.
18. Caviedes, P., Caviedes, R. and Rapoport, S.I. (2006) Altered calcium currents in cultured sensory neurons of normal and trisomy 16 mouse fetuses, an animal model for human trisomy 21 (Down syndrome). *Biol. Res.*, **39**, 471–481.
19. Li, H., Rao, A. and Hogan, P.G. (2011) Interaction of calcineurin with substrates and targeting proteins. *Trends Cell Biol.*, **21**, 91–103.
20. Yamato, F., Takaya, J., Yasuhara, A., Teraguchi, M., Ikemoto, Y. and Kaneko, K. (2009) Elevated intracellular calcium in neutrophils in patients with Down syndrome. *Pediatr. Int.*, **51**, 474–477.
21. De Stefani, D., Raffaello, A., Teardo, E., Szabo, I. and Rizzuto, R. (2011) A forty-kilodalton protein of the inner membrane is the mitochondrial calcium uniporter. *Nature*, **476**, 336–340.
22. Drago, I., Pizzo, P. and Pozzan, T. (2011) After half a century mitochondrial calcium in- and efflux machineries reveal themselves. *EMBO J.*, **30**, 4119–4125.
23. Peng, T.I. and Jou, M.J. (2010) Oxidative stress caused by mitochondrial calcium overload. *Ann. N. Y. Acad. Sci.*, **1201**, 183–188.
24. Chen, Y., Wang, Y., Chen, J., Chen, X., Cao, W., Chen, S., Xu, S., Huang, H. and Liu, P. (2012) Roles of transcriptional corepressor RIP140 and coactivator PGC-1alpha in energy state of chronically infarcted rat hearts and mitochondrial function of cardiomyocytes. *Mol. Cell. Endocrinol.*, **362**, 11–18.
25. Leone, T.C., Lehman, J.J., Finck, B.N., Schaeffer, P.J., Wende, A.R., Boudina, S., Courtois, M., Wozniak, D.F., Sambandam, N., Bernal-Mizrachi, C *et al.*. (2005) PGC-1alpha deficiency causes multi-system energy metabolic derangements: muscle dysfunction, abnormal weight control and hepatic steatosis. *PLoS Biol.*, **3**, e101.
26. Mitra, R., Nogee, D.P., Zechner, J.F., Yea, K., Gierasch, C.M., Kovacs, A., Medeiros, D.M., Kelly, D.P. and Duncan, J.G. (2012) The transcriptional coactivators, PGC-1alpha and beta, cooperate to maintain cardiac mitochondrial function during the early stages of insulin resistance. *J. Mol. Cell. Cardiol.*, **52**, 701–710.
27. Bersu, E.T., Ahmad, F.J., Schwei, M.J. and Baas, P.W. (1998) Cytoplasmic abnormalities in cultured cerebellar neurons from the trisomy 16 mouse. *Brain Res. Dev. Brain Res.*, **109**, 115–120.
28. John, G.B., Shang, Y., Li, L., Renken, C., Mannella, C.A., Selker, J.M., Rangell, L., Bennett, M.J. and Zha, J. (2005) The mitochondrial inner membrane protein mitofilin controls cristae morphology. *Mol. Biol. Cell*, **16**, 1543–1554.
29. Zerbes, R.M., Bohnert, M., Stroud, D.A., von der Malsburg, K., Kram, A., Oeljeklaus, S., Warscheid, B., Becker, T., Wiedemann, N., Veenhuis, M *et al.* (2012) Role of MINOS in mitochondrial membrane architecture: cristae morphology and outer membrane interactions differentially depend on mitofilin domains. *J. Mol. Biol.*, **422**, 183–191.
30. Darshi, M., Mendiola, V.L., Mackey, M.R., Murphy, A.N., Koller, A., Perkins, G.A., Ellisman, M.H. and Taylor, S.S. (2011) ChChd3, an inner mitochondrial membrane protein, is essential for maintaining crista integrity and mitochondrial function. *J. Biol. Chem.*, **286**, 2918–2932.
31. Zick, M., Rabl, R. and Reichert, A.S. (2009) Cristae formation-linking ultrastructure and function of mitochondria. *Biochim. Biophys. Acta*, **1793**, 5–19.
32. Lambert, A.J., Buckingham, J.A., Boysen, H.M. and Brand, M.D. (2008) Diphenyleneiodonium acutely inhibits reactive oxygen species production by mitochondrial complex I during reverse, but not forward electron transport. *Biochim. Biophys. Acta*, **1777**, 397–403.
33. Annerén, K.G., Korenberg, J.R. and Epstein, C.J. (1987) Phosphofructokinase activity in fibroblasts aneuploid for chromosome 21. *Hum. Genet.*, **76**, 63–65.
34. Selivanov, V.A., Votyakova, T.V., Pivtoraiko, V.N., Zeak, J., Sukhomlin, T., Trucco, M., Roca, J. and Cascante, M. (2011) Reactive oxygen species production by forward and reverse electron fluxes in the mitochondrial respiratory chain. *PLoS Comput. Biol.*, **7**, e1001115.
35. Adam-Vizi, V. and Starkov, A.A. (2010) Calcium and mitochondrial reactive oxygen species generation: how to read the facts. *J. Alzheimer Dis.*, **20**(Suppl. 2), S413–S426.
36. Feissner, R.F., Skalska, J., Gaum, W.E. and Sheu, S.S. (2009) Crosstalk signaling between mitochondrial Ca2+ and ROS. *Front. Biosci.*, **14**, 1197–1218.
37. Bush, C.R., Havens, J.M., Necela, B.M., Su, W., Chen, L., Yanagisawa, M., Anastasiadis, P.Z., Guerra, R., Luxon, B.A. and Thompson, E.A. (2007) Functional genomic analysis reveals cross-talk between peroxisome proliferator-activated receptor gamma and calcium signaling in human colorectal cancer cells. *J. Biol. Chem.*, **282**, 23387–23401.
38. Oyekan, A. (2011) PPARs and their effects on the cardiovascular system. *Clin. Exp. Hypertens*, **33**, 287–293.
39. Puigserver, P., Wu, Z., Park, C.W., Graves, R., Wright, M. and Spiegelman, B.M. (1998) A cold-inducible coactivator of nuclear receptors linked to adaptive thermogenesis. *Cell*, **92**, 829–839.
40. Gardiner, K. (2006) Transcriptional dysregulation in Down syndrome: predictions for altered protein complex stoichiometries and post-translational modifications, and consequences for learning/behavior genes ELK, CREB, and the estrogen and glucocorticoid receptors. *Behav. Genet.*, **36**, 439–453.
41. Rytinki, M.M. and Palvimo, J.J. (2009) SUMOylation attenuates the function of PGC-1alpha. *J. Biol. Chem.*, **284**, 26184–26193.
42. Powelka, A.M., Seth, A., Virbasius, J.V., Kiskinis, E., Nicoloro, S.M., Guilherme, A., Tang, X., Straubhaar, J., Cherniack, A.D., Parker, M.G *et al.* (2006) Suppression of oxidative metabolism and mitochondrial

biogenesis by the transcriptional corepressor RIP140 in mouse adipocytes. *J. Clin. Invest.*, **116**, 125–136.
43. Seth, A., Steel, J.H., Nichol, D., Pocock, V., Kumaran, M.K., Fritah, A., Mobberley, M., Ryder, T.A., Rowlerson, A., Scott, J *et al.* (2007) The transcriptional corepressor RIP140 regulates oxidative metabolism in skeletal muscle. *Cell Metab.*, **6**, 236–245.
44. Handschin, C., Rhee, J., Lin, J., Tarr, P.T. and Spiegelman, B.M. (2003) An autoregulatory loop controls peroxisome proliferator-activated receptor gamma coactivator 1alpha expression in muscle. *Proc. Natl Acad. Sci. USA*, **100**, 7111–7116.
45. Arron, J.R., Winslow, M.M., Polleri, A., Chang, C.P., Wu, H., Gao, X., Neilson, J.R., Chen, L., Heit, J.J., Kim, S.K *et al.* (2006) NFAT dysregulation by increased dosage of DSCR1 and DYRK1A on chromosome 21. *Nature*, **441**, 595–600.
46. Gittenberger-de Groot, A.C., Bartram, U., Oosthoek, P.W., Bartelings, M.M., Hogers, B., Poelmann, R.E., Jongewaard, I.N. and Klewer, S.E. (2003) Collagen type VI expression during cardiac development and in human fetuses with trisomy 21. *Anat. Rec. A Discov. Mol. Cell. Evol. Biol.*, **275**, 1109–1116.
47. Liu, C., Morishima, M., Yu, T., Matsui, S., Zhang, L., Fu, D., Pao, A., Costa, A.C., Gardiner, K.J., Cowell, J.K *et al.* (2011) Genetic analysis of Down syndrome-associated heart defects in mice. *Hum. Genet.*, **130**, 623–632.
48. Morgan, S.C., Relaix, F., Sandell, L.L. and Loeken, M.R. (2008) Oxidative stress during diabetic pregnancy disrupts cardiac neural crest migration and causes outflow tract defects. *Birth Defects Res. A Clin. Mol. Teratol.*, **82**, 453–463.
49. Miles, M.V., Patterson, B.J., Chalfonte-Evans, M.L., Horn, P.S., Hickey, F.J., Schapiro, M.B., Steele, P.E., Tang, P.H. and Hotze, S.L. (2007) Coenzyme Q10 (ubiquinol-10) supplementation improves oxidative imbalance in children with trisomy 21. *Pediatr. Neurol.*, **37**, 398–403.
50. Tiano, L., Carnevali, P., Padella, L., Santoro, L., Principi, F., Bruge, F., Carle, F., Gesuita, R., Gabrielli, O. and Littarru, G.P. (2011) Effect of Coenzyme Q10 in mitigating oxidative DNA damage in Down syndrome patients, a double blind randomized controlled trial. *Neurobiol. Aging*, **32**, 2103–2105.
51. Kerstens, H.M., Robben, J.C., Poddighe, P.J., Melchers, W.J., Boonstra, H., de Wilde, P.C., Macville, M.V. and Hanselaar, A.G. (2000) AgarCyto: a novel cell-processing method for multiple molecular diagnostic analyses of the uterine cervix. *J. Histochem. Cytochem.*, **48**, 709–718.
52. Reynolds, E.S. (1963) The use of lead citrate at high pH as an electron-opaque stain in electron microscopy. *J. Cell Biol.*, **17**, 208–212.
53. Gundersen, H.J. (2002) The smooth fractionator. *J. Microsc.*, **207**, 191–210.
54. Weibel, E.R., Kistler, G.S. and Scherle, W.F. (1966) Practical stereological methods for morphometric cytology. *J. Cell Biol.*, **30**, 23–38.
55. Marcos, R., Monteiro, R.A. and Rocha, E. (2012) The use of design-based stereology to evaluate volumes and numbers in the liver: a review with practical guidelines. *J. Anat.*, **220**, 303–317.
56. Piccoli, C., Scrima, R., Quarato, G., D'Aprile, A., Ripoli, M., Lecce, L., Boffoli, D., Moradpour, D. and Capitanio, N. (2007) Hepatitis C virus protein expression causes calcium-mediated mitochondrial bioenergetic dysfunction and nitro-oxidative stress. *Hepatology*, **46**, 58–65.
57. Cela, O., Piccoli, C., Scrima, R., Quarato, G., Marolla, A., Cinnella, G., Dambrosio, M. and Capitanio, N. (2010) Bupivacaine uncouples the mitochondrial oxidative phosphorylation, inhibits respiratory chain complexes I and III and enhances ROS production: results of a study on cell cultures. *Mitochondrion*, **10**, 487–496.
58. Barrientos, A., Fontanesi, F. and Diaz, F. (2009) Evaluation of the mitochondrial respiratory chain and oxidative phosphorylation system using polarography and spectrophotometric enzyme assays. *Curr. Protoc. Hum. Genet.*, **Chapter 19**, Unit19.13.

SUPPLEMENTARY MATERIALS

Table S1
Characteristics of the primary lines of foetal fibroblasts obtained from foetuses after therapeutic abortion at 18-22 gestational weeks.

		NAME	KARYOTYPE	HEART DEFECT
N-HFF		BIO-21	46,XY	NO
		BIO-23	46,XX	NO
		BIO-27	46,XX	NO
		BIO-29	46,XY	NO
		BIO-30	46,XY	NO
DS-HFF	**NCDS-HFF**	BIO-24	47,XY,+21	NO
		BIO-37	47,XY,+21	NO
		BIO-45	47,XX,+21	NO
		BIO-48	47,XY,+21	NO
	CDS-HFF	BIO-22	47,XX,+21	TOF
		BIO-36	47,XX,+21	TOF
		BIO-44	47,XX,+21	AVC
		BIO-55	47,XX,+21	AVC

N-HFF = fibroblasts from euploid human foeti; DS-HFF = fibroblasts from foeti with trisomy of Hsa21; CDS-HFF = fibroblasts from foeti with congenital heart defects; NCDS-HFF = fibroblasts from foeti without heart defects.

Heart defects: TOF= Tetralogy of Fallot; AVC= Atrio-Ventricular Canal defect.

TABLE S2. Genes analyzed in this study by qRT-PCR.

GENE NAME	PRIMER SEQUENCES
BTG3	**LEFT:** GAGGCAGTTGAGAGGTTTGC **RIGHT:** GAGTGAGCTCCTTTGGCAAG
ITSN1	**LEFT:** GTGAGCGGCACTGATTTGT **RIGHT:** GATCATGCTTCGCTCTTTCC
DYRK1A	**LEFT:** GATATCATATGGGTCAGGTCATTTT **RIGHT:**CTGGACTGTAACATAACACAGTATGC
SOD1	**LEFT:** GCATCATCAATTTCGAGCAG **RIGHT:** CAGCCTCTGTATTATCTCCAA
NRF1	**LEFT**: AAACGGAAACGGCCTCAT **RIGHT**: CTTGCTGTCCCACACGAGTA
IMMT	**LEFT**: AGTTTGTCCTCCGTCCATTG **RIGHT**: CCACCAATACCTCCACCAAC
PGC1A	**LEFT**: ACAGAACTGAGGGACCGTTTT **RIGHT**: TTTCAAGAGCAGCAAAAGCA
NRF2	**LEFT**: CCTGAACTGGTTGCACAGAA **RIGHT**: ACAAATCATGTCCCCATCGT
RIP140	**LEFT**: TGCCGTTGACAAAAAGTCTG **RIGHT**: CTTTGACAGGTGGGAAATGC
NDUFA1	**LEFT**: CTGGCTACTGCGTACATCCA **RIGHT**: TGCGCCTATCTCTTTCCATC
NDUFA8	**LEFT**: GTCATGCCGGGGATAGTG **RIGHT**:TTAAGCACAGCAGAACTAATTTTCA
NDUFB8	**LEFT**: GCCAAGAAGTATAATATGCGTGTG **RIGHT**: GTCAGGGAGCTTCGGGTAG
NDUFS2	**LEFT**: GAATGGGCACAGGAGTTTG **RIGHT**: GGCCCAAAGTTCAGGGTAAT
NDUFS6	**LEFT**: AGAAGGTCACGCACACTGG **RIGHT**: CACGGGCTGCTCTGCTAT
RCAN1	**LEFT:** TTTGCTCAGACCTTACACATAGGA **RIGHT:** GGGAGGGGAGATCAGAAACT
NFATC2	**LEFT:** GAGTTCACATCCCAGAGTCCA **RIGHT:** GAGCACTCGATGGGGTTAGA
NFATC3	**LEFT:** CTTTGCAATGGCAAGAGGA **RIGHT:** GATGAGGCACAGGCAAAGAT
NFATC4	**LEFT:** GTGAGATCATTGGCCGAGAC **RIGHT**: CCAGGTGATGACAGTTCACG
GAPDH	**LEFT:** TGCACCACCAACTGCTTAGC **RIGHT:** GGCATGGACTGTGGTCATGAG
RPL13A	**LEFT:** CCTGGAGGAGAAGAGGAAAGAGA **RIGHT:** TTGAGGACCTCTGTGTATTTGTCA

Left and Right primer sequences, obtained from Primer 3 software, are indicated for each analyzed gene.

Figure S1. Intramitochondrial calcium measurements in DS-HFF samples with aequorin.

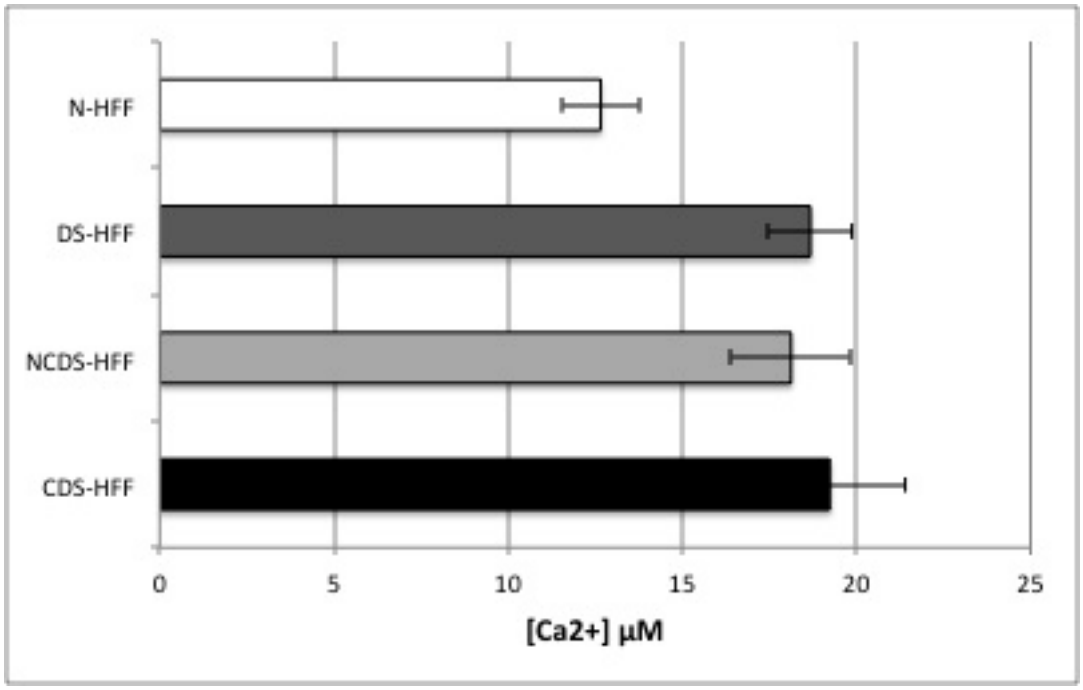

Starting from a calibration curve, we measured the mtCa^{2+} concentration in three samples per group on 15 coverslips for each sample. We found a significative 40% calcium overload in DS-HFF samples, irrespective of whether they were derived from cardiopathic trisomic foeti, when compared to the control group ($p<0.01$). Results are shown as mean of the determinations in each group ± standard error. N-HFF = Euploid fibroblasts, DS-HFF = Hsa21 trisomic fibroblasts, NCDS-HFF = Hsa21 trisomic fibroblasts from DS foeti without heart defects, CDS-HFF = Hsa21 trisomic fibroblasts from DS foeti with heart defects.

Table S3. Mitochondrial genes downregulated in DS heart tissues with NRF1 binding site in their promoter regions.

Gene name	Score	Promoter region position	Binding site sequence
ECGF1	1,00	-13	CGCATGCGCA
SCO2	1,00	-14	CGCATGCGCA
PIN4	0,98	-282	CGCGTGCGCA
IDH3A	0,97	-24	CGCTTGCGCA
UQCRC1	0,96	7	CGCTTGCGCG
NDUFB8	0,96	-9	CACATGCGCA
RPL10	0,96	-12	CACATGCGCA
ENDOG	0,91	-161	CGCCTGCGCA
FPGT-TNNI3K	0,91	23	CGCATGCGCC
SDHA	0,91	-88	CGCCTGCGCA
UQCRC2	0,91	-264	CGCATGCGCC
ETFB	0,90	-9	CGCCTGCGCG
GLUD1	0,90	-31	CGCCTGCGCG
NDUFAB1	0,90	-43	CGCCTGCGCG
CYCS	0,90	-208	CGCAAGCGCA
SDHB	0,90	-65	CGCATGCCCA
HSPA9	0,89	-171	CGCATGTGCG
MRPL15	0,88	-52	CGCGCGCGCA
SLC25A12	0,88	-63	CGCGTGCGGA
VDAC1	0,88	-59	TGCGTGCGCA
HCCS	0,88	-25	CGCGTGCCCG
IDH3B	0,87	-166	TGCTTGCGCA
IDH2	0,86	-262	CGCTTGCGAG
COX4NB	0,84	-292	CACGTCCGCA
COQ7	0,81	-363	CGCCCGCGCA
ETFA	0,81	-71	CGCCTGCCCA
GOT1	0,81	-395	CGCCCGCGCA
NDUFA13	0,81	-265	GGCCTGCGCA
NDUFS2	0,81	-78	CGCCTGCGTA
PDHA1	0,81	-165	CGCAGGCGCT
DLAT	0,80	33	AGCCTGCGCG
GCSH	0,80	-18	CGCCTCCGCG
MOSC2	0,80	-6	AGCCTGCGCG
AK2	0,80	-303	CCCACGCGCA

NRF1 target genes are sorted with a cut-off affinity score = 0.80.

Table S4. Mitochondrial genes downregulated in DS heart tissues with ERRa binding site in their promoter regions.

Gene name	Score	Promoter region position	Binding site sequence
HSPA9	0,95	-66	GACTCAAGGTCACA
MOSC2	0,94	-174	CGCTGAAGGTCATG
SDHA	0,93	-390	TTGTGGAGGTCACA
TXN2	0,92	-298	ATCACGAGGTCAAA
MRPL35	0,92	-231	ATCACAAGGTCAGG
BDH1	0,91	-193	GGATCAAGGACAGA
NDUFB8	0,90	-208	AGAAAAAGGACACA
COX7A2	0,90	-48	TCGAAAAGGTCAGG
SDHB	0,90	-446	ATCACGAGGTCAGG
DLAT	0,89	-428	AACTGAAGGTGACA
NDUFAB1	0,88	-417	AAAAAAAGGACAAA
COQ7	0,88	-108	TCGAAGAGGTCACG
MRPS12	0,88	23	ACCTAAAGGTGAGG
TIMM23	0,87	-6	CCCGGAAGGTCAGC
ETFA	0,87	-296	ACCCCGAGGTCAGC
ATP5B	0,87	-289	TGATCTAGGTGACA
IDH3B	0,86	-153	GTGGGGAGGTCATG
ECI1	0,86	-292	AGCTCGCGGTCACG
MRPL15	0,85	-112	ACTAAAAGGACAAC
ETFB	0,85	-449	ACATGGAGGTGAAG
COX4NB	0,85	-94	GCACGGAGGTCACC
CYCS	0,84	-367	ACCTAGAGGTCTCC
TNNI3K	0,84	-329	TTTTCAAGATCATT
UQCRFS1	0,84	-236	ATCTCTAGGTCTTC
SLC25A4	0,83	-205	GTTTAAAGGGCACA
GOT1	0,83	-405	TGGTCAAGGTCGCC
PIN4	0,83	-99	TCTTATTGGTCAGA
SCO2	0,81	-258	CCATGGCGGTCAGC
NFS1	0,81	-92	CGAGCGAGGTGAGG
CKMT2	0,81	-437	GGAAGGAGGTCCCT
IMMT	0,80	-41	ATATCCAGCTCATA
DLST	0,80	-191	TCCTGAAGGTGTAT
MIPEP	0,80	-265	GCCTGAAGGAGAAG
COX10	0,80	-14	GCCTGAAGGACTTC

ERRa target genes are sorted with a cut-off affinity score = 0.80. A possible target of *ERRa* is *IMMT* (in red), a gene involved in mitochondrial cristae pattern organization.

Text S1

Supplemental Methods

Mitochondrial calcium measurement using aequorin

Aequorin is a 21-kDa protein from various *Aequorea species* [1] which, in the active form, consists of an apoprotein and a covalently bound prosthetic group (coelenterazine). When Ca^{2+} ions bind to three high-affinity sites (EF-hand type), aequorin undergoes an irreversible reaction in which a photon is emitted.

Mitochondrial Calcium was measured by the method described by [2]. Cells were cultured on 13 mm-diameter coverslips in Chang medium B+C (Irvine scientific) at 37 °C and 5% CO_2 for 24 h and then infected with an adenoviral vector containing the plasmid with the cDNA coding for a mitochondrial-matrix addressed mutant form of aequorin. This construct includes the mitochondrial-targeting presequence of subunit VIII of human cytochrome c oxidase fused to the aequorin cDNA. Forty-eight hours after transfection, the cells were incubated for 1.5 h with 5 μM coelenterazine in Chang medium in a 5% CO_2 atmosphere. Coverslips with the transfected cells was placed in a saline solution-perfused chamber at 37 °C, and the number of emitted photons per second was measured after the stimulation with histamine using a photomultiplier with amplifier-discriminator. The output of the amplifier-discriminator was captured by a photon-counting board in a microcomputer and stored for further analysis. In order to calibrate the row luminescent signal in terms of $[Ca^{2+}]$ an algorithm has been developed that takes into account the instant rate of photon emission and the total number of photons that can be emitted by the aequorin of the sample. To obtain the latter parameter, at the end of each experiment the cells were lysed by a hyposmotic medium containing 10 mM $CaCl_2$ and 0,1% Triton X-100 in order to discharge all the aequorin that was not consumed during the experiment.

1. Shimomura O (1986) Isolation and properties of various molecular forms of aequorin. The Biochemical journal 234: 271-277.
2. Pinton P, Rimessi A, Romagnoli A, Prandini A, Rizzuto R (2007) Biosensors for the detection of calcium and pH. Methods in cell biology 80: 297-325.

Text S2

Supplemental Methods

Bionformatic binding analysis

The promoter regions from -450bp to +50bp of mitochondrial genes downregulated in DS heart tissues were analyzed in order to recognize DNA binding motifs for both NRF1 and ERRα matrices (from PSCAN software http://159.149.109.9/pscan/). The list of downregulated genes was ranked according to the prediction of binding affinity of their promoter regions to NRF1 and ERRα binding sites with a cut-off affinity score = 0.80 and p-value<0.003.